Universidade de Aveiro Departamento de Ambiente e Ordenamento
2013

Joana Patrícia Carvalho Pereira

Células de Combustível Passivas de Etanol Direto: estudos de modelação

Passive Direct Ethanol Fuel Cells: modeling studies

Universidade de Aveiro Departamento de Ambiente e Ordenamento
2013

Joana Patrícia Carvalho Pereira

Células de Combustível Passivas de Etanol Direto: estudos de modelação

Passive Direct Ethanol Fuel Cells: modeling studies

Dissertação apresentada à Universidade de Aveiro para cumprimento dos requisitos necessários à obtenção do grau de Mestre em Engenharia do Ambiente, realizada sob a orientação científica do Dr. António José Barbosa Samagaio, Professor Associado do Departamento de Ambiente e Ordenamento da Universidade de Aveiro, e da Dr.ª Alexandra Rodrigues Pinto, Professora Associada do Departamento de Engenharia Química da Faculdade de Engenharia da Universidade do Porto.

aos meus pais, que sempre me incentivaram a sonhar.
à minha avó, que muita força me deu.
ao Douglas, que me fez acreditar.

“What is now proved was once only imagined”
William Blake

o júri

presidente

Professor Doutor Luís António da Cruz Tarelho
Professor Auxiliar, Universidade de Aveiro

vogais

Professor Doutor Fernando Manuel Bico Marques
Professor Catedrático, Universidade de Aveiro

Professor Doutor António José Barbosa Samagaio
Professor Associado, Universidade de Aveiro

Professora Doutora Alexandra Maria Pinheiro da Silva Ferreira Rodrigues Pinto
Professora Associada, Faculdade de Engenharia da Universidade do Porto

agradecimentos

São muitas as pessoas que tornaram possível a realização deste trabalho, e todas elas merecem a minha maior consideração pelo seu inestimável apoio:

Agradeço, em primeiro lugar, à Professora Dr.ª Alexandra Pinto, pela confiança que depositou em mim e por me ter concedido esta valiosa oportunidade. Da mesma forma, agradeço ao Professor Dr. António Samagaio por ter tido a amabilidade de aceitar este desafio.
Sem eles, este projeto não teria sido possível.

À Dr.ª Vânia Oliveira, pela sua preciosa orientação científica e, sobretudo, pela enorme disponibilidade e amabilidade, demonstradas durante todo o desenvolvimento deste trabalho.

Agradeço também à Dr.ª Daniela Falcão, pela atenção, interesse e simpatia que sempre me disponibilizou.

A todos os amigos que estiveram ao meu lado, e que me fizeram sorrir nas horas fáceis e difíceis. Um agradecimento especial ao André, Catarina, Ariana, Filipe, João, porque às vezes os almoços também alimentam a alma. Ao Douglas. Pela companhia fantástica nos dias de sol e pelo brilho nos dias de chuva. Pelas tertúlias nas mesas dos cafés, nos bancos dos jardins, nas longas viagens. Uns mais próximos, outros mais distantes, mas todos presentes.

A todos, o meu Muito Obrigada!

palavras-chave

Células de combustível passivas de etanol direto, Modelação, Transporte de calor e massa, Atravessamento de etanol, Atravessamento de água

resumo

O presente trabalho teve como objetivo o estudo de modelação de uma célula de combustível com injeção direta e passiva de etanol operando em condições ambientais. Este estudo foi desenvolvido tendo em conta a importância crescente dos sistemas com alimentação direta e passiva de etanol como solução para as aplicações portáteis.

No decurso deste trabalho, foi desenvolvido um modelo matemático para a célula passiva, em estado estacionário e a uma dimensão, incorporando o transporte de calor e massa bem como as reações eletroquímicas que ocorrem no ânodo e no cátodo da célula de combustível. Este modelo simplificado pode ser rapidamente implementado usando métodos numéricos simples existentes no Excel, e reproduz de modo satisfatório os dados experimentais obtidos.

Neste trabalho, foi também desenvolvida uma instalação laboratorial para determinação experimental das curvas de polarização e de potência da célula. Para esse fim, foi concebida e construída uma célula com uma área ativa de 25 cm^2. Um estudo experimental detalhado para a célula passiva operando sob condições ambientais é apresentado nesta tese.

As previsões do modelo foram comparadas com os resultados experimentais e verificou-se uma grande concordância entre ambos. Deste modo, o funcionamento da célula de combustível com injeção direta e passiva de etanol foi explicado à luz das previsões do modelo para o atravessamento de metanol e de água através da membrana.

O efeito das condições de operação (tais como a concentração de etanol na alimentação ao ânodo e a densidade de corrente), bem como de parâmetros de configuração (materiais que constituem as camadas de difusão e espessura da membrana polimérica), no desempenho da célula foi estudado detalhadamente, e as previsões do modelo reproduziram satisfatoriamente os resultados obtidos.

Dada a escassa informação existente sobre este tema na literatura atual, os resultados obtidos neste estudo são de elevado interesse e apresentam grande importância para o futuro desenvolvimento de células de combustível com injeção direta e passiva de etanol.

keywords Passive direct ethanol fuel cells, Modeling, Heat and mass transfer, Ethanol crossover, Water crossover

abstract

Bearing in mind that the passive feed Direct Ethanol Fuel Cell (DEFC) systems emerge as a solution for portable applications, the main objective of this thesis was the modelling study of a passive feed DEFC working under ambient conditions.

A steady state, one dimensional and non-isothermal model was developed, accounting for coupled heat and mass transfer processes along with the electrochemical reactions occurring in the fuel cell. This simplified model was rapidly implemented using simple numerical tools as Excel, and reproduced with satisfactory accuracy the experimental data.

An experimental set-up was implemented in order to determine the cell polarization and power density curves. For the experimental studies, an "in-house" passive feed DEFC with an active area of 25 cm^2 was designed, and a detailed experimental characterization of the cell working under ambient conditions was performed.

The model predictions were compared with the experimental results, and a very successful accuracy was found. Therefore, the experimental results could be explained under the light of the model predictions concerning both ethanol and water crossover.

Moreover, the effect of operating conditions (ethanol feed concentration and current density) and design parameters (anode diffusion layer material and thickness, anode catalyst loading and membrane thickness) on the fuel cell performance was intensively investigated. The model proved to predict accurately the trends of the effect of the different parameters on both ethanol and water crossover, and subsequently on the cell performance.

Given the lack of information concerning this issue in the actual literature, the results achieved in this work provide very interesting and useful information for the future development of passive DEFCs.

Table of Contents

1. Motivation and Objectives 1

2. Introduction 3
2.1. Fuel Cells for Sustainable Energy 3
2.2. Brief History of Fuel Cells 4
2.3. Working Principles of Fuel Cells 5
2.4. Performance of Fuel Cells 6
2.5. Types of Fuel Cells Available 7
2.5.1. Alkaline Fuel Cells (AFC) 7
2.5.2. Phosphoric Acid Fuel Cells (PAFC) 8
2.5.3. Molten Carbonate Fuel Cells (MCFC) 8
2.5.4. Solid Oxide Fuel Cells (SOFC) 8
2.5.5. Proton Exchange Membrane Fuel Cells (PEMFC) 8
2.5.6. Direct Alcohol Fuel Cells (DAFC) 9
2.6. Benefits and Constraints of Fuel Cells 9

3. Direct Ethanol Fuel Cells: state-of-the-art 13
3.1. Introduction to DEFCs 13
3.2. Passive feed DEFCs 14
3.3. Working Principle of Passive DEFCs 14
3.4. Fundamentals of DEFCs 17
3.4.1. Thermodynamics of DEFCs 17
3.4.2. Electrochemistry of DEFCs 18
3.4.2.1. Membrane Electrode Assembly 19
3.4.2.2. Electro-catalysts for Ethanol Oxidation and Oxygen Reduction 23
3.5. Mass Transport Phenomena 30
3.5.1. Ethanol Crossover 30
3.5.2. Water Management 32
3.6. Operating Conditions 34
3.6.1. Ethanol Concentration 34
3.6.2. Fuel Cell Temperature 35
3.6.3. Catalyst Loading 36

3.7. Mathematical Modeling 36
3.8. Applications 38
3.9. Summary and Scope of the Present Work 40

4. Model Formulation for a Passive Feed DEFC 43
4.1. General Model Structure 43
4.2. Model Assumptions 44
4.3. Governing Equations and Boundary Conditions 45
4.3.1. Mass Transport 45
4.3.2. Heat Transport 54
4.3.3. Cell Performance 57
4.4. Results and Discussion 58
4.5. Concluding Remarks 64

5. Experimental Setup for a Passive Feed DEFC 65
5.1. Fuel Cell Design 65
5.2. Test Kit Testing Unit 68
5.3. Experimental Procedure 69

6. Experimental and Modeling Studies 71
6.1. Model Validation 71
6.2. Results and Discussion 73
6.2.1. Effect of the Ethanol Concentration 73
6.2.2. Effect of the Membrane Thickness 77
6.2.3. Effect of the Anode Catalyst Loading 80
6.2.4. Effect of the Anode Diffusion Layer Material 82
6.3. Concluding Remarks 86

7. Conclusions and Suggestions for Future Work 87
7.1. Conclusions 87
7.2. Suggestions for Future Work 88

8. References 91

APPENDICES 101
Appendix A: Uncertainty Analysis 102
Appendix B: Physical properties of the materials used 105
Appendix C: Diffusion coefficients 109

List of Figures

Fig.2.1| Schematic representation of an individual fuel cell system 3

Fig.2.2| Typical design of a fuel cell system 5

Fig.2.3| Schematic representation of a typical fuel cell polarization curve, adapted from Ref. [38] 6

Fig.3.1| Schematic representation of typical design of a passive DEFC 15

Fig.3.2| Schematic representation of perfluorinated sulfonic acid membranes chemical structure, adapted from Ref. [39] 20

Fig.3.3| Schematic representation of the reaction pathways of DEFCs using platinum in acidic media, reprinted from Ref. [34] 23

Fig.3.4| Schematic representation of ethanol electro-oxidation using Pt-Sn catalysts, reprinted from Ref. [13] 27

Fig.3.5| Polarization curves and power density curves in single DEFC at 90°C. Electrolyte: Nafion™ 115 membrane. Anode: ethanol solution: 1.0 M; flow rate: 1.0 ml min^{-1}. Cathode: Pt/C 1.0 mg cm^{-2} Reprinted from Ref. [107] 28

Fig.3.6| Performance of single DEFCs for different anode catalysts at 200 mV and 80°C. Ethanol solution: 1.0 M; flow rate: 2.0 ml min^{-1}. Reprinted from Ref. [119] 29

Fig.3.7| Maximum conversion of ethanol at different temperatures, reprinted from Ref. [36] 35

Fig.3.8| Examples of transport modes powered by fuel cell technology 39

Fig.3.9| Examples of portable power tools powered by fuel cell technology 40

Fig.3.10| Examples of fuel cell chargers powered by fuel cell technology 40

Fig.4.1| Schematic representation of the passive feed DEFC used in the model formulation 43

Fig.4.2| Predicted ethanol concentration profiles through the DEFC for different current densities. Membrane: Nafion™ 117; Diffusion layers: Carbon Cloth; Anode: ethanol solution 1.0 M, Pt-Ru/C 4.0 mg cm^{-2}; Cathode: Pt/C 2.0 mg cm^{-2}; Temperature: 293 K. ... 60

Fig.4.3| Predicted leakage current for different ethanol feed concentrations. Membrane: Nafion™ 117; Diffusion layers: Carbon Cloth; Anode: Pt-Ru/C 4.0 mg cm^{-2}; Cathode: Pt/C 2.0 mg cm^{-2}; Temperature: 293 K. 60

Fig.4.4| Predicted water concentration profile across the anode and membrane. Membrane: Nafion™ 117; Diffusion layers: Carbon Cloth; Anode: ethanol solution 1.0 M, Pt-Ru/C 4.0 mg cm^{-2}; 61

Fig.4.5| Predicted net water transport coefficients for different ethanol feed concentrations. Membrane: Nafion™ 117; Diffusion layers: Carbon Cloth; Anode: Pt-Ru/C 4.0 mg cm^{-2}; Cathode: Pt/C 2.0 mg cm^{-2}; Temperature: 293 K. 62

Fig.4.6| Influence of ethanol concentration on the net water transport coefficients for different current densities. Membrane: Nafion™ 117; Diffusion layers: Carbon Cloth; Anode: ethanol solution 1.0 M, Pt-Ru/C 4.0 mg cm^{-2}; Cathode: Pt/C 2.0 mg cm^{-2}; Temperature: 293 K. 63

Fig.4.7| Predicted temperature profiles across the DEFC for different current densities. Membrane: Nafion™ 117; Diffusion layers: Carbon Cloth; Anode: ethanol solution 1.0 M, Pt-Ru/C 4.0 mg cm^{-2}; Cathode: Pt/C 2.0 mg cm^{-2}; Temperature: 293 K. 63

Fig.5.1| Nafion-based Membrane Electrode Assembly (MEA) 65

Fig.5.2| Diffusion layers made of (a) Carbon cloth; (b) Carbon paper; (c) ELAT 66

Fig.5.3| Current collector plate made of stainless steel 66

Fig.5.4| Isolating rubber plate 66

Fig.5.5| Acrylic end plates used in the (a) anode side; (b) cathode side 67

Fig.5.6| 3D CAD drawing of the “in-house” passive feed DEFC 67

Fig.5.7| Fabricated “in-house” passive feed DEFC 68

Fig.5.8| Test unit used for the experimental studies of the passive feed DEFC 69

Fig.6.1| Comparison of the model predictions for (a) cell potential and (b) power density curves and the experimental results for different ethanol concentrations. Membrane: Nafion™ 117; Diffusion layers: Carbon Cloth; Anode: Pt-Ru/C 4.0 mg cm^{-2}; Cathode: Pt/C 2.0 mg cm^{-2}; Temperature: 293 K. Dots: experimental data; Lines: model predictions. 72

Fig.6.2| Carbon dioxide formation on the anode side of the cell during the experimental studies 73

Fig.6.3| Influence of ethanol concentration on (a) cell voltage and (b) power density. Membrane: Nafion™ 117; Diffusion layers: Carbon Cloth; Anode: Pt-Ru/C 4.0 mg cm^{-2}; Cathode: Pt/C 2.0 mg cm^{-2}; Temperature: 293 K. 75

Fig.6.4| Predicted ethanol crossover for different ethanol concentrations. Membrane: Nafion™ 117; Diffusion layers: Carbon Cloth; Anode: Pt-Ru/C 4.0 mg cm^{-2}; Cathode: Pt/C 2.0 mg cm^{-2}; Temperature: 293 K. 76

Fig.6.5| Predicted net water transport coefficient for different ethanol concentrations. Membrane: Nafion™ 117; Diffusion layers: Carbon Cloth; Anode: Pt-Ru/C 4.0 mg cm^{-2}; Cathode: Pt/C 2.0 mg cm^{-2}; Temperature: 293 K. 76

Fig.6.6| Influence of membrane thickness on (a) cell voltage and (b) power density for different ethanol concentrations. Diffusion layers: Carbon Cloth; Anode: Pt-Ru/C 4.0 mg cm^{-2}; Cathode: Pt/C 2.0 mg cm^{-2}; Temperature: 293 K. 78

Fig.6.7| Predicted ethanol crossover for different membrane thicknesses. Diffusion layers: Carbon Cloth; Anode: ethanol solution 1.0 M, Pt-Ru/C 4.0 mg cm^{-2}; Cathode: Pt/C 2.0 mg cm^{-2}; Temperature: 293 K. 79

Fig.6.8| Predicted net water transport coefficients for different membrane thicknesses. Diffusion layers: Carbon Cloth; Anode: ethanol solution 1.0 M, Pt-Ru/C 4.0 mg cm^{-2}; Cathode: Pt/C 2.0 mg cm^{-2}; Temperature: 293 K. 79

Fig.6.9| Influence of the anode catalyst loading on (a) cell voltage and (b) power density for different ethanol concentrations. Membrane: Nafion™ 117; Diffusion layers: Carbon Cloth; Anode: Pt-Ru/C 4.0 mg cm^{-2} (HL) or Pt-Ru/C 2.0 mg cm^{-2} (LL); Cathode: Pt/C 2.0 mg cm^{-2}; 80

Fig.6.10| Model predictions for the effect of the anode catalyst loading on the anode overpotentials for different ethanol concentrations. Membrane: Nafion™ 117; Diffusion layers: Carbon Cloth; Anode: Pt-Ru/C 4.0 mg cm^{-2} (HL) or Pt-Ru/C 2.0 mg cm^{-2} (LL); Cathode: Pt/C 2.0 mg cm^{-2}; Temperature: 293 K. 81

Fig.6.11| Model predictions for the effect of the anode catalyst loading on the ethanol crossover. Membrane: Nafion™ 117; Diffusion layers: Carbon Cloth; Anode: ethanol solution 1.0 M, Pt-Ru/C 4.0 mg cm^{-2} (HL) or Pt-Ru/C 2.0 mg cm^{-2} (LL); Cathode: Pt/C 2.0 mg cm^{-2}; Temperature: 293 K. 81

Fig.6.12| Influence of the anode diffusion layer material on (a) cell voltage and (b) power density for different ethanol concentrations. Membrane: Nafion™ 117; Anode: Pt-Ru/C 4.0 mg cm^{-2}; Cathode: Pt/C 2.0 mg cm^{-2}; Temperature: 293 K. 83

Fig.6.13| Predicted ethanol crossover for different anode diffusion layer materials. Membrane: Nafion™ 117; Anode: Ethanol concentration: 2M; Pt-Ru/C 4.0 mg cm^{-2}; Cathode: Pt/C 2.0 mg cm^{-2}; 84

Fig.6.14| Predicted anode overpotentials for different anode diffusion layer materials. Membrane: Nafion™ 117; Anode: Ethanol concentration: 2M; Pt-Ru/C 4.0 mg cm^{-2}; Cathode: Pt/C 2.0 mg cm^{-2}; Temperature: 293 K. 85

Fig.6.15| Predicted net water transport coefficient for different anode diffusion layer materials. Membrane: Nafion™ 117; Anode: Ethanol concentration: 2M; Pt-Ru/C 4.0 mg cm^{-2}; Cathode: Pt/C 2.0 mg cm^{-2}; Temperature: 293 K. 85

List of Tables

Table 4.1 | Values considered for the parameters used in the modeling studies..... 59

Table 5.1 | Specifications of the different components of the passive feed DEFC 68

Table 6.1 | Specifications of the different diffusion layer materials used in passive feed DEFC as in Ref. [46] 82

Table A.1 | Values of parameters and uncertainties regarding ethanol concentration... 103

Table A.2 | Values of parameters and uncertainties regarding the cell current 103

Table A.3 | Values of parameters and uncertainties regarding the cell potential 103

Table A.4 | Values of parameters and uncertainties regarding the cell power..... 104

Table B.1 | Densities 103

Table B.2 | Specific heat..... 103

Table B.3 | Standard enthalpies of formation 106

Table B.4 | Standard Gibbs free energy..... 106

Table B.5 | Viscosities 106

Table B.6 | Liquid molar volumes 106

Table B.7 | Parachor values 107

Table B.8 | Diffusion volumes..... 107

Table B.9 | Tortuosity..... 107

Table B.10 | Porosity..... 107

Table B.11 | Thermal conductivities 108

Nomenclature

A_a	Active area, cm^2
A_{holes}	Total area of the holes, cm^2
A_{surf}	Total area without the holes, cm^2
C	Concentration, mol cm^{-3}
$C_{O_2,\ ref}$	Reference concentration of oxygen, mol cm^{-3}
Cp	Specific heat, J mol^{-1} K^{-1}
$\partial E_{cell}/\partial T$	Rate of change of electromotive force, V K^{-1}
D	Diffusion coefficient, cm^2 s^{-1}
D^{eff}	Effective diffusion coefficient, cm^2 s^{-1}
E_{cell}	Thermodynamic equilibrium potential, V
E_{rev}	Reversible voltage, V
F	Faraday's constant, C mol^{-1}
G	Gibbs free energy, J mol^{-1}
g	Gravitational acceleration, cm^2 s^{-1}
H	Enthalpy of reaction, J mol^{-1}
h_{mass}	Mass transfer coefficient, cm s^{-1}
h_{heat}	Heat transfer coefficient, W cm^{-2} K^{-1}
i	Current, A
i_{cell}	Cell current density, A cm^{-2}
$i_{C_2H_5OH}$	Leakage current density due to ethanol crossover, A cm^{-2}
$i_{0,\ ref}^{C_2H_5OH}$	Exchange current density of ethanol, A cm^{-2}
$i_{0,\ ref}^{O_2}$	Exchange current density of oxygen, A cm^{-2}
k	Thermal conductivity, W cm^{-1} K^{-1}
$K_{2–9}$	Partition coefficients
L	Length of the active area, cm
n	Number of electrons
$n_{C_2H_5OH}$	Electro-osmotic drag coefficient of ethanol
n_d	Electro-osmotic drag coefficient of water
N	Molar flux, mol cm^{-2} s^{-1}
Nu	Nusselt number, dimensionless

P_{air}	Pressure of the ambient air, atm
Pr	Prandtl number, dimensionless
Q	Heat transfer, W cm^{-2}
R	Ideal law gas constant, J mol^{-1} K^{-1}
R_{cond}	Conduction resistance, K W^{-1}
R_{conv}	Convection resistance, K W^{-1}
$R_{thermal}$	Total thermal resistance, K W^{-1}
Ra	Rayleigh number, dimensionless
S	Entropy change in the system, J mol^{-1} K^{-1}
Sc	Schmidt number, dimensionless
Sh	Sherwood number, dimensionless
T	Temperature, K
V_{cell}	Cell voltage, V
W_{elec}	Electrical work, W
$x_{C_2H_5OH}$	Molar fraction of ethanol, dimensionless
x	Coordinate direction normal across the fuel cell, cm

Greek Letters

α	Net water transport coefficient
α_A	Anodic transfer coefficient
α_C	Cathodic transfer coefficient
β	Parameter
Δ	Variation
ε	Porosity
ε_{fuel}	Fuel utilization efficiency
ε_{real}	Real electric efficiency
ε_{rev}	Reversible efficiency
$\varepsilon_{voltage}$	Voltage efficiency
η	Overpotential, V
κ	Ionic conductivity of membrane, S cm^{-1}
λ	Membrane hydration coefficient
μ	Dynamic viscosity, mol cm^{-1} s^{-1}

v	Kinematic viscosity, $cm^2\ s^{-1}$
θ	Stoichiometric coefficient
δ	Thickness, cm

Superscripts

0	Initial conditions
AAP	Anode Acrylic plate
AC	Anode Catalyst
ACP	Anode Collector Plate
AD	Anode Diffusion
CAP	Cathode Acrylic Plate
CC	Cathode Catalyst
CCP	Cathode Collector Plate
CD	Cathode Diffusion
M	Membrane

Subscripts

A	Anode
air	air
C	Cathode
cell	Fuel cell
C_2H_5OH	Ethanol
CO_2	Carbon dioxide
j	Species j
H_2O	Water
O_2	Oxygen

Acronyms

1D	One dimension
AAP	Anode Acrylic plate
AC	Anode Catalyst
ACP	Anode Collector Plate
AD	Anode Diffusion
CAP	Cathode Acrylic Plate
CC	Cathode Catalyst
CCP	Cathode Collector Plate
CD	Cathode Diffusion
CFD	Computational Fluid Dynamics
DAFC	Direct Alcohol Fuel Cell
DFC	Direct Fuel Cell
DEFC	Direct Ethanol Fuel Cell
DMFC	Direct Methanol Fuel Cell
DTM	Decal Transfer Method
ErTFO	Erbium Triflate
GE	General Electric
HL	High Load
LL	Low Load
MEA	Membrane Electrode Assembly
MCFC	Molten Carbonate Fuel Cell
NASA	National Aeronautics and Space Administration
PAFC	Phosphoric Acid Fuel Cell
PEM	Polymer Electrolyte Membrane
PEMFC	Polymer Electrolyte Membrane Fuel Cell
PTFE	Polytetrafluoroethylene (Teflon)
PVA	Poly(vinyl alcohol)
SOFC	Solid Oxide Fuel Cell
sPEEK	Sulphonated Poly(etheretherketone)

1. Motivation and Objectives

In the last decades, fuel cells received great attention as a promising substitute power source for compact and mobile applications, mainly due to their simplicity, efficiency, low level of emissions, quick refueling, and a potentially renewable fuel source [1-10]. In particular, the research and development of direct alcohol fuel cells (DAFC) as battery replacers have been remarkable, based on their properties such as high energy densities, durable runtime and instant recharging. Furthermore, DAFCs can use fuels in liquid form, commonly methanol, ethanol or formic acid, and are able to run at ambient temperature, which makes them easy to handle and enables them to be designed at small and micro scales [10].

Among the different types of DAFCs, the direct methanol fuel cells (DMFCs) are the most intensively investigated as promising candidates for portable power sources because they work at lower temperatures, they use a quick refueling system, do not require any fuel processing, and thus they result in a simpler design and operation, together with higher reliability [3-5, 11]. However, methanol is volatile, flammable and highly toxic, and thus direct ethanol fuel cells (DEFCs) have been receiving particular attention as alternative compact power source [12-15]. Ethanol is an attractive fuel because it is easy to handle, it is non-toxic, and it is renewable as it can be produced from agricultural biomass. Therefore, its application in fuel cells has been investigated by many authors [12-20]. In order to improve the power output as well as the energy conversion efficiency in direct ethanol fuel cells, key issues concerning the crossover phenomena of water [21], oxygen [22, 23] and ethanol [24-30] through the cell membrane, as well as the electrochemical oxidation of ethanol [31-37] are still under study.

Concerning the different concepts of fuel handling and delivery, the direct fuel cells can be categorized as active or passive systems [3]. Passive feed systems are especially desirable because they are less expensive, more compact and simpler than the active ones. Additionally, the refueling is fast and durable, and since the parasitic power losses are lower, they become more efficient [2-4]. For that reason, passive systems are cost competitive within the actual market size and they are more suitable for portable power sources, but further research is needed on this issue.

Accounting for the introduction of passive DEFCs in the market, the main goal of the present study is to design a direct ethanol fuel cell, and to develop a simplified model that can accurately describe the main transport phenomena and reproduce experimental data. Mathematical modeling is crucial in the design and optimization of fuel cells, since models allow a better comprehension of the parameters affecting the system performance [38]. Moreover, mathematical models can be used to appropriately adjust the cell operating conditions, so that adequate levels of energy density can be achieved for real applications [10, 38].

A concise overview of the different types of fuel cells available, as well as their main characteristics is made in this work. Also, the result of an exhaustive review on recent studies concerning experimental and modeling studies of active and passive DEFCs is presented.

2. Introduction

2.1. Fuel Cells for Sustainable Energy

In the last few decades, mainly due to the global population growth and parallel expansion of the economy, the demand for energy has been increasing rapidly [1]. To fulfill human needs, the improvement of technology and electronic devices has been extraordinary, and nowadays portable devices as cell phones, laptop computers and multimedia equipment are widespread. However, these devices use batteries which are charged by fossil fuel-based electrical resources [2, 3], and which are becoming inadequate for the increasing power requirements of portable electronic devices [3-5].

Since the dawn of the industrial revolution, fossil fuels were used as the driving force behind the industrialized world and its economic growth. Presently, about 80% of all primary energy in the world is derived from fossil fuels with oil accounting for 32.4%, coal for 27.3% and natural gas for 21.4% [6]. Biofuels and waste (10.0%), nuclear power (5.7%) and hydroelectric dams (2.3%) account for only a minor share of the global primary energy supply, and only 0.9% of the world's primary energy is derived from alternative energy sources, such as solar, wind or geothermal [6]. As is known, the use of fossil fuel-based resources causes serious negative environmental impacts since these are non-renewable resources, and the existing reserves are being currently depleted [1]. Moreover, the burning of fossil fuels is responsible for water and air pollution, enhances the greenhouse effect and contributes to global warming [1-3, 7]. Therefore, the supply of clean and sustainable energy is urgent, and became an important scientific and technical challenge in the 21st century.

In view of the aforementioned, fuel cells emerge as an environmentally friendly solution, able to replace the conventional batteries for portable applications [2-5].

A fuel cell is, among a variety of electrochemical power sources, a device designed to convert the chemical energy directly into electrical energy (Fig. 2.1) [7-10]. A schematic diagram of a fuel cell is shown in Figure 2.1.

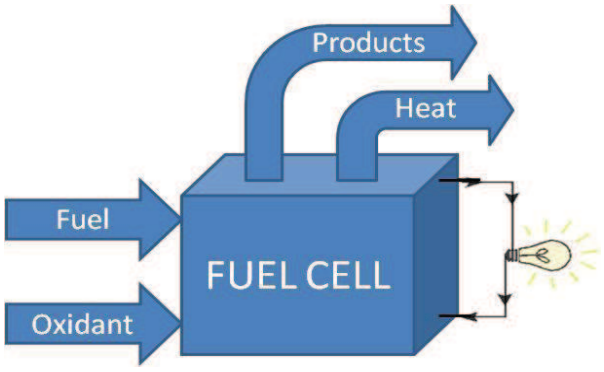

Fig. 2.1 | Schematic representation of an individual fuel cell system

Fuel cells are supplied by gaseous or liquid reactants, and as long as fuel and oxidant are provided they operate for extended time without recharging [10]. Since fuel cells rely on electrochemical reactions, the level of pollutants released is very low, which further contributes to the idea of achieving clean energy.

2.2. Brief History of Fuel Cells

It was in the early nineteenth century that William Nicholson and Anthony Carlisle demonstrated the first principle of what became fuel cells [38]. However, only in 1839, Welsh scientist Sir William Robert Grove was able to demonstrate the first fuel cell and publish his findings on the Philosophical Magazine and Journal of Science. Sir Grove established the possibility of reverting the electrolysis process to obtain water and electricity generation from hydrogen and oxygen. To prove his theory, Sir Grove built the world's first “fuel cell” based on two bottles containing oxygen and hydrogen, respectively. He arranged two platinum electrodes, with one end immersed in a container of sulfuric acid and the other separately sealed within the oxygen and hydrogen bottles, verifying that electric current could flow between the electrodes [9, 38].
Much of the theoretical understanding of how fuel cells operate was provided by the Nobel Prize Friedrich Wilhelm Ostwald. In 1893, he experimentally determined the interconnected roles of the various components of the fuel cell, namely electrodes, electrolyte, oxidizing and reducing agents, anions, and cations, and his work became the foundation for many other scientists and researchers [38].
Throughout the 20th century, many researchers increased efforts to make this technology commercially available. In 1955, a General Electric Company (GE) scientist named W. Thomas Grubb made advances in the field of Polymer Electrolyte Membrane Fuel Cell (PEMFC), modifying the original fuel cell design by using a sulphonated polystyrene ion-exchange membrane [38, 39]. Three years later, also from GE, Leonard Niedrach managed to deposit a catalyst onto the membrane, improving the hydrogen oxidation and oxygen reduction reactions. This became known as the “Grubb-Niedrach fuel cell” [38]. Later, GE cooperated with NASA and McDonnell Aircraft to develop this technology, leading to the first commercial use of a fuel cell [8, 39].
From the mid-1960s, Shell was involved with developing direct methanol fuel cells, where the use of liquid fuel was considered to be a great advantage for vehicle applications [39]. The research and development of fuel cells was largely accelerated by the oil crisis in the later 1970s. Since then, efforts have been made to attempt a larger commercialization of fuel cells, and thus investigation has been made in order to reduce the cost of the product, to find efficient fuel sources and to develop new materials that could improve the overall system. Substantial technical and commercial development continued in the 1990s, notably in the area of direct fuel cells. Carmakers such as General Motors, and

Toyota invested in PEMFC research. Other companies, namely Ballard, continued PEMFC research for automotive and stationary clean power. Ballard went on to supply PEMFC units to Daimler and Ford [8, 39].
Significant advances in fuel cell technology occurred as PEMFC technology was adapted for direct methanol portable devices. Early applications included power for devices such as laptops, PADs and mobile phones [8, 39]. Actually, fuel cells are a subject of vigorous research and development, engineering and testing on a broad scale in universities, research centers and private companies in different sectors of economy. Although many fuel cell companies are still far from being profitable, the opportunities for growth in the future appear to be very promising.

2.3. Working Principles of Fuel Cells

Fuel cells perform the direct conversion of the chemical energy stored in a fuel into electricity, by means of an electrochemical reaction. There are several different types of fuel cell but they are all based around a central design. They consist of an anode (negative side), a cathode (positive side) and an electrolyte, as illustrated in Figure 2.2. The chemical reactions occur at the interfaces of these three different segments, resulting in fuel consumption, production of water and other products, and electric current flow that can be used to power electrical devices [8-10].

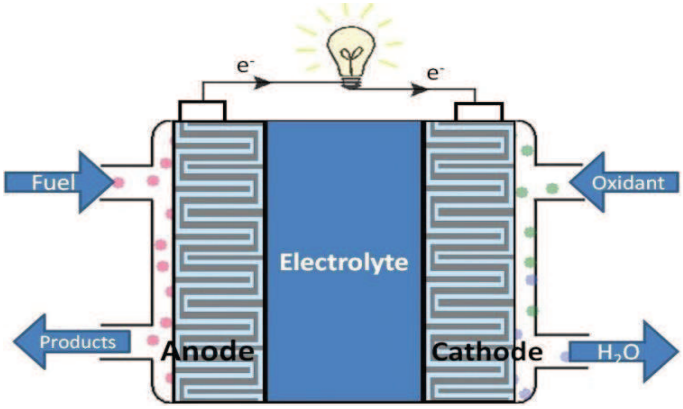

Fig. 2.2 | Typical design of a fuel cell system

In order to enhance the performance of the fuel cell, flow field plates can be used to increase the reaction surface area. These are provided with numerous thin channels that carry and distribute fuel and oxidant, enhancing the reactant delivery [9, 40].
The fuel is supplied to the anode while the oxygen, typically in the form of ambient air, is delivered to the cathode. Since the electrolyte is specifically designed to be permeable to ions but impermeable to gases, the fuel and the oxygen cannot react directly. Thus, the electrochemical reactions occur at the electrodes where ions and electrons are either produced or consumed [8, 9].

The ions produced migrate across the electrolyte, and this flux is balanced by an electron flux through an external circuit, generating electricity. The electrolyte plays a key role in this process, as it must permit only the appropriate ions to pass between the electrodes. If free electrons or other substances travel through the electrolyte, they disrupt the chemical reaction and lower the efficiency of the cell [8, 9].
Although the process appears to be quite simple, the electricity produced by the fuel cell depends on the fastness of the electrochemical reactions, and catalysts are commonly used to improve the process. One of the main challenges in fuel cell research is to improve the efficiency and durability of the catalysts in order to process more fuel [8, 40]. Besides electric power, by-products such as water, depleted fuel and heat are also formed throughout the process and need to be removed, as if they accumulate, they poison the membrane preventing the new fuel and oxidant from reacting [8].

2.4. Performance of Fuel Cells

The performance of a fuel cell can be described in a so-called polarization curve, a current-voltage ($i - V_{cell}$) graph which shows the voltage output of the fuel cell for a given current output (Fig 2.3). Since larger fuel cells can provide more electricity than smaller devices, these curves are usually normalized by fuel cell area, in order to make results comparable [10].

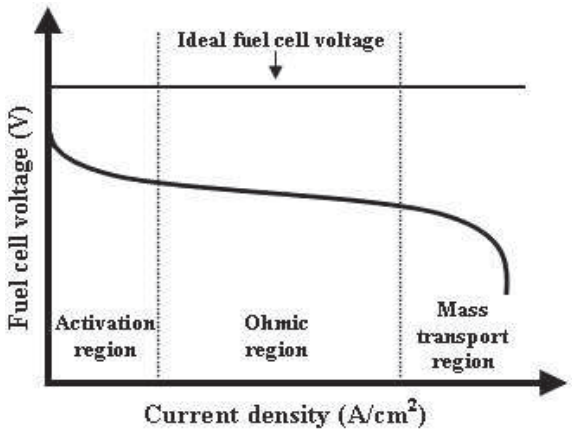

Fig. 2.3 | Schematic representation of a typical fuel cell polarization curve, adapted from Ref. [38]

As long as supplied with adequate amounts of fuel, ideal fuel cells would supply any amount of current while maintaining a constant voltage as determined by thermodynamic principles. However, the real voltage outputs are usually lower than the thermodynamically due to unavoidable losses [9, 10, 38]. There are three major types of losses that contribute to the characteristic shape of fuel cell $i - V_{cell}$ curves, each of them depending on the cell voltages and current density, and thus predominating in different regions, as indicated in Figure 2.3. The activation losses, occurring in the activation

region, are caused due to the energy consumption of the electrochemical reactions, which is higher than that predicted for ideal cases. These are mainly dominant when operating a cell at high voltage and low current densities. In the Ohmic region, the Ohmic losses are mostly caused by the ionic and electronic conduction. In the mass transport region, the concentration losses are responsible for the fuel cell low performance when working at high current densities [9, 10]. The voltage output of a fuel cell works as a measure of its efficiency, and it is therefore critical to maintain a high fuel cell voltage even when working under high current loads.

2.5. Types of Fuel Cells Available

All different fuel cells work under the same electrochemical principles. However different characteristics can be used to distinguish them, such as working temperature, reactant type and electrolyte type [8, 10].
Concerning the working temperature, one distinguishes low-temperature fuel cells (working at no more than 120 to 150°C); intermediate-temperature fuel cells (150 to 250°C); and high-temperature fuel cells (over 650°C). In the last years, fuel cells working in the temperature range of 200 to 650°C have also been introduced [8].
The reactant type may also vary among fuel cells. As reducing agent, sources as hydrogen, methanol, methane, carbon monoxide and other organic as well as some inorganic substances can be used. As oxidizing agent, fuel cells can use pure oxygen, air, hydrogen peroxide and even chlorine [40].
Most commonly, fuel cells are classified according to the nature of the electrolyte they employ, since this determines the kind of reactions occurring in the cell, the type of catalyst and fuel required, and other operating factors. There are five major types of fuel cells, concerning the type of electrolyte employed:

2.5.1. Alkaline Fuel Cells (AFC)

Alkaline fuel cells (AFCs) were one of the first fuel cell technologies developed. These fuel cells use an aqueous solution of potassium hydroxide as electrolyte, whose concentration can be varied according to the cell working temperature (60 to 250°C) [8, 10].
AFCs performance depends on the rate at which chemical reactions take place in the cell, and efficiencies near 60 percent were demonstrated in spatial applications [39]. The major disadvantage of this fuel cell is its sensitivity to poisoning by carbon dioxide. In fact, even the carbon dioxide found in common air can affect the performance of the cell, making it necessary to purify both the hydrogen and oxygen used. Besides being costly, susceptibility to poisoning also affects the cell's lifetime [10].

2.5.2. Phosphoric Acid Fuel Cells (PAFC)

This type of fuel cell uses liquid phosphoric acid as electrolyte, and since the ionic conductivity of this acid is low at low temperature, PAFCs need to operate under higher temperature ranges [8, 10]. When used for co-generation of electricity and heat, they can be 70 percent efficient [10]. However, they are less powerful than other types of fuel cells, given the same weight and volume. As a result, these fuel cells are typically large and heavy. These properties lead them to be used for stationary power generation, and also to power large vehicles such as city buses [8].

2.5.3. Molten Carbonate Fuel Cells (MCFC)

Molten carbonate fuel cells are high-temperature fuel cells that use an electrolyte composed by a molten carbonate salt mixture, usually lithium carbonate and potassium carbonate [10]. Working at 650°C, MCFCs can reach efficiencies approaching 50 percent, and when the heat generated as by-product is used in co-generation, overall fuel efficiencies can be as high as 90 percent [10]. MCFCs don't require an external reformer to convert fuels into hydrogen. Due to the high temperatures at which MCFCs operate, the fuels are converted within the fuel cell itself by internal reforming, which reduces its cost. However, the primary disadvantage of current MCFC technology is durability. The high temperatures at which these cells operate and the corrosive electrolyte used accelerate component breakdown and corrosion, decreasing cell lifetime [8, 10].

2.5.4. Solid Oxide Fuel Cells (SOFC)

Solid oxide fuel cells use a hard, non-porous ceramic material as electrolyte. Due to this characteristic, SOFCs are able to operate at very high temperatures, around 1000°C, and overall fuel use efficiencies could reach 90 percent when working in co-generation. Concerning the conversion of fuel into electricity, SOFCs are expected to be around 50-60 percent efficient [10].
SOFCs are the most sulfur-resistant fuel cell type, and they are not poisoned by carbon monoxide (CO), which can even be used as fuel [8]. However, high-temperature operation has disadvantages, resulting in a slow start up and places stringent durability requirements on materials. Thus, the development of low-cost materials with high durability is a technical challenge facing this technology [8, 10].

2.5.5. Proton Exchange Membrane Fuel Cells (PEMFC)

The proton exchange fuel cell capitalizes on the essential simplicity of the fuel cells. Also known as polymer electrolyte membrane fuel cells, they use a polymer membrane which

is permeable to protons, and they require only hydrogen, oxygen from the air, and water to operate, thus they can be used with increased facility [8, 10, 40].
Since the polymer membrane must be hydrated with water to maintain adequate conductivity, the working temperature of the PEMFC is limited under 90°C, which allows a quick start (less warm-up time) and less usage of the system components, resulting in higher durability [10]. However, the low temperatures also lead to slow reaction rates, and for this reason, they require the use of sophisticated catalysts and electrodes to overcome that fact [8, 10, 40].
Platinum is generally the catalyst used, and although it is expensive, developments in recent years allowed the use of only minute amounts of this compound, reducing the cost of PEMFCs [9, 40]. In addition, these fuel cells deliver higher power densities and offer the advantages of low weight and volume, compared to other fuel cells. Due to these characteristics, PEMFCs are particularly suitable for portable applications [10].

2.5.6. Direct Alcohol Fuel Cells (DAFC)

Direct alcohol fuel cells (DAFC) are a subcategory of PEMFCs that are able to directly use liquid or vapor forms of fuel, such as methanol and ethanol, instead of hydrogen [8, 40]. This type of fuel cell was largely overlooked in the early 1990s because of its low efficiency, and companies rather preferred the PEMFC. However, in the beginning of this century special attention was given to DAFCs, and tremendous progress has been made [40]. In Section 3, the result of an exhaustive research on the recent work done on this type of cell is presented. Detailed information about active and passive DEFCs is also provided, as well as a review on experimental and modeling studies concerning this type of fuel cell.

2.6. Benefits and Constraints of Fuel Cells

The progress in the fuel cell field is fast, and this technology is already widely used throughout the economy in a vast range of applications. Moreover, fuel cells provide various advantages when compared to conventional power sources, such as internal combustion engines or batteries. Although some of the attributes of fuel cells are only valid for some applications, most of the benefits are general [8-10, 39]:

- Fuel cells have a higher efficiency than diesel or gas engines, as they rely on electrochemical reactions rather than combustion reactions.
- Fuel cells based on hydrogen fuel produce only water and air as by-products. If the hydrogen comes from the electrolysis of water driven by renewable energy, then using fuel cells eliminates greenhouse gases over the whole cycle. When other

fuels are used, such as methanol or ethanol, by-products such as carbon dioxide can be formed. Nevertheless, the emissions generated do not approach those of other conversion technologies, and thus fuel cells can reduce pollution caused by burning fossil fuels.

- Since hydrogen can be produced anywhere where there is water and a source of power, generation of fuel can be distributed and does not have to be grid-dependent. Therefore, fuel cells can be located almost anywhere, including dense urban areas, providing power wherever electricity is needed, making the whole electric power grid more robust and reliable.

- Unlike batteries, that must be disposed once their chemicals are depleted, fuel cell reactions do not degrade over time and can theoretically provide continuous electricity, as long as a fuel source is provided. The refueling process is much faster and simpler than that of recharging a battery.

- Since there are no moving parts in the system, the maintenance of fuel cells is simple and they are more reliable and quieter than generators. Moreover, fuel cells are not exposed to high temperatures, corrosion or any structural weaknesses found in other engines, which improves their durability.

- Economically, fuel cells represent a prudent path to provide electric power because they can reduce economic dependence on oil producing countries, generating a greater energy security worldwide. Each fuel cell type has its own operational characteristics, offering advantages to particular applications. Moreover, they can achieve high efficiencies at any size scale, making them perfect for a broader range of applications than any other currently available power source, from small portables to transportation and residential uses. Furthermore, higher temperature fuel cells produce high-grade process heat along with electricity and are well suited to cogeneration applications (such as combined heat and power for residential use).

Notwithstanding all the benefits and attractive aspects of fuel cells aforementioned, some constraints still limit the use and commercialization of this technology.
One of the main constraints is related to the cost associated with fueling. Although abundant in the universe, hydrogen is fairly rare in our atmosphere, meaning that it has to be extracted. This process can be cost prohibitive and inefficient, and brings great difficulty when dealing with fuel manufacture and storage [8, 10]. Also, high costs arise from the catalysts used to promote the electrochemical reactions, since they usually rely on rare and expensive metals [8, 40].

In the past, fuel cells were large and extremely expensive to manufacture, but their cost will quickly decrease to consumer-affordable levels once mass production exists. Currently, many fuel cell companies are seriously investing to accelerate the mass manufacturing, while also trying to develop a variety of markets for this type of products. A good example is the increased market significance of DAFCs, which can presently use less costly fuels such as alcohols thus becoming an affordable technology.

3. Direct Ethanol Fuel Cells: state-of-the-art

3.1. Introduction to DEFCs

It is widely recognized that PEMFCs have attracted particular attention in the last decades, mainly due to their applicability to transportation systems and portable electronic products. However, the major advantages of PEMFCs could not be entirely appreciated given the difficulties and hazards associated with handling, storing, transporting and distributing gaseous reactants such as hydrogen [8, 9].

In order to overcome these issues, several efforts were made for the development of direct fuel cells, which could use liquid fuels directly without a reforming step [9]. This new technology provided considerable weight and volume advantages over the traditional PEMFCs. Moreover, liquid fuels as methanol and ethanol have higher volumetric energy densities than hydrogen, thus DAFCs can be simultaneously compact and be recharged more quickly, by simply pouring some drops of alcohol [9].

Among all the investigated fuels, methanol was the most favorite due to its handling and distribution facility, relatively higher electrochemical activity and low cost. Thus, great progress has been made concerning the performance of DMFCs [41, 42] and their modeling [11, 43-46]. However methanol is toxic for human beings, especially for the optical nerve [13], it is inflammable with a low boiling point (65°C) and it is not a primary fuel [15]. Based on these limitations, several materials were investigated as possible fuels for DAFCs and ethanol emerged as the most attractive and promising option to overcome the problems detected in DMFCs [12-15].

Ethanol has a higher theoretical mass energy density than methanol (8.0 vs. 6.1 kWh kg^{-1}), and it is known that ethanol is non-toxic for humans, it is naturally available and it can be easily renewed by the fermentation of sugar-containing agricultural biomass [7, 12-15, 48]. Also, the carbon dioxide emitted from direct ethanol fuel cells can be recycled by planting, allowing a zero green-house contribution to the atmosphere [13, 48].

In the last decade many efforts have been made to improve the ethanol electrical performance when used in a DEFC, and thus exhaustive work has been made concerning thermodynamic [33-36], experimental [49-55] and modeling [56-60] aspects of DEFCs. Furthermore, Song et al. [28] found that ethanol shows lower crossover rates than methanol, and presents less negative effect on the cathode performance due to its smaller permeability through the membrane and its slower electrochemical oxidation kinetics on the cathode.

Due to its attractive characteristics, DEFCs are important candidates as sustainable electric power source for a vast range of devices, and especially for compact systems. However, despite the advantages that make this technology especially appealing, DEFCs

are rather new and further investigation is needed to optimize and improve their performances.

3.2. Passive feed DEFCs

Depending on how the reactants are supplied to the system, direct alcohol fuel cells can be categorized as active or passive systems [3]. Additionally semi-passive systems, that are a combination of both passive and active systems, have been tested [4].
Active fuel cells supply fuel and oxidant by using additional components such as pumps, fans, and reactant controllers, improving the flow mass transport and the electrochemical activity of this type of system [5]. However, the use of extra components is related to higher costs and lower system energy density, and thus active systems are better suitable for large fuel cells.
Passive feed systems, on the other hand, do not require any moving accessory components or additional power consumption, since all the processes are accomplished by natural capillary forces, gravity, diffusion, convection and evaporation [4, 5]. Thus, oxygen diffuses from the ambient air into the cathode by an air-breathing mechanism, and the fuel diffuses from a built-in reservoir into the anode due to a concentration gradient existing between both media. This fact helps to decrease the volume, as well as parasitic power losses [3]. Moreover, passive fuel cells operate at low current densities resulting in less heat production and lower fuel delivery requirements, thus the refueling is fast and the fuel is long-lasting. For the reasons aforementioned, passive fuel cells are compact, simple, reliable, and efficient, making them more suitable for portable applications which require low power [2-5, 61].
Several studies have been conducted in the last decade by many researchers concerning the improvement of passive DMFCs [2-5, 61-102]. However, the present development of passive DEFCs is not as satisfying, and few references have been found related to this new technology [103]. For this reason, it is urgent to investigate and explore the most significant challenges and feasibility of passive DEFCs.

3.3. Working Principle of Passive DEFCs

Direct ethanol fuel cells perform the direct conversion of chemical energy into electricity, by means of ethanol oxidation coupled to oxygen reduction. Similarly to the PEMFCs these fuel cells use a polymer membrane as electrolyte, and their anatomy is very similar to the regular fuel cell, previously shown in Figure 2.2. However, the main difference settles on the reactants supply, on the current collectors and on the membrane electrode assembly (MEA), responsible for the good performance of the electrochemical reactions [40].

A schematic representation of a passive direct ethanol fuel cell is shown in Figure 3.1, and as can be seen, the structure of a passive DEFC is composed by a polymer electrolyte membrane (PEM), placed between the anode and the cathode. On both sides of the PEM there are the anode and cathode catalyst layers (AC and CC respectively) where the reactions occur, followed by the anode and cathode diffusion layers (AD and CD), responsible for the enhanced delivery of the reactants along the catalysts. These three sandwich structured components are often referred as the membrane electrode assembly [40]. As depicted in Figure 3.1, the MEA is placed between an anode and a cathode current collector plate (ACP and CCP) that gather the generated electric current, and the entire cell setup is held between an anode and cathode fixture, namely the ethanol reservoir end plate (AAP) and the cathode end frame where the air breathing occurs (CAP).

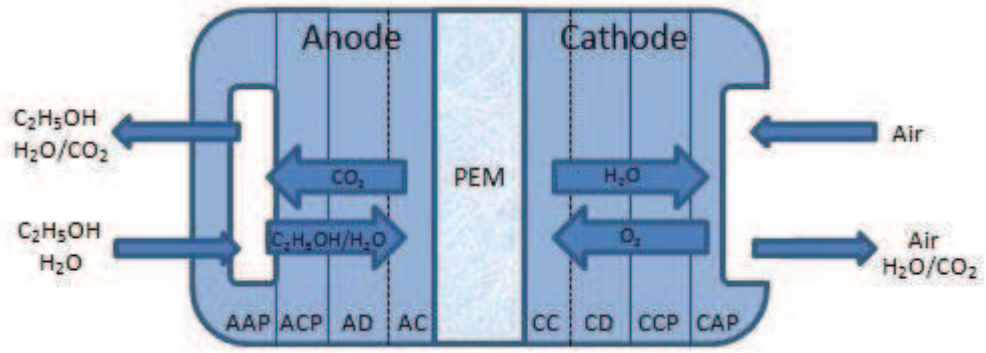

Fig. 3.1 | Schematic representation of typical design of a passive DEFC

In a passive air-breathing fuel cell, the current collector plates usually present an open pattern, in order to promote an appropriate reactant delivery. Generally, holes are perforated on the metal plates, which act as both current collectors and reactant distributors [102].

The current collectors must comprise characteristics such as high electric conductivity, good mechanical strength and uniform transport area [76]. Stainless steel is the mostly common material employed as current collector in passive fuel cells because of its intrinsic properties, such as corrosion resistance, high electrical conductivity and rigidity, and thus it was used by many authors [61-78, 98-101]. On the other hand, materials like copper have also been studied by Oliveira et al. [5, 80]. Some authors [5, 62-66, 77-80, 99] employed gold plated current collectors, since gold has proved to eliminate any contact resistance at the current-collector electrode interface [99]. The free open ratio of the current collector was found to be an important factor influencing the mass transfer characteristics of passive fuel cells, and it has also been investigated by some authors [76, 100, 102]. The findings suggest that a higher open ratio of the current collector helps to enhance the cell performance, due to the improvement of mass transfer. On one hand, a higher open ratio facilitates fuel, water and oxygen diffusion within the electrode surface

area. On the other hand, it also provides an efficient expelling path for the products [76, 100, 102].

Acrylic materials are frequently used by many authors to make both the anode and cathode end plates [2, 5, 72-76, 80], since the use of transparent materials allow the visualization of the internal activity of the cell, and also provides sufficient rigidity to support the unit.

In a passive feed fuel cell, the pure ethanol or ethanol aqueous solution, as well as the oxidant (usually air or pure oxygen), are supplied to the reaction zone by natural convection [98]. The transportation of ethanol from the anode reactant compartment (AAP) towards the anode reaction zone occurs mainly by natural diffusion. Reaching the catalyst layer (AC), with the aid of the electro-catalysts the ethanol is oxidized to produce carbon dioxide, releasing simultaneously protons and electrons. The ethanol oxidation in the anode can be described by [15]:

$$C_2H_5OH + 3\ H_2O \rightarrow 2\ CO_2 + 12\ H^+ + 12\ e^- \quad (3.1)$$

As the membrane is ideally impermeable to gases, the resultant carbon dioxide moves counter-currently to the fuel tank, and eventually emerges as gas bubbles through the AC. The protons cross through the PEM to the cathode, while the electrons flow through an external circuit, generating electric current on their way to reach the cathode. At the CC, the electrons transported from the anode combine with protons and the oxidant to produce water. The electro-reduction of oxygen taking place on the cathode is given by [15]:

$$O_2 + 4\ H^+ + 4\ e^- \rightarrow 2\ H_2O \quad (3.2)$$

The water produced in CC moves then counter-currently to the CCP or, under specific operating conditions, by back diffusion to the anode. The overall reaction of these two combined electrochemical reactions occurring at each side of the PEM is given by:

$$C_2H_5OH + 3\ O_2 \rightarrow 2\ CO_2 + 3\ H_2O \quad (3.3)$$

Mainly due to the membrane properties, an operating temperature below 100 °C is required. However, these two half-reactions would normally occur very slowly at such conditions. Thus, catalysts are used both on the anode and cathode to increase the rates of each half-reaction [8]. The final products of the overall cell reaction are electric power, carbon dioxide, water and heat. Cooling is thus required to maintain the temperature of the fuel cell below 100 °C.

3.4. Fundamentals of DEFCs

3.4.1. Thermodynamics of DEFCs

It is commonly known that thermodynamics is the branch of natural science concerned with energy changing from one form to another. As already mentioned, a fuel cell converts the energy stored within a fuel into other forms of energy, thus the predictions that can be made using thermodynamic equations are crucial for understanding and modeling fuel cell performances.

The total intrinsic energy of a fuel can be quantified in terms of internal energy, which is associated with the chemical bonds of the atoms. However, fuel cells convert only a portion of this energy into electrical energy, being this established by the first and second laws of thermodynamics [10]. Fundamentally, in a fuel cell the maximum amount of energy that can be extracted from a fuel depends whether this is done by means of heat or work. In an isothermal, isobaric system, the maximum heat energy that can be extracted from the ethanol is given by its enthalpy of reaction (ΔH) equal to -1367.9 kJ mol^{-1} at 25°C and 1 atm [27]. On the other hand, the maximum electrical work (W_{elec}) that the system can perform under isothermal and isobaric conditions is measured by the free energy change associated with the chemical reaction, which is directly converted into electrical energy. This is given by the negative change in Gibbs free energy (ΔG) for the process [10, 38]:

$$W_{elec} = -\Delta G \tag{3.4}$$

The Gibbs free energy expresses the amount of useful work that can be obtained from the system when it changes from one set of steady-state to another, and for ethanol it equals -1326.7 kJ mol^{-1} under 25°C and 1 atm [27]. Considering isothermal processes, the Gibbs free energy can also be computed from the enthalpy of the system according to [10]:

$$\Delta G = \Delta H - T\Delta S \tag{3.5}$$

where ΔS represents the entropy change in the system, and T is a given temperature.

The potential of a system to perform electrical work by moving a charge carried out by electrons through an electrical potential difference E_{cell}, in volts, can also be represented by [10, 38]:

$$W_{elec} = n\,F\,E_{cell} \tag{3.6}$$

where n is the number of moles of electrons transferred, and F is the Faraday constant (96.485 coulombs per mole of electrons), the maximum reversible voltage provided by a DEFC can be calculated from [10, 38]:

$$E_{rev} = -\frac{\Delta G}{nF} \quad (3.7)$$

The term "reversible" is frequently used concerning fuel cells, and it implies that the fuel cell voltage is produced at thermodynamic equilibrium. Recalling equation 3.3, 12 electrons result from each molecule of ethanol. Thus, the thermodynamic cell potential for a liquid feed DEFC working under standard conditions, i.e. 25°C and 1 atm, approximates a theoretical value of 1.145 V for the reversibly working cell [15, 27, 33].
Accordingly, and taking into account that the thermodynamic efficiency ε of a fuel cell is defined as the ratio of the maximum electrical work and the total chemical energy, the reversible efficiency of an ideal fuel cell is obtained by [15, 38]:

$$\varepsilon_{rev} = \frac{\Delta G}{\Delta H} \quad (3.8)$$

Working under standard conditions, the theoretical thermodynamic efficiency of a DEFC can reach 97%. However, it has been verified that DEFC real efficiencies are substantially lower to the reversible efficiencies, mainly due to losses related to reaction, conduction and mass transport steps within the fuel cell [10, 36].
The voltage efficiency of the fuel cell $\varepsilon_{voltage}$ incorporates losses due to irreversible kinetic effects, and is given by the ratio of the real operating voltage V_{cell} to the thermodynamically reversible voltage of the cell E_{rev}:

$$\varepsilon_{voltage} = \frac{V_{cell}}{E_{rev}} \quad (3.9)$$

The real operating voltage of the fuel cell depends on the current i, as given by $i - V_{cell}$ curves, and thus $\varepsilon_{voltage}$ depends on the current drawn from the cell [10].
The fuel utilization efficiency ε_{fuel} due to the ethanol crossover phenomena is defined as:

$$\varepsilon_{fuel} = \frac{i_{cell}}{i_{cell} + i_{C_2H_5OH}} \quad (3.10)$$

where i_{cell} is the actual current produced, and $i_{C_2H_5OH}$ is the parasitic current due to ethanol crossover. Therefore, the real electric efficiency of a DEFC, ε_{real} accounting for the overall losses may be calculated as [10]:

$$\varepsilon_{real} = \varepsilon_{rev} \times \varepsilon_{voltage} \times \varepsilon_{fuel} \quad (3.11)$$

3.4.2. Electrochemistry of DEFCs

The overall PEM fuel cell electrochemical reactions were introduced in Section 3.3, and although these reactions do not seem overly complicated, the actual reactions proceed through many steps and generate many intermediate species.

Since the electrochemical reactions involve the transfer of electrons between the electrode surface and chemical species adjacent to the electrode surface, the current produced by the DEFCs depends on the reaction rate, i.e. its kinetics. Only a detailed knowledge of the intermediate and adsorbed species, the reaction paths and the rate determining steps would allow an increase of the overall reaction rates.

The primary goal to enhance the kinetics of DEFCs is to find electrode materials that enable the chemical reactions to occur at potentials as close as possible to their thermodynamic equilibrium potential. Increasing the operating temperature and adopting more active catalysts could help to improve the kinetics and the performance of DEFCs [15]. However, considering the limited working temperature ranges of the usual membranes (<100ºC), the kinetics enhancement in DEFCs is not only dependent on the development of novel electrolyte materials with higher proton conductivity, increased tolerance to higher temperatures, and higher impermeability to ethanol, but mainly on the investigation of new electro-catalysts with desired catalytic activity for ethanol electro-oxidation and higher selectivity for CO_2 production [36].

3.4.2.1. Membrane Electrode Assembly

As abovementioned, the membrane electrode assembly is the main responsible for the good performance of a DEFC, and it is composed by the polymer electrolyte membrane surrounded by the catalyst layers (AC and CC), and the diffusion layers (AD and CD), as previously illustrated on Figure 3.1.

The catalyst layers provide the active surface for the occurrence of the electrochemical reactions, and play the role of reactant and product transporters. The main processes occurring in the catalyst layers include mass transport of the reactants, interfacial reactions of the reactants at the electrochemically active sites, proton transport in the electrolyte phase, and electron conduction in the electronic phase, besides the transport of some by-products [40]. Thus, it is important that they are designed so as to generate high rates of the desired reactions, and to minimize the amount of catalyst necessary for reaching the required levels of power output. Usually, catalyst inks are made from a porous mixture composed of catalyst, carbon powders, binders, and solvent, and they can be either applied at the surface of the diffusion layers or directly on the surface of the membrane (catalyst coated membrane) [40].

The diffusion layers provide the basic mechanical support to the MEA and electrical pathway for the electrons [9]. Although they do not have a direct participation in the electrochemical reactions, they allow the access of the reactants and the removal of products from the catalyst layers, as well as heat removal, and thus they must be sufficiently porous and electrically and thermally conductive [9]. To accomplish these features, they usually consist of a backing layer composed of porous carbon paper or carbon cloth, and a micro porous layer which is created by mixing carbon blacks with

polytetrafluoroethylene (PTFE) solution [40, 104]. Although the carbon paper shows excellent electronic conductivity, the carbon cloth is more porous and less tortuous, thus both materials are widely used. The PTFE solution applied in the cathode diffusion media enhances the water removal from the cathode catalyst layer given its hydrophilic character, thus preventing flooding. Moreover, the strong bonds between the fluorine and the carbon make it durable and resistant to chemical attack [9], and a concise review on PTFE-bonded MEAs proved that these resulted in higher fuel cell performances when PTFE was used as a binder in the cathode [9, 40].

One of the main problems of DEFCs relies on the crossover of products between the anode and the cathode, which leads to serious poisoning of cathode catalysts and lower efficiency of fuel consumption [21-28]. Thus, the polymer electrolyte membrane plays an important role as an effective barrier separating fuel and reactants. The PEM is actually a porous polymer membrane acting as a barrier for the fuel, which ideally allows the penetration of protons and water molecules, and must accomplish important characteristics such as chemical and mechanical stability within the fuel cell, as well as high proton conductivity [9, 104].

The most frequently used electrolytes in DEFCs are made of perfluorocarbon-sulfonic acid ionomer, a compound resulting from the combination of tetrafluoroethylene and perfluorosulfonate monomers. The chemical structure of perfluorinated sulfonic acid membranes is presented in Figure 3.2. These membranes have been developed since 1960s by DuPont, and they are commercially available under the name of Nafion™, existing in many different thicknesses, usually related to a number in mills [12, 13].

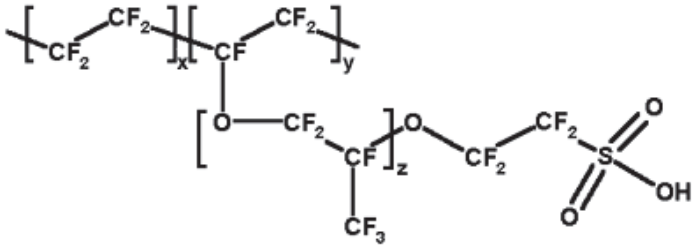

Fig. 3.2 | Schematic representation of perfluorinated sulfonic acid membranes chemical structure, adapted from Ref. [39]

The conductivity of Nafion™ membranes is heavily dependent on their hydrate state, and thus their working temperatures is limited to less than 100°C [29]. The use of Nafion™ 115 membranes in DEFCs was investigated by Song et al. [28, 29], and it was found that the membrane porosity, also known as the degree of membrane swelling, increases with ethanol concentration. Microscopic and macroscopic bulk swelling exist for Nafion™ membranes in aqueous ethanol solutions, concerning the amount of water adsorbed by the ionic clusters, or the ethanol that penetrates and plasticizes the fluorocarbon matrix, respectively [29, 52]. According to the authors [28], the high macroscopic swelling degree

of Nafion™ membranes in the presence of ethanol enhanced the distortion between the electrode and the electrolyte, resulting in fast delamination of the catalyst layer from the membrane and shortening the longevity of DEFCs. These findings are in agreement with that reported by Elliot et al. [52], who studied the bulk swelling of Nafion™ membranes in mixtures of ethanol and water, and verified that the ethanol was able to plasticize the fluorocarbon matrix, allowing the ionic material to be redistributed into numerous clusters.

The influence of the polymer electrolyte membranes on the performance of DEFCs was analysed by Andreadis et al. [17] by using an ethanol concentration of 1.0 M and comparing the thicknesses of Nafion™ 112 (0.051mm) and 117 (0.178 mm). According to the authors, the use of Nafion™ 117 leads to lower ethanol crossover rates, lower parasitic currents and lower mixed potential values. Thus, when the cell operates at low current densities, the use of a thick membrane is adequate to reduce the negative effect caused by ethanol crossover. However, the authors [17] also stated that considering higher current densities, a thinner membrane like Nafion™ 112 could reduce the ohmic overpotential, leading to higher power density values.

The method used on the preparation of MEAs also has an influence on the cell performance. Song et al. [26] investigated the effect of MEA preparation procedure on ethanol crossover and single DEFC performance, by comparing MEAs prepared through both the conventional and the decal transfer method (DTM). The main difference between these two electrode preparation procedures is that the catalyst layer is applied onto the gas diffusion layers on the conventional method, while on the DTM it is applied onto the electrolyte membrane with a transfer process at higher temperatures. The authors [26] verified that, although the MEA-DTM presented higher ethanol crossover, single DEFCs using these membranes exhibited improved performance and lower internal resistance in comparison with the conventional MEAs.

The performance of the state-of-the-art DEFCs using Nafion™ as the electrolyte for the most common catalysts is still far below the theoretical value of 1.145 V [36], and thus other polymer binders were investigated in order to reduce the fuel permeability, such as trifluoromethanesulfonic acid (triflic acid) and erbium triflate (ErTFO). Barbora et al. [49] developed composite membranes of ErTFO/Nafion™, and verified a reduction of about 80% in alcohol permeability, together with a rise of 38% in proton conductivity when compared to pure Nafion™ membranes. Moreover, the authors stated that these membranes were chemically stable and suitable for use in DEFCs.

In recent years, new materials such as poly (vinyl alcohol) (PVA) and sulfonated poly (ether ether ketone), most commonly known as sPEEK, have also been studied for the manufacture of membranes for DEFCs [51]. PVA is considered a versatile polymer and it has been investigated due to its good film-forming properties, good chemical resistance, reduced ethanol permeability, and low cost [51, 53]. Gomes and Filho [53] tested hybrid membranes composed of PVA, impregnated with phosphotungstic acid hydrate and

(diethylenetriamine)pentaacetic acid, and obtained ethanol permeabilities two orders of magnitude smaller than common Nafion™ 117. sPEEK materials were was also tested by researchers as a modified polymeric matrix [54, 55]. However, domains such as proton conductivity and membrane stability are still under research for these compounds [55].
Concerning passive DAFCs, so far no work was found for direct ethanol fuel cells. Nevertheless, Nafion™ membranes were widely investigated for passive DMFCs.
Achmad et al. [2] compared both Nafion™ 112 and 117 membranes regarding passive DMFCs, and stated that the performance of Nafion™ 117 was superior to the one with Nafion™ 112 membrane. Liu et al. [73] also studied the effect of the membrane thickness on the efficiency of passive DMFCs and verified that for low fuel concentrations (2.0 M), thicker membranes led to good performances at lower current densities, but lower performances at higher current densities. However, when tested with high fuel concentrations (4.0 M), the different membranes exhibited similar cell voltages over a wide range of current densities. Additionally, the authors [73] observed that thicker membranes would yield higher efficiency regarding fuel utilization. This was supported by Bae et al. [84] who compared both Nafion™ 115 and 117 membranes, and verified that although it had little effect on the cell's performance, the fuel lasted longer when using thicker membranes. For this reason, the authors [84] suggested that thicker membranes should be used when the fuel cell was used for portable power sources. On the other hand, singular studies suggested that adopting thinner membranes such as Nafion™ 212 could provide more proton conductivity and less resistance when compared to thicker membranes, thus increasing the water back flow rate, and improving both cell hydration and performance [4]. Moreover, a study by Yuan et al. [90] where Nafion™ membranes were modified by decreasing the ionomer size in the anode catalytic layer, showed that this decrease was beneficial to an improvement in both catalyst and Nafion™ ionomer utilization, thus enhancing the cell performance.
Currently, other alternative polymeric membranes are being investigated for passive DMFCs. Higa et al. [74] prepared PEMs from PVA and a modified PVA polyanion containing 2-methyl-1-propanesulfonic acid groups as a copolymer. According to the authors [74], the proton selectivity obtained was almost three times higher than the Nafion™ 117, and thus the PVA-based electrolytes are potential candidates for fuel cells working with high fuel concentrations. Lufrano et al. [89] developed PEMs based on sulfonated polysulfone for application in a DMFC mini-stack operating at room temperature and detected fewer problems with interfacial delaminating between the electrode layer and the membrane, which has been considered a critical factor in terms of durability.

3.4.2.2. Electro-catalysts for Ethanol Oxidation and Oxygen Reduction

The poor performance of electro-catalysts, especially anode catalysts at lower temperatures, is still an obstacle to overcome before the commercialization of DEFCs.
Ethanol electro-oxidation involves the cleavage of the C–C bond, which is very difficult at lower temperatures [105] and the production of adsorbed species as acetate and carbon monoxide, that inhibit the formation of CO_2 and lead to the formation of stable intermediate products such as acetaldehyde and acetic acid [33-37, 57]. This process releases just a couple of electrons per ethanol molecule, and hence generates low currents. The complete conversion of ethanol to CO_2 would release a total of 12 electrons per molecule and generate higher currents, but that requires higher potentials to break the strong bond between the two carbon atoms [34]. This would make the process inefficient, since almost all of the voltage produced by oxidizing the ethanol would sustain the reaction, reducing the net power output. Due to these issues, the improvement of the activity of the anode catalysts is of major importance. Additionally, efficient catalysts would prevent the fuel crossover, since the fuel concentration on the interface between anode and proton electrolyte is lowered as the fuel is consumed more exhaustively, consequently reducing the alcohol crossover [106].
Several studies have been performed to evaluate the influence of different catalysts on direct ethanol fuel cells [105-117] and the most extensively investigated catalysts are based on platinum (Pt). Since the efficiency of catalysis is dependent on the contact area, the active phase is usually dispersed on a conductive support as carbon, in order to augment the available surface [18].
Kutz et al. [34] investigated the ethanol electro-oxidation reaction (EOR) pathways on polycrystalline Pt surfaces in acidic media. The mechanism proposed for the reaction pathways is schematically represented in Figure 3.3.

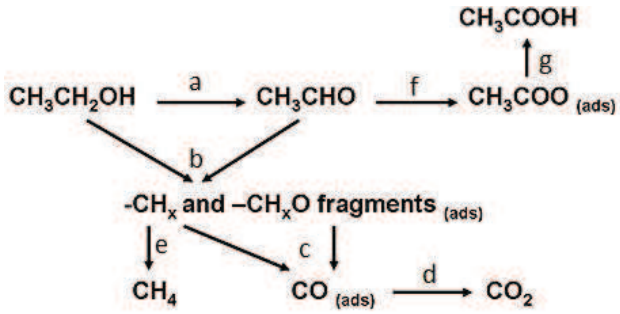

Fig. 3.3 | Schematic representation of the reaction pathways of DEFCs using platinum in acidic media, reprinted from Ref. [34]

As can be seen in Figure 3.3, the formation of acetaldehyde occurs in step (a) from the dehydrogenation of ethanol, and both adsorbed ethanol and acetaldehyde experience the cleavage of the C–C bond, generating surface-adsorbed $–CH_x$ and $–CH_xO$ fragments in step (b). These fragments may oxidize to generate adsorbed CO, as can be seen in step

(c), and as long as the electrode potential is higher than 0.4 V this is further oxidized to CO_2 in step (d) [34]. However, the reaction not always follows this path and, as can be seen in step (e), the adsorbed $–CH_x$ may be reduced to CH_4 which then desorbs from the surface and is dissolved in the bulk electrolyte. Moreover, when the C–C bond is not broken, acetaldehyde may oxidize to adsorbed acetate in step (f), followed by conversion to acetic acid in step (g) [34].

It is strongly expected that these products affect the total cell performance of DEFCs, since a considerable loss of the available energy occurs when the ethanol molecule is oxidized to acetaldehyde or acetic acid [33, 37]. Moreover, when used in acidic media Pt is vulnerable to poisoning by CO adsorbing species [105-108], and experiences a self-inhibition phenomenon, especially in the steady state operation mode [105].

An ideal catalyst for ethanol oxidation should accomplish the cleavage of acetaldehyde C–H bonds followed by the cleavage of C–C bond and subsequent oxidation of intermediates to CO_2 in the presence of adsorbed OH [116].

Efforts to mitigate these issues have been concentrated on the addition of co-catalysts, and it is known that all the additives can promote the electro-catalytic activity of platinum towards ethanol oxidation [13, 18]. The analysis of the literature review further indicate that ruthenium (Ru) and tin (Sn), as well as the binary Pt–Ru and Pt–Sn [105-118] and the correlated ternary Pt–Ru–based and Pt–Sn–based catalysts [103, 119-124], are the most commonly used.

The advanced performance of binary and ternary catalysts for the ethanol oxidation is mainly attributed to the bifunctional effect [107, 125] and to the electronic interaction between Pt and other alloyed metals [125].

According to the bifunctional mechanism [107], the electro-oxidation of strongly adsorbed species is facilitated by the presence of Ru or Sn, since these alloys activate water molecules and provide preferential sites for OH adsorption at lower potentials. The abundance of OH_{ads} species enhances the complete oxidation of poisoning intermediates to CO_2 [15, 107]. Additionally, it has been verified that these alloys modify the electronic structure of Pt, enhancing the mechanism of adsorption of oxygen-containing species [125].

It is well known that Pt–Ru materials are good catalysts for methanol oxidation [125], and several researchers have employed Pt–Ru as catalyst on the anode of passive DMFCs [61-70, 79-90]. Moreover, it has been reported that the oxidation of adsorbed CO species with a Pt–Ru electrode occurred at potentials at least 200 mV below those observed with pure platinum [15]. Therefore, several researchers investigated this catalyst concerning the electro-oxidation of ethanol in DEFCs [105-108, 110-114, 126], and many studies indicated that cells with carbon supported Pt–Ru as anode material achieve better performances than those using pure carbon supported Pt [107, 112-114, 126].

Lee et al. [113] investigated the ethanol electro-oxidation at carbon supported Pt and Pt–Ru anode catalysts and observed that the cell current increase doubles when using Pt–

Ru/C for temperatures in the range of 25 – 80°C, compared to Pt/C. According to the authors [113], the addition of Ru promotes the dehydrogenation mechanism, and generates higher currents due to the bifunctional effect. Liu et al. [114] used a microwave-assisted polyol process to prepare nano-sized Pt and Pt–Ru colloids, and investigated the electro-oxidation of liquid ethanol on these catalysts at room temperature by cyclic voltammetry. The results demonstrated that the alloy catalysts were more active than pure Pt, suggesting that Ru facilitates the oxidation of freshly chemisorbed species and display an enhanced activity for ethanol electro-oxidation [114]. The authors proposed the following mechanism for the ethanol reaction in the presence of Ru catalysts:

$$Pt–Ru–OH_{ads}+Pt–Ru=C=O \rightarrow 2Pt–Ru+CO_2+H^+ +e^- \quad (3.11)$$

$$2Pt–Ru–OH_{ads}+(CH_3–COOH)_{ads} \rightarrow 2Pt–Ru+2CO_2+6H^+ +6e^- \quad (3.12)$$

Moreover, preliminary tests on a single DEFC indicated that the Pt–Ru/C anode catalyst with a molar ratio of 52:48 was the best electrocatalyst at an operating temperature of 80°C [114], achieving an open circuit voltage (OCV) of 830 mV and a maximum power density of 60 mW cm^{-2} for a current density of 130 mA cm^{-2}. These results are much higher than those determined by Zhou et al. [106] for DEFCs at 90°C, where the OCV was 680 mV and the peak power densities was only 28 mW cm^{-2} for a current density of 130 mA cm^{-2}, using Pt–Ru/C with a lower molar ratio (20:10).

The influence of Pt–Ru atomic composition on the yields of ethanol oxidation was also investigated by Camara et al. [112]. The authors reported the existence of a promoting effect favoring the pathway forming CO_2 with increasing concentrations of Ru up to an optimum Pt:Ru atom ratio of 3:2. It was also verified that the yield of CO_2 was much lower than that of the sum of acetic acid and acetaldehyde, and thus the main effect of increasing Ru was reflected in the production of acetic acid [112]. This was explained as being due to two opposite effects of Ru, namely the positive effect favoring CO oxidation, and the negative effect on inhibiting ethanol adsorption [112]. The reaction kinetics and the product distribution at the anode of DEFCs was also examined by Nakagawa et al. [120] at 80°C using both Pt and Pt–Ru catalysts. The authors found that the addition of Ru increased the power density and the cell current when compared to pure Pt, however it also decreased the rate of conversion of acetaldehyde to CO_2, as well as the selectivity for CO_2 [120]. These results indicate that Pt–Ru catalysts have a poor activity concerning the cleavage of the C–C bond [112, 120]. Similarly, other studies supported that although the addition of Ruthenium increased the catalytic activity, it was not capable of enhancing the C–C bond cleavage [12, 113].

Several studies point toward the addition of tin to enhance the activity of Pt, especially in acidic media, showing better single DEFC performance than the ones with pure Pt or

binary Pt–Ru catalysts [20, 105-107]. Moreover, the addition of Sn has been proved to favor the C–C bond cleavage and to prevent CO poisoning [105-108].

Zhou et al. [106] investigated the performance of direct alcohol fuel cells at 90°C by using carbon supported Pt, Pt–Ru and Pt–Sn as anode catalysts, and stated that single Pt lead to poor performances even when using high catalyst loadings. According to the authors [106], the addition of Ru or Sn would dramatically enhance the electro-oxidation of alcohols, and Pt–Sn was more suitable for ethanol achieving an OCV of 810 mV and peak power density of 52 mW cm^{-2}. Additionally, it was observed that CO_2 was one of the main products of DEFCs with Pt–Sn/C showing higher productivity than with Pt–Ru/C [106]. Accordingly, Li and Pickup [20] examined the performance of DEFCs operating under low temperatures (80°C) with different anode catalysts, and verified that cells with Pt–Sn or Pt–Ru had much higher performances than cells with single Pt, indicating higher catalytic activities for ethanol oxidation. Moreover, the cell with Pt–Sn as anode catalyst showed the best performance, but the power density was lower than the one found in the literature due to the use of air as oxidant [20].

The influence of the Sn content in Pt–Sn catalysts was also investigated, and controversial results have been reported concerning the performance of DEFCs.

Purgato et al. [115] synthesized carbon-supported Pt-based catalysts for ethanol oxidation at low temperatures (90°C) by the method of thermal decomposition. The best results were obtained for Pt–Sn/C with a molar ratio of 80:20, reaching an OCV of 750 mV and a power density of 37 mW cm^{-2} at 90 mA cm^{-2} [115]. Simões et al. [116] evaluated the catalytic activity of various compositions of Pt–Sn electrodes prepared by thermal decomposition for ethanol electro-oxidation, and stated that the presence of tin was necessary to activate the catalyst and convert CO to CO_2 at lower potentials than those observed for single Pt catalysts. According to the electrochemical characterization by cyclic voltammetry and chronoamperometry, the authors [116] found that Pt–Sn 60:40 is the best catalyst for ethanol oxidation. However, Pt–Sn 90:10 exhibited the highest catalytic activity, with an open circuit voltage (OCV) of 810 mV and a power density of 72 mW cm^{-2} at 160 mA cm^{-2}. Furthermore, the research group of Zhou [108, 109] performed a detailed investigation of the effect of Sn content in the Pt–Sn alloy catalysts, and found that Pt–Sn/C electro-catalysts with Pt:Sn molar ratios of 66:33, 60:40 and 50:50 are more active than electro-catalysts with 75:25 and 80:20 molar ratios, with the optimum composition in the range of 33 – 40 at.%, depending on DEFC operation temperature. According to the authors [108, 109], the higher content of Sn could lead to an increased content of Sn oxide, affecting negatively the anode electronic conductivity.

Spinacé et al. [117] investigated the effect on DEFCs of Pt–Sn/C electro-catalysts prepared by different methods and concluded that besides the atomic ratio, the performance of Pt–Sn/C electro-catalysts also depends on the preparation procedure. The activity of Pt–Sn/C (2:1) catalysts prepared using different methods was also investigated by Song et al. [105] for ethanol oxidation. The research group [105] prepared carbon supported Pt–Sn

catalysts by deposition of Sn on preformed Pt/C (Pt–Sn/C-a), and also using the polyol method (Pt–Sn/C-b). The results indicated that the behavior of both cells was similar for low current densities, but when increasing the current density the performance of the cell with Pt–Sn/C-a decreases. According to the authors [105], this could be attributed to a higher content of Sn oxide in Pt–Sn/C-a, leading to a higher internal cell resistance and consequently affecting the cell performance. Additionally, the efficiency of these catalysts was compared to that of Pt–Ru/C (1:1) catalysts as anode materials, and it was found that both cells using Pt–Sn/C catalysts have better performances than the ones with commercial and in-house prepared Pt–Ru/C [105].

Based on previous studies by the research group of Song [13], the authors proposed a possible mechanism for ethanol electro-oxidation over Pt–Sn catalysts, and it is schematically presented in Figure 3.4. The adsorption and decomposition of ethanol and its intermediate reaction products happen on Pt active sites, while the dissociative adsorption of water occurs over Sn sites to form oxygen-containing surface species. The bifunctional role of Pt and Sn is manifested in the steps marked with a gray star, as is shown in Figure 3.4.

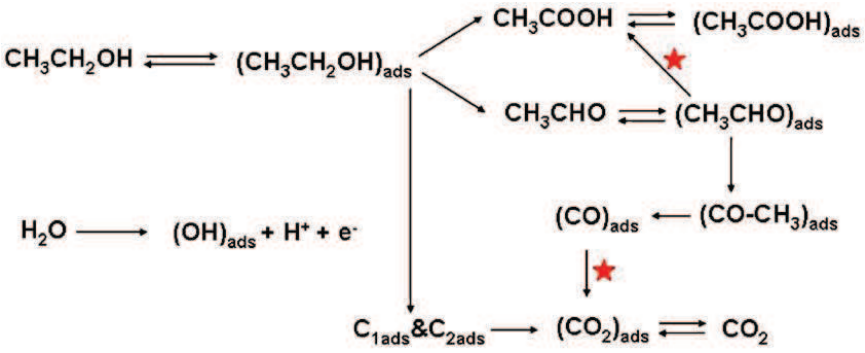

Fig. 3.4 | Schematic representation of ethanol electro-oxidation using Pt-Sn catalysts, reprinted from Ref. [13]

Other binary catalysts have been investigated for the ethanol oxidation reaction (EOR), and generally these catalysts presented an EOR activity higher than that with Pt but lower than that with Pt–Ru and Pt–Sn [107].

Attempting to identify the suitable electro-catalysts for ethanol oxidation, Zhou et al. [107] studied and tested several Pt-based binary and ternary metallic anode catalysts in single direct ethanol fuel cells at lower temperatures in order to identify the most appropriate. The results are shown in Figure 3.5, and it is clear that tin, ruthenium and wolfram (W) are the best additives, affecting the activity of ethanol electro-oxidation in the following sequence: Pt–Sn/C > Pt–Ru/C > Pt–W/C > Pt–Pd/C > Pt/C. The single cell test demonstrated that, from a practical point of view, Pt/C and Pt–Pd/C do not seem to be good catalysts for ethanol oxidation, while W and Ru can dramatically enhance the activity of Pt due to the so-called synergetic effect. Moreover, the authors stated that the addition of W and molybdenum (Mo) to the bimetallic catalyst Pt–Ru could improve its

activity. Although the trimetallic Pt–Ru–W and Pt–Ru–Mo catalysts showed excellent behavior toward ethanol electro-oxidation, it would still be lower to that with Pt–Sn/C, which is evidently the most suitable bimetallic catalyst for DEFCs [107].
The addition of Mo to bimetallic Pt–Ru/C and Pt–Sn/C was also investigated by Neto et al. [127] and Lee et al. [128], respectively, and both studies indicated that the ternary catalysts show better performance than the bimetallic catalysts, being very promising anode catalysts for DEFCs. Other catalyst mixtures using three additives instead of single or binary catalysts have been recently studied, mainly using metals as nickel (Ni) [119], lead (Pb) [126], iridium (Ir) [122], rhenium (Re) [123, 124], and rhodium (Rh) [120, 121].

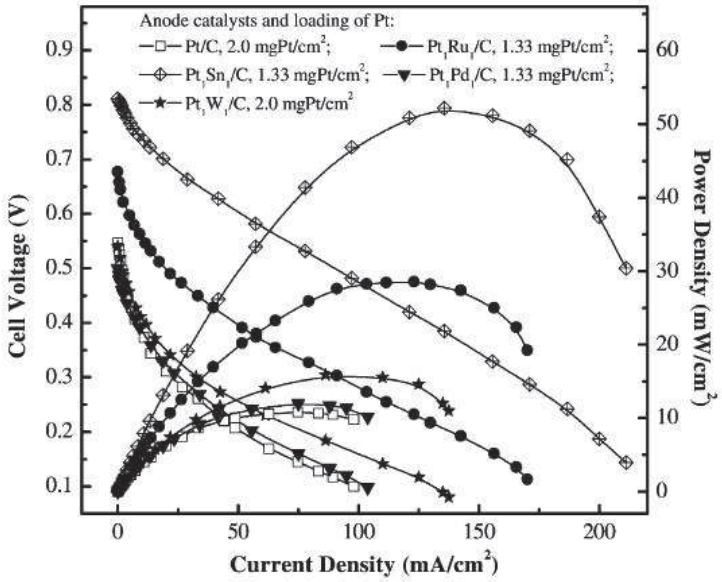

Fig. 3.5 | Polarization curves and power density curves in single active DEFC at 90°C. Electrolyte: Nafion™ 115 membrane. Anode: ethanol solution: 1.0 M; flow rate: 1.0 ml min^{-1}. Cathode: Pt/C 1.0 mg cm^{-2} Reprinted from Ref. [107]

Ribadeneira [119] conducted an experimental comparison of Pt–Ru, Pt–Sn, Pt–Ru–Sn, Pt–Ru–Ni and Pt–Sn–Ni electro-catalytic mixtures to determine the most suitable catalytic mixture for use in DEFCs, and the results show that the current generated by Pt–Ru and Pt–Sn mixtures was similar, in opposition to what was found in other studies [105-107]. The current used to reach a voltage of 200 mV was evaluated in each fuel cell, and the results obtained are shown in Figure 3.6. It is clear that the addition of Ni significantly improved the cell performance, with trimetallic catalytic mixtures producing higher currents relative to bimetallic catalysts. On the other hand, the cell performance depends much on the variations in the atomic ratio and Pt–Ru–Ni/C (75:15:10) demonstrates higher efficiency when compared to other catalysts in the anode [119].

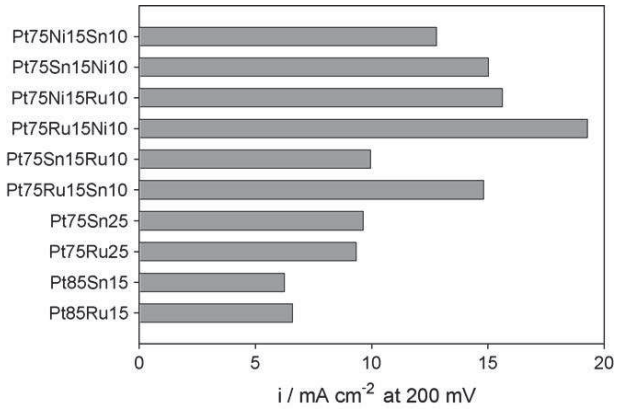

Fig. 3.6 | Performance of single DEFCs for different anode catalysts at 200 mV and 80°C. Ethanol solution: 1.0 M; flow rate: 2.0 ml min^{-1}. Reprinted from Ref. [119]

The same trend was verified using trimetallic mixtures with other alloys. Li and Pickup [126], investigated the addition of Pb to Pt and Pt–Ru and found that after addition of Pb, the catalytic activity of Pt and Pt–Ru for ethanol oxidation increased, especially at high potentials. Tayal et al. [122] tested different combinations of bimetallic and trimetallic Pt, Sn and Ir as anode catalysts in DEFCs, and revealed that the addition of small amounts of Ir to Pt–Sn/C catalysts resulted in higher electro-catalytic activity. The same authors tested binary and ternary Pt based catalysts with addition of Sn and Re, and verified that Re enhances the breaking of C–C bond. The trimetallic combination of Pt–Sn–Re/C (20:15:5) showed a higher activity towards ethanol electro-oxidation than the bimetallic combinations of Pt–Sn/C (20:20) and Pt–Re/C (20:20) [124]. This finding was supported by Goel and Basu [123], who studied the performance of a DEFC for different compositions of Pt–Sn–Re /C catalysts.

The use of rhodium in anode bimetallic Pt–Rh electrodes for ethanol oxidation was also shown to improve the CO_2 yield when compared to pure platinum electrodes [18]. However, Nakagawa et al. [120] investigated the effects of Rh addition to Pt–Ru on the product distribution and the electro-oxidation mechanism in DEFCs, and stated that although Pt–Ru–Rh/C showed higher current density than Pt–Ru/C, the addition of Rh decreased the selectivity for CO_2. Neto et al. [121] also investigated Rh addition to Pt and Pt–Sn catalysts, and concluded that Pt–Sn–Rh/C generated a higher current density than those with Pt–Rh/C and commercial Pt–Ru/C, however Pt–Sn/C proved to be more efficient than the ternary mixtures.

In summary, all ternary Pt–Ru-based catalysts tested for the ethanol oxidation perform better than the bimetallic Pt–Ru, however the bimetallic Pt–Sn or other Pt–Sn–based catalysts have been reported to be more efficient, and seem to be the most promising anode materials for DEFCs [105-107, 121-124].

Concerning the cathode, the catalyst material must accomplish properties such as high activity for the oxygen reduction reaction and high ethanol tolerance. The literature review revealed a wide consensus on the use of carbon supported Pt catalysts [13, 15-19].

Moreover, it has been reported that the oxygen reduction kinetics on Pt electro-catalyst is excellent when compared to ethanol electro-oxidation on Pt based electro-catalysts [58].

Andreadis et al. [17] investigated the effect of the catalyst loading on the cathode in the range of 0.2 – 1.0 mg Pt cm^{-2}, and found that an increase of the Pt loading leads to higher values of the specific reaction surface area, resulting in better cell performances.

However, at the cathode, ethanol and oxygen adsorption compete for available surface sites as a result of ethanol crossover, and thus it has been suggested that the addition of a second metal to Pt could enhance the oxygen reduction reaction [18]. In fact, in the temperature range of 60 – 100°C single DEFCs proved to have better performances using Pt–Co/C as cathode catalyst [18]. Additionally, Lopes et al. [129] studied the influence of palladium (Pd) addition to Pt catalysts, and found that it could also enhance DEFCs performance, since Pt–Pd/C catalysts present higher ethanol tolerance than Pt in case of fuel crossover. Furthermore, in order to circumvent the effect of fuel crossover through the membrane, Lamy et al. [15] suggested the replacement of the Pt catalysts by transition metal compounds such as macrocycles or chalcogenides. Although this would also help to avoid the platinum cathode depolarization, these compounds are unstable in strong oxidizing environments under medium temperatures (60 – 100°C), and thus their utility is still dubious.

3.5. Mass Transport Phenomena

As been aforementioned, in order to produce electricity, the direct ethanol fuel cell must be continually supplied with ethanol and oxygen. Analogously, to ensure the continuity and stabilization of the DEFC the products formed must be continuously removed, to avoid poisoning the cell. These processes of supplying reactants and removing products are accomplished by mass transport phenomena, and these apparently simple tasks can turn out to be dramatically complex mainly due to poor mass transport which leads to significant losses in fuel cell performances [10, 38].

3.5.1. Ethanol Crossover

A common challenge for direct ethanol fuel cells relies on fuel crossover, where the fuel fed to the anode compartment permeates through the electrolyte to the cathode, leading to a mixed potential on the cathode side with a consequent decrease on the cell performance [24-28]. The research group of Song [28] investigated the consequences of crossover in DAFCs and found that ethanol exhibits lower crossover rates than methanol, possibly due to its larger molecular size. As a result, it has a lower effect on the cathode performance, due to its lower permeability, and also slower electrochemical oxidation kinetics over Pt/C. However, when ethanol permeates through the membrane to the

cathode, one of the major consequences for the fuel cell is the fuel loss, which otherwise would be used to produce electricity [27]. Instead, ethanol crossover generates poisoning products such as CO_2, acetaldehyde and acetic acid in the cathode catalyst layer, inducing the competition with oxygen at the cathode and creating a mixed potential that leads to higher overpotentials [25, 27].

Several studies were performed to analyze ethanol crossover in DEFCs, and it was found that the ethanol crossover rate is mainly dependent on the ethanol feed concentration, membrane thickness, current densities, and cell operating temperature [20, 24-29]. Song et al. studied the ethanol crossover on DEFCs using a Nafion™ 115 membrane, and observed that the crossover rate is positively influenced by the temperature. According to the authors [29], this is probably due to the fact that at higher temperatures the kinetics of the reaction is accelerated, and furthermore the polymer backbone expands due to a softening of the fluorinated chain, leading to higher ethanol permeation rates as well as higher water transport rates. Additionally, the authors [29] verified that the crossover rate also increases with the ethanol concentration, and stated that the permeation of water and ethanol through Nafion™ membranes takes place under the driving forces of concentration and pressure gradients. The ethanol crossover in DEFCs was also investigated by Andreadis and Tsiakaras [24], who found a linear relationship between ethanol crossover rate and ethanol feed concentration, until a maximum ethanol concentration of 8.0 M. Moreover, the authors [24] pointed out that the combined effect of low current density values and highly concentrated ethanol solutions enhances the crossover rate. This fact was also confirmed in recent studies by Suresh and Jayanti [27], who verified that the crossover flux was enhanced by the electro-osmotic drag as the current density increases, considering ethanol concentrations above 2.0 M. On the other hand, considering concentrations below 1.0 M the crossover decreases with an increase of the current density, becoming null at limiting current densities [27]. According to the authors [27], the electro-osmotic drag of ethanol is small at such low concentrations, since the consumption of ethanol makes it less available for crossover flux.

Li and Pickup [20] observed that ethanol crossover rates increase dramatically with an increase of concentration and temperature. However, they were much lower if the membrane thickness was augmented. According to the authors [20], the crossover would be reduced by half with a Nafion™ 117 membrane when compared to Nafion™ 115, for the same ethanol concentration (1.0 M). Song et al. [26] went further and analyzed the effect of the membrane electrode assembly preparation procedure on both ethanol crossover and DEFC performance recurring to distinct MEAs prepared by the conventional and the decal transfer methods. The authors [26] found that the ethanol crossover current density was almost 1.5 times higher in the decal transfer method electrode than with the conventional MEA for all the temperatures studied, indicating an obvious effect of the electrode preparation procedure on ethanol crossover and DEFC performance.

Although the use of diluted ethanol solutions could avoid the fuel crossover, it would also cause specific energy losses in the DEFC system, and thus the main approach to solve this problem is to improve the MEAs used in DEFCs. Wan et al. [30] made efforts to mitigate the ethanol crossover in DEFCs by fabricating a composite anode comprising an inner catalyst layer of Pt–Sn nanoparticles. This layer, directly deposited on the Nafion™ membrane surface, served both as ethanol filter and electrode, and proved to reduce the ethanol crossover and to improve the cell performance [30].
Other attempts to modify or adopt new electrolyte materials to avoid or at least decrease ethanol crossover have been reported in the last years [53-55]. Hybrid membranes composed of PVA have been proved to reduce ethanol permeabilities of about two orders of magnitude when compared to Nafion™ 117 [53]. Maab and Nunes [54] prepared sPEEK membranes from two classes of materials, one of them based on sPEEK coated with carbon molecular sieves, and another based on sPEEK/polyimide blends. Both approaches led to a substantial reduction of ethanol crossover through the membranes, when compared to plain sPEEK or to Nafion™ 117 membranes. Particularly in DEFC experiments performed at 90°C, the sPEEK/polyimide membranes had an effective reduction of ethanol crossover [54].

3.5.2. Water Management

In direct ethanol fuel cells there are two major sources of water, one of them resulting from the aqueous dilution of ethanol at the anode, and the other arising from the oxygen reduction reaction at the cathode. The water crossover occurring through the membrane generally results from the effect of the electro-osmotic drag caused by proton transport through the electrolyte, and the diffusion phenomenon caused by water concentration gradients from the anode to the cathode [21, 47].
The water management concerning DEFCs is detrimental to enhance the fuel cell performance and durability, especially due to the most commonly used type of membranes in DEFCs, the Nafion™ membranes. As been aforementioned, the Nafion™ membranes require a certain level of hydration in order to achieve acceptable proton conductivity. Once the membrane is deprived of the necessary hydration, an increase in the electrical resistance may occur, followed by consequent heating and enlargement of the ohmic losses [21]. The local heating is additionally prejudicial for the membrane since it may increase the local dryness of the membrane and induce further water evaporation, limiting the membrane lifetime and the cell durability.
In a conventional DEFC fed with a dilute ethanol solution, the water supply from the aqueous solution at the anode reservoir should easily hydrate the electrolyte membrane and fully provide water for the anode reaction. Nevertheless, another problem of water management relates to the water balance within the electrolyte, since in practice some

parts of the membrane may be correctly hydrated, but others may be too dry or even flooded [47, 80].

Due to the aforementioned, the water management in fuel cells, and especially in passive feed systems, is still of major concern to assure the water removal from the cathode preventing its flooding, and to keep good water content in the anode avoiding an increase on proton conductive resistance. Although the work on water management in passive DMFCs is quite extensive [80-83], the same for DEFCs is insufficient. The water management issue was intensively studied by Oliveira et al. concerning both active DMFCs [41, 45-47] and passive DMFCs [5, 80]. The authors [5] developed a semi-analytical 1D model considering coupled heat and mass transfer, along with the electrochemical reactions occurring in a passive DMFC. This model was used to predict the concentration profiles along the cell and it was shown that both water and fuel crossover could be lowered by decreasing the fuel concentration and increasing the membrane thickness, the anode diffusion layer thickness and the catalyst layers thicknesses [80]. Based on these results, the authors [80] proposed a tailored MEA using a Nafion™ 212 membrane to reduce ohmic losses, thick anode diffusion and catalyst layers to reduce fuel and water crossover, and a thicker cathode catalyst layer to enhance oxygen reduction. The water management was also investigated by Li et al. [83] concerning semi-passive DMFCs fed with concentrated methanol solutions, and it was verified that the water crossover is positively dependent on the water content in the feeding solution, but also on the current density. According to the authors [83], the water back flow from the cathode to the anode is crucial to hydrate the electrolyte and to provide lower membrane resistance when operating at higher current densities.

Although no work was found concerning the water management in passive feed DEFCs, the continuous flow field design emerges as one of the water management approaches applied to active feed DEFCs. Pramanik and Basu [58] investigated the use of serpentine flow channels in active feed DEFCs, and verified that these were able to control the humidity within the fuel cell. Belchor et al. [130] also made an attempt to improve the water management in fuel cells operating with low water content by comparing a parallel serpentine-baffle flow field design (PSBFFP) design and a parallel serpentine flow field (PSFFP). According to the authors [130], the fuel cell fitted with the PSBFFP presented better performances under low humidity, since this could retain the water within the channels.

Recently, Nowak et al. [131] attempted to improve the water management in fuel cells by developing electrically conductive and hydrophilic coatings for stainless steel bipolar plates, in order to minimize voltage losses and facilitate the liquid water transport in plate channels. The coatings were based on a multifunctional silane mixed with conductive carbon composite, and exhibited promising results by displaying long term wetting behavior under realistic fuel cell testing conditions [131].

3.6. Operating Conditions

Published work has shown that the direct ethanol fuel cell performance is significantly affected by the employed operating conditions [16-20, 26-29]. Issues as the catalyst loading, temperature and ethanol concentration were found to have great influence on the ethanol crossover rate and on the cell performance in general, and thus they were studied by many authors.

3.6.1. Ethanol Concentration

The effect of ethanol concentration on ethanol crossover and membrane porosity was investigated by the group of Song et al. [26, 28, 29] using a Nafion™ 115 membrane and Pt–Ru as anode catalyst. The authors concluded that Nafion™ membranes have an increased swelling degree with the ethanol concentration increment, showing a negative effect on the electrode structure [26, 28]. This occurrence leads to a higher ethanol crossover through the membrane, which increases as the ethanol concentration is increased above 1.0 M [28, 29]. This fact was supported by Li and Pickup [20], who observed that ethanol crossover rates increase dramatically with an increase of ethanol concentration.

Alzate et al. [16] also studied the effect of the ethanol concentration on the performance of DEFCs, and found that the different regions in the polarization curve have different dependences on the ethanol concentration. Both, the OCV and the fuel cell performance in the kinetic region increase with decreasing ethanol concentration, while in the mass transfer region the performance of the fuel cell increases with increasing ethanol concentration up to 2.0 M. At very low ethanol concentration the performance suddenly drops due to mass transfer limitations [16]. Additionally, Andreadis et al. [17] found that the increase of the ethanol feed concentration from 0.25 M to 1.0 M improves both the cell discharge behavior and the cell power density. However, by further increasing the ethanol feed concentration up to 4.0 M the cell performance as well as the cell power density decrease. This is due to the fact that higher ethanol feed concentrations lead to higher ethanol crossover rates, which are directly related to higher parasitic current generation [17].

Heysiattalab et al. [19] also investigated the performance of DEFCs using different ethanol concentrations, and found that the augmentation of ethanol concentration increases the reaction rate and enhances the diffusion phenomena rate. The authors [19] stated that when the ethanol concentration is low, the concentration losses are augmented because proper amounts of ethanol do not reach the catalyst layers.

3.6.2. Fuel Cell Temperature

Heysiattalab et al. [19] investigated the influence of temperature on the efficiency of DEFCs and verified that the fuel cell performance increases with temperature considering the entire polarization curve. Based on their experimental studies, it was concluded that temperature has an important effect in fuel cell performance since it increases the reaction rate, the diffusion phenomena rate and the conductivity of the membrane [19].
These findings are in agreement with the results of Li and Pickup [20], who found that the anode performance was markedly improved at higher operating temperatures, mainly due to the increase of the ethanol oxidation and mass transport rates.
Song et al. [29] also investigated the operating temperature effect on the performance of DEFCs, and found that increasing the temperature can accelerate the ethanol oxidation kinetics and improve the single DEFC performance. However, according to the authors [29], increasing the temperature can also lead to a higher ethanol crossover rate, affecting negatively the DEFC performance. This may counteract the positive effect of temperature on the DEFC performance to some extent [29].
The research group of Song et al. [36] also investigated the maximum conversion of ethanol in DEFCs for temperatures in a range of 0 – 300°C, and the results are presented in Figure 3.7. The group found that the maximum conversion of ethanol concerning the desired reaction (3) is less than 14% for temperatures below 100°C, and considerably lower than 2.5% for temperatures close to ambient conditions, which consequently leads to lower fuel cell efficiencies [36].

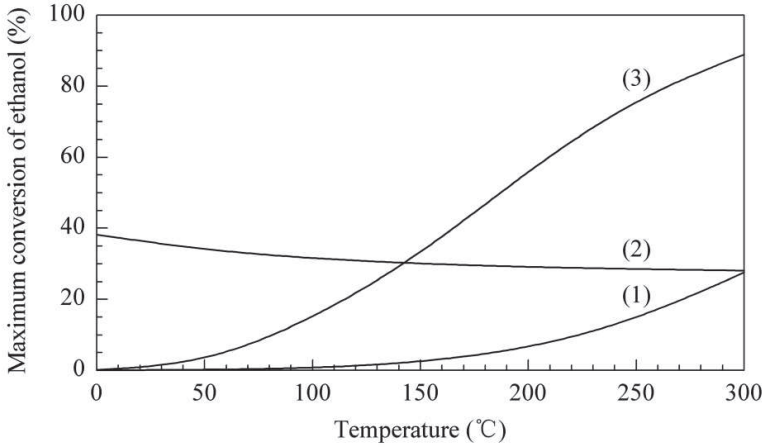

Fig. 3.7 | Maximum conversion of ethanol at different temperatures, reprinted from Ref. [36]

(1) $CH_3CH_2OH \rightarrow CH_3CHO+H_2$

(2) $CH_3CH_2OH+H_2O \rightarrow CH_3COOH+2H_2$

(3) $CH_3CH_2OH+3H_2O \rightarrow 2CO_2+6H_2$

3.6.3. Catalyst Loading

Few studies were found concerning the effect of the catalyst loading on the DEFCs performance. Andreadis et al. [17] investigated the effect of the anode and cathode catalyst loadings on the fuel cell performance using Platinum on both sides, and found that an increase of the Pt loading leads to higher values of the specific reaction surface area, resulting in better cell performance. According to the model predictions, an increase of the anode catalyst loading compared to an equal one of the cathode catalyst loading has greater impact on the cell power density [17]. This is explained due to the fact that the ethanol electro-oxidation reaction over the anode catalyst layer is much slower than the oxygen reduction reaction over the cathode catalyst layer. As a consequence, a higher anode specific reaction surface area has more significant effect on the cell operation compared to a higher cathode specific reaction surface area [17].

3.7. Mathematical Modeling

Mathematical modeling is essential for the development of fuel cells because it allows an extensive comprehension of the parameters that affect the fuel cell performance. Nowadays, with the available computational power, the model simulations are getting more complex, including a high level of details directly related to the basic fuel cell modeling features and to the simplifications and assumptions that are usually made by the authors. It is important to understand all the assumptions made, in order to recognize the limitations and to accurately interpret the results provided by each model. The majority of the fuel cell models aims to describe the interactions occurring among the several physical and electrochemical phenomena within the different layers of the cell, and many studies were performed for DEFCs [17, 24, 27, 56-60].

Meyer et al. [57] developed a one-dimensional mathematical model for a DEFC where the electrochemical oxidation of ethanol in the catalyst layers is described by several reaction steps. The authors [57] assume a bifunctional reaction mechanism for the activation of water on a binary catalyst, and the chemical reactions are coupled with the charge and reactant transport. Additionally, the model accounts for the crossover of the reactants through the membrane, leading to the phenomenon of anode and cathode mixed potentials due to the parasitic oxidation of ethanol and reduction of oxygen, respectively [57]. Although this is a very interesting approach, the model still needs to be validated with further experimental data.

Pramanik and Basu [58] worked on a mathematical model for DEFCs considering the effect of the distinct overpotentials. In this model, the activation overpotential term is formulated considering the Butler–Volmer equation, and the ohmic overpotential is modeled based on the proton conductivity of Nafion™ membrane and ohmic losses at the electrodes, current collectors and electrode-current collector interfaces. Furthermore,

the concentration overpotential is formulated using Fick's law, the modified Butler–Volmer equation and transport process through the electrodes and electro-catalyst layers. Using this model, the authors [58] were able to predict the experimental data on current-voltage with reasonable agreement considering temperatures in the range of 40 – 60°C.

Andreadis and Tsiakaras [24] reported a simple 1D, steady-state and single phase mathematical model with the purpose of describing the mass transport and the performance of a DEFC. The model was implemented in FORTRAN language, assuming steady-state isothermal conditions and atmospheric pressure conditions in both anode and cathode compartments. The ethanol transport in the diffusion layer is a combination of diffusion and convection, while in the catalyst layer the ethanol oxidation is described by the Tafel equation. For the sake of simplification, the water transport through the membrane was based on the assumption that both anode and cathode are fully hydrated. The authors [24] used this model to predict the effect of operating parameters on the cell performance, and found a relatively good agreement between theory and experimental results related to both ethanol crossover rates and DEFC performance, considering operating temperatures of 75 and 90°C.

Suresh and Jayanti [27] proposed a comprehensive 1D, single phase, isothermal model for a DEFC, taking into account the mass transport and electrochemical phenomena on both anode and cathode sides. Tafel equation was used to describe the electrochemical oxidation of ethanol at the anode and the simultaneous ethanol oxidation and oxygen reduction reaction at the cathode, and the model fully accounts for the mixed potential effect caused by ethanol crossover at the cathode. Although the model is validated using very limited data from the literature, it predicts reasonably well the limiting current and the polarization behavior for different cell parameters, as well as the effect of key operating parameters on ethanol crossover and cathode overpotential [27].

Specific modeling and simulation of the anode in DEFCs was also investigated as an attempt to better understand the anodic process [56, 60]. Andreadis et al. [56] developed a mathematical model that explained in one phase and one dimension the ethanol mass transport throughout the anode compartment and proton exchange membrane. The cell operates under steady-state and atmospheric pressure conditions, and the driving force for both water and ethanol transport through the catalyst layer consists on the diffusion and the electro-osmotic drag. The effect of main parameters such as current density, temperature and ethanol concentration on both ethanol crossover and anode overpotential were investigated, and the authors found a good agreement between the simulated and experimental results for a temperature range of 30 – 75°C [56]. Sousa Jr. et al. [60] proposed a mechanistic model that could supply details of the physical system, such as the concentration profiles of the various intermediates generated in the anode and the coverage of the adsorbed species on the electrode surface, as well as the anode overpotential-current relationship. This model uses the Navier–Stokes equations for fluid

flow and the Darcy's Law for porous media flow, and the heat transfer is modeled considering diffusion, convection and conduction. For the cathode, a standard model is used. The simulations were performed using the software Comsol Multiphysics®, an interactive environment for modeling scientific and engineering systems based on partial differential equations, and the authors obtained a good agreement between model predictions and experimental results [60].

Any modeling studies were found in the literature for passive feed DEFCs. However, very interesting mathematical models exist for passive feed DMFCs, namely considering the heat transfer effect [5, 71, 80].

Chen and Zhao [71] developed a 1D model coupling heat and mass transport along with the electrochemical reactions occurring in a passive DMFC. In order to simplify the complex heat and mass transport processes, the authors introduced several simplifications and assumptions, and developed the analytical solutions for methanol and oxygen concentrations, as well as temperature distributions through the cell layers. From the predictions of the model, the authors concluded that the thermal management in passive DMFCs is critical to improve the cell performance [71]. The research group of Oliveira et al. [5, 80] also developed a 1D, steady state and non-isothermal model to simulate the operation of a passive DMFC. The model can be used to predict the methanol, oxygen and water concentration profiles in the anode, cathode and membrane as well as to estimate the methanol and water crossover and the temperature profile across the cell. Due to its simplicity, the model is rapidly implemented and can be easily used to optimize the cell performance by studying the impact of design parameters such as membrane thickness, catalyst loading and diffusion layer material and thickness. Using this model, the authors [5] successfully predicted the influence of the methanol feed concentration on the cell performance and the correct trends of the current density and methanol feed concentration on methanol and water crossover. Additionally, the authors used this model to deeply investigate the effect of different design and operating parameters on water management and on the performance of passive DMFCs [80].

3.8. Applications

Although direct ethanol fuel cells are still new in the market, they already proved to have the capability to assume an important role as one of the green energy sources in the new era. Like the other types of fuel cells, DEFC technology is a great source of clean alternative energy with the advantage of using a liquid fuel, which excludes the need of a fuel reformer and easily reduces the size and weight of the system. Furthermore, the use of a biodegradable fuel such as ethanol will prevent the environment from the pollution caused by the dumping of other types of fuels.

Nowadays fuel cells are used in stationary applications, providing primary or backup power to small communities. Using fuel cell technology for the electrical needs can reduce energy costs by 20% to 40% over the conventional energy services, which makes them perfect to be used in power generation. Moreover, fuel cell technology can help to provide electrical power and ensure the energy supply to critical areas where the electric grid is insufficient. Also, fuel cell technology can be used in generators to provide hot water and heating for residential use.

Nowadays, these revolutionary devices are also applied in various transport modes such as scooters, buses and even trains. In the Shell Eco Marathon University of Offerburg in 2007, a DEFC powered vehicle was used and its demonstration was considered quite impressive due to its practicality.

However, the main advantage of DEFCs is that they can be applied wherever a battery is needed, especially in the area of portable power tools, such as mobile phones, laptops, PDAs, pagers, video recorders, and also low power remote devices, such as hearing aids, domestic alarms, smoke detectors and hotel locks, with the advantage of providing energy for longer time than regular batteries. NDC Power created the EOS Direct Ethanol Fuel Cell, a device that works on ethanol and air, and that is remarkably used for portable applications. Moreover, Horizon Fuel Cell has developed many fuel cell portable applications such as the Fuel Cell Car Science Kit, the Hydrogen Education Kit and the Bio-Hydrogen Discovery Kit.

In Figures 3.8 – 3.10, some examples of the applications of fuel cell technology are shown.

Fig. 3.8 | Examples of transport modes powered by fuel cell technology [7, 12, 132, 133]

Fig. 3.9 | Examples of portable power tools powered by fuel cell technology [39, 133]

Fig. 3.10 | Examples of fuel cell chargers powered by fuel cell technology [39, 133]

3.9. Summary and Scope of the Present Work

In the present work, the fundamental transport processes of ethanol and water occurring in direct ethanol fuel cells have been reviewed. Additionally, a summary of the actual models and experimental studies developed in this area has been presented. However, the commercialization of DEFCs is still dependent on critical challenges that keep these revolutionary devices away from competing with traditional batteries. For overcoming these challenges, a better understanding of the basic transport phenomena is essential to improve new design concepts.

Material problems concerning the membrane and the catalyst properties have been intensively investigated by many research groups, and remain an important issue for the enhancement of DEFCs. Moreover, the development of mathematical models describing the transport phenomena occurring in DEFCs has received increased attention in the last years. However, the majority of these models lack to describe the simultaneous ethanol, water and heat transport processes within the fuel cell, as well as the passive feed systems.

The main objective of the present work is to develop a model considering the effects of coupled heat and mass transfer, along with the electrochemical reactions occurring in a passive feed DEFC. The model should be able to satisfactorily predict the ethanol, water and oxygen concentration profiles at the anode, membrane and cathode, as well as to estimate the water and ethanol crossover and the temperature profiles across the cell. Additionally, the model should also be used to estimate the effect of operating conditions (ethanol concentration and current density) and design parameters (active area and material properties used in the cell fabrication) on the concentration and temperature profiles along the cell, and on water and ethanol crossover.

There is a lack of published work on DEFCs operating at atmospheric pressure and low temperatures, and these less severe conditions are favorable especially for portable applications. It is also a main objective of this work to study the effect of operating and configuration parameters on fuel cell performance and power density of a passive DEFC.

4. Model Formulation for a Passive Feed DEFC

The development of this work has been strongly motivated by the introduction of passive DEFCs in the market, especially as a promising alternative for portable rechargeable batteries. For this to happen, the formulation of an adequate model is crucial to help understanding the internal processes within the cell.
Therefore, it is here described a steady-state, one-dimensional (1D) model accounting for the electrochemical reactions occurring in a passive feed DEFC, as well as the effects of coupled heat and mass transfer, based on the work developed for passive DMFCs by Oliveira et al. [5]. The main goal of this model is to accurately predict the experimental data, and to predict ethanol, oxygen and water profiles in the anode, cathode and membrane of the fuel cell. Moreover, the model can be used to adequately estimate ethanol and water crossover, as well as the temperature profile across the cell [5].

4.1. General Model Structure

A schematic representation of a passive feed direct ethanol fuel cell is shown in Fig. 4.1, comprising the following elements:

- An acrylic plate (AAP) containing the fuel tank, a current collector plate (ACP), a diffusion layer (AD) and a catalyst layer (AC) at the anode side;
- A polymer electrolyte membrane (M);
- A catalyst layer (CC), a diffusion layer (CD), a current collector plate (CCP), and an acrylic plate (CAP) at the cathode side.

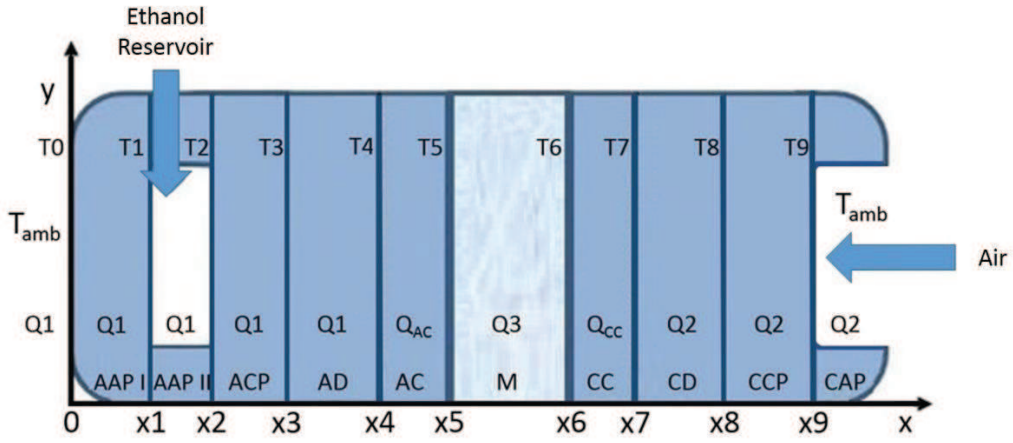

Fig. 4.1 | Schematic representation of the passive feed DEFC used in the model formulation

In a passive feed DEFC, the fuel, usually an aqueous ethanol solution, and the oxidant, usually the environment air, are supplied to the reaction zone by natural convection. From the ACP through the AD, and from the AC through the M, the ethanol solution is

transported primarily by diffusion. In a similar way, the transport of oxygen on the CCP, CD and CC is accomplished by diffusion. In the AC, the ethanol oxidation generates gaseous carbon dioxide that exits the cell by moving counter-currently towards the fuel tank. When the current densities are sufficiently high, the carbon dioxide emerges in the form of gas bubbles from the surface of the AC. In the CC, oxygen reacts with protons and electrons generating water, and this moves counter-currently towards the open holes of the CCP. Under some operating conditions, the water generated can also move by back diffusion towards the anode.

4.2. Model Assumptions

The direct ethanol fuel cell is a multiphase system which involves simultaneous mass, charge and energy transfer. Modeling all of these different phenomena for the different species in all the different domains would be an arduous task. To make this complex system simpler, it is here presented as a one-dimensional transport (along the x direction), with the following assumptions [5, 45]:

- The fuel cell is assumed to operate under steady-state conditions.
- The solutions are considered ideal and diluted.
- The carbon dioxide is assumed to be dissolved in solution, thus only the liquid phase is considered in the anode side; on the other hand, in the cathode side gaseous ethanol and water vapor are also considered.
- The local equilibrium at the interfaces is represented by partition functions.
- The pressure gradient across the layers is assumed to be negligible.
- Both the anode and cathode kinetics are described by the simplified Tafel equation [24, 56], considering that a large amount of net current is produced, and assuming this as a case of an irreversible reaction process dominated by the forward-reaction direction.
- The thermal energy model is based on the differential thermal energy conservation equation (Fourier's law) [38].
- The mass transport in the diffusion layers and membrane is described using the effective Fickian models [38].
- The ethanol and water transport through the membrane is assumed to depend on the combined effect of the concentration gradient between the anode and the cathode and the electro-osmotic force.

- The heat and mass transfer of the ethanol from the bulk solution to the ACP on the anode side, and air from the environment to the CCP on the cathode side, are assumed to be driven by natural convection.
- The heat and mass transfer through the gas diffusion and catalyst layers is assumed to be a diffusion-predominated process, and the convective transport can be safely ignored in this case [10].
- The anodic and cathodic overpotentials are considered to be constant through the catalyst layers.
- The catalyst layers are assumed to be macro-homogeneous porous electrodes, and thus reactions in these layers are considered to be homogeneous.
- The heat generated by the electrochemical reactions occurring in the catalyst layers is considered in this model, while the heat released by joule effects is ignored.
- The heat flux generated in the catalyst layers is assumed to be constant.

4.3. Governing Equations and Boundary Conditions

4.3.1. Mass Transport

The ethanol is fed to the fuel cell under standard conditions, reacting at the anode:

$$\text{Ethanol oxidation: } C_2H_5OH + 3H_2O \rightarrow 2CO_2 + 12H^+ + 12e^- \quad (4.1)$$

Simultaneously, the air from the environment enters the cell reacting at the cathode:

$$\text{Oxygen reduction: } O_2 + 4H^+ + 4e^- \rightarrow 2H_2O \quad (4.2)$$

The overall reaction results as:

$$\text{Ethanol oxidation: } C_2H_5OH + 3O_2 \rightarrow 2CO_2 + 3H_2O \quad (4.3)$$

The ethanol and water are supplied to the anode at a concentration C^0, and the transport of the reactants from the fuel tank to the ACP is dominated by fluid flow and natural convection [10]. The molar fluxes can be determined from [5]:

$$N_j = h_{mass,j}^{AAP}\left(C_j^0 - C_j^{AAP}\right) \quad (4.4)$$

where j stands for the ethanol or water, and $h_{mass,j}^{AAP}$ represents the mass transfer coefficient of the species j.

In mass convection analysis, it is often convenient to express the mass transfer coefficient in a non-dimensional form in terms of the dimensionless Sherwood number, defined as [134]:

$$Sh = \frac{h_{mass}\, L}{D} \tag{4.5}$$

where L is the length of the active area, and D is the diffusion coefficient. The value of h_{mass} is dependent on the physical properties of the species involved, the geometry of the fuel tank, and its orientation [134]. Considering the actual case of natural convection flow occurring in vertical plates, it may be determined from [5, 134]:

$$Sh = \left[0.825 + \frac{0.387\, Ra^{1/6}}{\left(1+\left(0.492/Sc\right)^{9/16}\right)^{8/27}}\right]^2 \tag{4.6}$$

where Ra stands for the Rayleigh number $\left(Ra = Sc\frac{g\Delta C L^3}{Cv^2}\right)$, and Sc is the Schmidt number $\left(Sc = \frac{v}{D}\right)$ [5, 134].

Within the inner layers of the fuel cell, the tortuous and sheltering geometry of the electrodes insulates the reactant molecules from the convective forces and hence the transport is dominated by diffusion [10]. Thus, the molar fluxes of ethanol and water across the ACP, AD and AC layers are related to the concentration gradients, and can be determined by the principles of Fick's law according to the following equations [5]:

$$N_j = -D_j^{ACP}\, \frac{dC_j^{ACP}}{dx} \tag{4.7}$$

$$N_j = -\, D_j^{eff,AD}\, \frac{dC_j^{AD}}{dx} \tag{4.8}$$

$$N_j = -\, D_j^{eff,AC}\, \frac{dC_j^{AC}}{dx} \tag{4.9}$$

Due to the porous structure of the electrodes, the diffusion of the molecules is hardened by the pore walls, and so the diffusion flux must account for this effect. Commonly, the correction of Bruggemann is employed to calculate the effective diffusivity D^{eff} [10]. Thus $D_j^{eff,AD}$ and $D_j^{eff,AC}$ represent the effective diffusion coefficients in the AD and AC, respectively.

Since local equilibrium is assumed at the AAP–ACP, ACP–AD and AD–AC interfaces, the concentration of the reactants is determined by using the partition coefficients K_2, K_3 and K_4, respectively. As a result, the boundary conditions for the previous equations (4.7), (4.8) and (4.9) are obtained from [5]:

$$C_{2,j}^{ACP} = K_2 C_j^{APP}, \text{ at } x = x_2 \tag{4.10}$$

$$C_{3,j}^{AD} = K_3 C_{3,j}^{ACP}, \text{ at } x = x_3 \quad (4.11)$$

$$C_{4,j}^{AC} = K_4 C_{4,j}^{AD}, \text{ at } x = x_4 \quad (4.12)$$

$$C_j^{AC} = C_{5,j}^{AC}, \text{ at } x = x_5 \quad (4.13)$$

As is known, the fuel cell produces electricity at a given current density, i_{cell}, leading to a flux of reactants and products within the cell layers. Considering steady-state, the rate of consumed reactants must equal the rate of product supply, and therefore the molar flux can be related to the current density by the following equation [10]:

$$i_{cell} = n F N_j \quad (4.14)$$

Accordingly [5], the molar flux of ethanol in a DEFC can then be related to the current density accounting for the crossover flux of ethanol through the membrane from the anode to the cathode, $N_{C_2H_5OH}^M$, by:

$$N_{C_2H_5OH} = \frac{i_{cell}}{12F} + N_{C_2H_5OH}^M \quad (4.15)$$

Similarly [5], the water molar flux in the anode is related to the current density, accounting for the ratio of the net water flux though the membrane from the anode to the cathode normalized by the protonic flux, represented by the net water transport coefficient α:

$$N_{H_2O} = \frac{i_{cell}}{4F} (\alpha + 1) \quad (4.16)$$

Combining equations (4.4) and (4.15), it is possible to achieve the ethanol concentration profile in the AAP according to:

$$C_{C_2H_5OH}^{AAP} = C_{C_2H_5OH}^0 - \frac{1}{h_{mass,C_2H_5OH}^{AAP}} \left(\frac{i_{cell}}{12F} + N_{C_2H_5OH}^M \right) \quad (4.17)$$

Accordingly, by merging equations (4.4) and (4.16), it is possible to determine the water concentration profile in the AAP:

$$C_{H_2O}^{AAP} = C_{H_2O}^0 - \frac{i_{cell}}{4F\, h_{mass,H_2O}^{AAP}} (\alpha + 1) \quad (4.18)$$

The concentration profile in the ACP can be determined by coupling the equations (4.7), (4.10) and (4.15) for the ethanol or (4.16) for water respectively, yielding:

$$C_{C_2H_5OH}^{ACP} = K_2 C_{C_2H_5OH}^{AAP} + \frac{x_2 - x}{D_{C_2H_5OH}^{ACP}} \left(\frac{i_{cell}}{12F} + N_{C_2H_5OH}^M \right) \quad (4.19)$$

$$C_{H_2O}^{ACP} = K_2 C_{H_2O}^{AAP} + \frac{x_2 - x}{D_{H_2O}^{ACP}} \frac{i_{cell}}{4F} (\alpha + 1) \quad (4.20)$$

Analogously, the concentration profiles in the AD layer can be established from the combination of equations (4.8), (4.11) and (4.15) or (4.16) for ethanol or water respectively:

$$C^{AD}_{C_2H_5OH} = K_3 C^{ACP}_{3,C_2H_5OH} + \frac{x_3 - x}{D^{eff,AD}_{C_2H_5OH}} \left(\frac{i_{cell}}{12F} + N^{M}_{C_2H_5OH} \right) \quad (4.21)$$

$$C^{AD}_{H_2O} = K_3 C^{ACP}_{3,H_2O} + \frac{x_3 - x}{D^{eff,AD}_{H_2O}} \frac{i_{cell}}{4F} (\alpha + 1) \quad (4.22)$$

The same procedure can be applied for the AC layer by combining the equations (4.9), (4.12) and (4.15) or (4.16), according to the following:

$$C^{AC}_{C_2H_5OH} = K_4 C^{AD}_{4,C_2H_5OH} + \frac{x_4 - x}{D^{eff,AC}_{C_2H_5OH}} \left(\frac{i_{cell}}{12F} + N^{M}_{C_2H_5OH} \right) \quad (4.23)$$

$$C^{AC}_{H_2O} = K_4 C^{AD}_{4,H_2O} + \frac{x_4 - x}{D^{eff,AC}_{H_2O}} \frac{i_{cell}}{4F} (\alpha + 1) \quad (4.24)$$

Within the membrane, the mass transport of both ethanol and water is assumed to be dependent on the effect of the concentration gradient coupled to the electro-osmotic force [5, 24]. As a result, the permeation fluxes through the membrane can be described by the following [5]:

$$N^{M}_{C_2H_5OH} = - D^{eff,M}_{C_2H_5OH} \frac{dC^{M}_{C_2H_5OH}}{dx} + n_{C_2H_5OH} \frac{i_{cell}}{F} \quad (4.25)$$

$$N^{M}_{H_2O} = \alpha \frac{i_{cell}}{4F} = - D^{eff,M}_{H_2O} \frac{dC^{M}_{H_2O}}{dx} + n_d \frac{i_{cell}}{F} \quad (4.26)$$

The electro-osmotic drag coefficient, defined as the number of ethanol or water molecules dragged by each proton when traveling through the membrane, is represented correspondingly by $n_{C_2H_5OH}$ and n_d in equations (4.25) and (4.26).

The boundary conditions for the previous equations (4.25) and (4.26), assuming local equilibrium in the AC–M interface, are determined from [5]:

$$C^{M}_{5,j} = K_5 C^{AC}_{5,j}, \text{ at } x = x_5 \quad (4.27)$$

where j represents ethanol or water.

In the membrane, the ethanol and water concentration profiles can be deduced by merging equation (4.27) with equations (4.25) or (4.26), respectively:

$$C^{M}_{C_2H_5OH} = K_5 C^{AC}_{5,C_2H_5OH} + \frac{x_5 - x}{D^{eff,M}_{C_2H_5OH}} \left(N^{M}_{C_2H_5OH} - n_{C_2H_5OH} \frac{i_{cell}}{F} \right) \quad (4.28)$$

$$C_{H_2O}^{M} = K_5 C_{5,H_2O}^{AC} + \frac{x_5 - x}{D_{H_2O}^{eff,M}} \frac{i_{cell}}{F}\left(\frac{\alpha}{4} - n_d\right) \tag{4.29}$$

Analogously to that assumed for the anode, the principles of Fickian diffusion [38] can also be used to determine the molar fluxes of ethanol, water and oxygen within the cathode catalyst layer according to:

$$N_j = -D_j^{eff,CC} \frac{dC_j^{CC}}{dx} \tag{4.30}$$

where j stands for ethanol, water or oxygen. Since the oxygen permeation through the membrane is considered negligible, the oxygen concentration at the M–CC interface is assumed to be zero. Also, it is assumed that the ethanol crossing through the membrane is totally consumed at the cathode catalyst layer, and thus its concentration at the CC–CD interface is null [5, 45]. As a result, the boundary conditions for equation (4.30), assuming local equilibrium for the concentration of water and ethanol at the M–CC interface, as well as the concentration of water and oxygen at the CC–CD interface, are [5]:

$$C_{6,j}^{CC} = K_6 C_{6,j}^{M}, \text{ and } C_{6,O_2}^{CC} = 0 \text{ at } x = x_6 \tag{4.31}$$

where j represents ethanol or water, and

$$C_{C_2H_5OH}^{CC} \cong 0,\ C_{H_2O}^{CC} = C_{7,H_2O}^{CC} \text{ and } C_{O_2}^{CC} = C_{7,O_2}^{CC} \text{ at } x = x_7 \tag{4.32}$$

The permeation flux of ethanol through the membrane with a thickness equal to δ^M can be determined from the following equation:

$$N_{C_2H_5OH}^{M} = \frac{D_{C_2H_5OH}^{eff,M}}{\delta^M}\left(K_5 C_{5,C_2H_5OH}^{AC} - C_{6,C_2H_5OH}^{M}\right) + n_{C_2H_5OH}\frac{i_{cell}}{F} \tag{4.33}$$

and the net water transport coefficient α can be deduced from the equation (4.26) according to:

$$\alpha = \frac{4F}{i_{cell}} \frac{D_{H_2O}^{eff,M}}{\delta^M}\left(C_{5,H_2O}^{M} - C_{6,H_2O}^{M}\right) + 4n_d \tag{4.34}$$

Due to the ethanol crossover, part of the oxygen supplied is consumed at the CC layer by unwanted side reactions, generating an internal current and a mixed potential. The oxygen flux in the cathode can thus be related to the current density coupled to the permeation of ethanol through the membrane by [5, 45]:

$$N_{O_2} = \theta_{O_2}\frac{i_{cell}}{4F} + \theta_{cross,O_2} N_{C_2H_5OH}^{M} \tag{4.35}$$

where θ is the stoichiometric coefficient of oxygen in the cathode and overall reactions, and thus $\theta_{O_2} = 1$ and $\theta_{cross,O_2} = 3$ (recall equations (4.2) and (4.3)). Since the oxygen is

provided to the fuel cell in the cathode, its flux across the layers occurs in the opposite direction to that of ethanol and water, and thus $N_{O_2} = -N_j$.

The molar flux of water in the cathode must also account for the effect of water crossover, coupled to the water generation occurring in the catalyst layer due to the oxygen reduction and ethanol crossover oxidation. It can thus be described according to [5]:

$$N_{H_2O} = -\theta_{H_2O}\frac{i_{cell}}{4F} - \theta_{cross,H_2O}N^M_{C_2H_5OH} - N^M_{H_2O} \tag{4.36}$$

where θ is the stoichiometric coefficient of water in the cathode and overall reactions, and thus $\theta_{H_2O} = 2$ and $\theta_{cross,H_2O} = 3$ (recall equations (4.2) and (4.3)).

By employing a suitable combination of the equations (4.30), (4.31), (4.32), (4.33) and (4.34), the concentration profiles in the cathode catalyst layer can be established for ethanol and water by using the following equations respectively:

$$C^{CC}_{C_2H_5OH} = K_6 C^M_{6,C_2H_5OH} + \frac{x_6 - x}{D^{eff,CC}_{C_2H_5OH}}\left(\frac{i_{cell}}{12F} - N^M_{C_2H_5OH}\right) \tag{4.37}$$

$$C^{CC}_{H_2O} = K_6 C^M_{6,H_2O} + \frac{x - x_6}{D^{eff,CC}_{H_2O}}\left((2+\alpha)\frac{i_{cell}}{4F} + 3N^M_{C_2H_5OH}\right) \tag{4.38}$$

In the cathode diffusion layer and cathode current collector, the oxygen and water molar fluxes can be determined as previously, by assuming Fickian diffusion:

$$N_j = -D^{eff,CD}_j \frac{dC^{CD}_j}{dx} \tag{4.39}$$

$$N_j = -D^{CCP}_j \frac{dC^{CCP}_j}{dx} \tag{4.40}$$

where j in this case represents oxygen or water vapor.

The boundary conditions for the previous equations (4.39) and (4.40), assuming local equilibrium at the CC–CD and CD–CCP interfaces, are given by:

$$C^{CD}_{7,j} = K_{7,j}C^{CC}_{7,j}, \text{ at } x = x_7 \tag{4.41}$$

$$C^{CCP}_{8,j} = K_{8,j}C^{CD}_{8,j}, \text{ at } x = x_8 \tag{4.42}$$

The concentration profiles can be established in the CD and CCP layers for oxygen and water, by employing a suitable combination of the equation (4.35) or (4.36) and equations (4.39) and (4.41) concerning the CD layer, or (4.40) and (4.42) concerning the CCP layer respectively:

$$C^{CD}_{O_2} = K_7 C^{CC}_{7,O_2} + \frac{x - x_7}{D^{eff,CD}_{O_2}}\left(\frac{i_{cell}}{4F} + 3N^M_{C_2H_5OH}\right) \tag{4.43}$$

$$C_{H_2O}^{CD} = K_7 C_{7,H_2O}^{CC} + \frac{x-x_7}{D_{H_2O}^{eff,CD}} \left((2+\alpha) \frac{i_{cell}}{4F} + 3N_{C_2H_5OH}^{M} \right) \quad (4.44)$$

$$C_{O_2}^{CCP} = K_8 C_{8,O_2}^{CD} + \frac{x-x_8}{D_{O_2}^{CCP}} \left(\frac{i_{cell}}{4F} + 3N_{C_2H_5OH}^{M} \right) \quad (4.45)$$

$$C_{H_2O}^{CCP} = K_8 C_{8,H_2O}^{CD} + \frac{x-x_8}{D_{H_2O}^{CCP}} \left((2+\alpha) \frac{i_{cell}}{4F} + 3N_{C_2H_5OH}^{M} \right) \quad (4.46)$$

Similarly to that described for the anode, the oxygen from the environment is supplied to the cathode side at a concentration C^0 by natural convection. As simplification, it is assumed that the air in the CAP is in a saturated state, mainly due to the water generation on the cathode and water permeation from the anode. Therefore the oxygen and water vapor fluxes within the acrylic plate can be determined from:

$$N_j = h_{mass,j}^{CAP} \left(C_j^0 - C_{9,j}^{CAP} \right) \quad (4.47)$$

where $h_{mass,j}^{CAP}$ represents the mass transfer coefficient of oxygen, and can be determined according to equation (4.6). The water vapor feed concentration $C_{H_2O}^0$ can be determined from P_{sat}/RT, where $P_{sat} = 10^{(-2.1794+0.02953T-9.1837\times10^{-5}T^2+1.4454\times10^{-7}T^3)}$ [71].
The boundary condition for this equation, assuming local equilibrium at the CCP–CAP interfaces, is:

$$C_{9,j}^{CAP} = K_{9,j} C_{9,j}^{CCP}, \text{ at } x = x_9 \quad (4.48)$$

The oxygen and water concentration profiles in the CAP can be determined according to:

$$C_{9,O_2}^{CAP} = C_{O_2}^0 - \frac{1}{h_{mass,O_2}^{CAP}} \left(\frac{i_{cell}}{4F} + 3N_{C_2H_5OH}^{M} \right) \quad (4.49)$$

$$C_{9,H_2O}^{CAP} = C_{H_2O}^0 + \frac{1}{h_{mass,H_2O}^{CAP}} \left((2+\alpha) \frac{i_{cell}}{4F} + 3N_{C_2H_5OH}^{M} \right) \quad (4.50)$$

Due to the mass transfer limitations related to the reactant transport, the decrease in the concentration of ethanol results in a concentration overpotential as the anode is not immediately restocked with fuel. The rate of the electrochemical oxidation of ethanol can be described using the Tafel equation [24, 56]:

$$i_{cell} = i_{0,ref}^{C_2H_5OH} \frac{C_{C_2H_5OH}^{AC}}{C_{C_2H_5OH,ref}^{AC}} \exp\left(\frac{F\alpha_A}{RT^{AC}} \eta_A \right) \quad (4.51)$$

where $i_{0,ref}^{C_2H_5OH}$ and $C_{C_2H_5OH,ref}^{AC}$ represent, respectively, the reference exchange current density on the anode and the reference concentration of ethanol, $C_{C_2H_5OH}^{AC}$ is the average ethanol concentration within the anode catalyst layer, α_A is the anodic charge transfer coefficient, T^{AC} is the temperature at the anode catalyst layer and η_A is the anode

overpotential. Assuming that η_A is constant in the anode catalyst layer, equation (4.51) can be used to determine the anode overpotential for a given current density [5] according to:

$$\eta_A = \frac{RT^{AC}}{F\alpha_A} \ln\left(\frac{i_{cell}\, C^{AC}_{C_2H_5OH,ref}}{i^{C_2H_5OH}_{0,ref} C^{AC}_{C_2H_5OH}}\right) \tag{4.52}$$

$C^{AC}_{C_2H_5OH}$ is determined from the average of the ethanol concentrations at the catalyst interfaces, $C^{AC}_{4,\,C_2H_5OH}$ and $C^{AC}_{5,\,C_2H_5OH}$ respectively, according to the following:

$$C^{AC}_{4,\,C_2H_5OH} = K_4K_3K_2C^0_{C_2H_5OH} - Ct_1\left(\frac{i_{cell}}{12F} + N^M_{C_2H_5OH}\right) \tag{4.53}$$

where

$$Ct_1 = \frac{K_4K_3K_2}{h^{AAP}_{mass,C_2H_5OH}} + \frac{K_4K_3\delta^{ACP}}{D^{ACP}_{C_2H_5OH}} + \frac{K_4\delta^{AD}}{D^{eff,AD}_{C_2H_5OH}} \tag{4.54}$$

and

$$C^{AC}_{5,\,C_2H_5OH} = K_4K_3K_2C^0_{C_2H_5OH} - Ct_2\left(\frac{i_{cell}}{12F} + N^M_{C_2H_5OH}\right) \tag{4.55}$$

where

$$Ct_2 = Ct_1 + \frac{\delta^{AC}}{D^{eff,AC}_{C_2H_5OH}} \tag{4.56}$$

The ethanol crossover through the membrane can be calculated from:

$$N^M_{C_2H_5OH} = \frac{n_{C_2H_5OH}\frac{i_{cell}}{F} + K_5C^{AC}_{5,\,C_2H_5OH}\frac{D^{eff,M}_{C_2H_5OH}}{\delta^M} - \frac{i_{cell}}{12FK_6}\frac{\delta^{CC}D^{eff,M}_{C_2H_5OH}}{\delta^M D^{eff,CC}_{C_2H_5OH}}}{1-\frac{\delta^{CC}D^{eff,M}_{C_2H_5OH}}{K_6\delta^M D^{eff,CC}_{C_2H_5OH}}} \tag{4.57}$$

The water concentration at the membrane interface can be determined from:

$$C^M_{5,\,H_2O} = K_5K_4K_3K_2C^0_{H_2O} - Ct_3\left(\frac{i_{cell}}{4F}(\alpha+1)\right) \tag{4.58}$$

where

$$Ct_3 = \frac{K_5K_4K_3K_2}{h^{AAP}_{mass,H_2O}} + \frac{K_5K_4K_3\delta^{ACP}}{D^{ACP}_{H_2O}} + \frac{K_5K_4\delta^{AD}}{D^{eff,AD}_{H_2O}} + \frac{K_5\delta^{AC}}{D^{eff,AC}_{H_2O}} \tag{4.59}$$

Accordingly, the water concentration at the membrane interface on the cathode side can be determined from:

$$C^{M}_{6,\,H_2O} = \frac{C^{0,sat}_{H_2O}}{K_9K_8K_7K_6} + Ct_4\left((2+\alpha)\frac{i_{cell}}{4F} + 3N^{M}_{C_2H_5OH}\right) \tag{4.60}$$

and

$$Ct_4 = \frac{1}{K_9K_8K_7K_6h^{CAP}_{mass,H_2O}} - \frac{\delta^{CCP}}{K_8K_7K_6D^{CCP}_{H_2O}} - \frac{\delta^{CD}}{K_7K_6D^{eff,CD}_{H_2O}} - \frac{\delta^{CC}}{K_6D^{eff,CC}_{H_2O}} \tag{4.61}$$

The water permeation through the membrane can be calculated by using the following equation:

$$\alpha = \frac{\frac{4FD^{eff,M}_{H_2O}}{i_{cell}\delta^{M}}\left[\left(K_5K_4K_3K_2C^{0}_{H_2O} - Ct_3\frac{i_{cell}}{4F}\right) - \left(\frac{C^{0,sat}_{H_2O}}{K_9K_8K_7K_6} + Ct_4\left(\frac{i_{cell}}{2F} + 3N^{M}_{C_2H_5OH}\right)\right)\right] + 4n_d}{1 + (Ct_3 + Ct_4)\frac{D^{eff,M}_{H_2O}}{\delta^{M}}} \tag{4.62}$$

On the cathode, the overpotential is affected by the phenomenon of ethanol crossover. To account for this effect, it is assumed that the ethanol crossing from the anode completely reacts electrochemically on the cathode, and thus the internal current due to ethanol oxidation on the cathode ($i_{C_2H_5OH}$) is determined from:

$$i_{C_2H_5OH} = 12\,F\,N^{M}_{C_2H_5OH} \tag{4.63}$$

The oxygen reduction reaction taking place at the cathode is also modeled according to the Tafel equation accounting for the mixed potential generated by fuel crossover:

$$i_{cell} + i_{C_2H_5OH} = i^{O_2}_{0,ref}\frac{C^{CC}_{O_2}}{C^{CC}_{O_2,ref}}\exp\left(\frac{F\alpha_C}{RT^{CC}}\eta_C\right) \tag{4.64}$$

where $i^{O_2}_{0,ref}$ and $C^{CC}_{O_2,ref}$ represent the reference exchange current density on the cathode and the reference concentration of oxygen, respectively, $C^{CC}_{O_2}$ is the oxygen concentration at the catalyst interface, α_C is the cathodic transfer coefficient and T^{CC} is the temperature in the cathode catalyst layer. Thus, the cathode activation overpotential η_C can be determined from the following equation [5, 71]:

$$\eta_C = \frac{RT^{CC}}{F\alpha_C}\ln\left(\frac{(i_{cell}+i_{C_2H_5OH})\,C^{CC}_{O_2,ref}}{i^{O_2}_{0,ref}\,C^{CC}_{7,O_2}}\right) \tag{4.65}$$

The oxygen concentration can then be determined from:

$$C^{CC}_{7,\,O_2} = \frac{C^{0}_{O_2}}{K_9K_8K_7} - Ct_5\left(\frac{i_{cell}}{4F} + 3N^{M}_{C_2H_5OH}\right) \tag{4.66}$$

where

$$Ct_5 = \frac{1}{K_9K_8K_7h^{CAP}_{mass,O_2}} + \frac{\delta^{CCP}}{K_8K_7D^{CCP}_{O_2}} + \frac{\delta^{CD}}{K_7D^{eff,CD}_{O_2}} \tag{4.67}$$

4.3.2. Heat Transport

When the heat is conducted through two adjacent materials with different thermal conductivities, the heat flux through a finite cross-sectional area A_a can be described according to the Newton's law of cooling [134]:

$$Q = -h_{heat} A_a \Delta T \tag{4.68}$$

where h_{heat} represents the heat transfer coefficient due to natural convection, and A_a is the active area. Considering the present case of natural convection flow occurring in vertical plates, h_{heat} may be determined from the dimensionless Nusselt number according to [38, 134]:

$$h_{heat} = \frac{k}{L} Nu = \frac{k}{L}\left[0.825 + \frac{0.387\, Ra^{1/6}}{\left(1+\left({}^{0.492}/_{Pr}\right)^{9/16}\right)^{8/27}}\right]^2 \tag{4.69}$$

where $Ra = Pr\frac{g\Delta T L^3}{Tv^2}$, and Pr is the Prandtl number $\left(Pr = \frac{\mu Cp}{k}\right)$. On the other hand, when a temperature gradient occurs within a homogeneous substance, there is an energy transfer in the form of heat through the medium by means of conduction. The rate of heat transfer in the x-direction through a finite cross-sectional area A_a is described according to the Fourier's law [38]:

$$Q = -kA_a \frac{dT}{dx} \tag{4.70}$$

where k is the effective thermal conductivity of the substance.
Having in mind the simplifications assumed previously for the heat transfer in passive direct ethanol fuel cells, and recalling Figure 4.1, the general heat transfer process can here be described according to the following [5]:

$$Q_1 + Q_2 = Q^{AC} + Q^{CC} \tag{4.71}$$

Additionally, according to the energy balance, the total heat generated within the cell must equal the heat losses to the surroundings at the anode and cathode, and thus:

$$Q_3 = Q^{AC} - Q_1 = Q_2 - Q^{CC} \tag{4.72}$$

On the anode, the heat generated by the electrochemical reaction occurring in the AC layer can be described by the following equation [5, 98]:

$$Q^{AC} = i_{cell}\left(\eta_A - \left(\frac{\Delta H_A - \Delta G_A}{12F}\right)\right) \tag{4.73}$$

where the first term represents the heat generation due to the activation and mass transfer overpotential η_A and the second term accounts for the entropy change of the anodic electrochemical reaction with ΔH_A denoting the anodic reaction enthalpy and $\Delta G_A$the Gibbs free energy. The previous equation can be rewritten in the following form [71]:

$$Q^{AC} = i_{cell}\eta_A - \frac{i_{cell}}{12F}\left[\beta_1 + \beta_2\left(T^{AC} - 298\right)\right] \quad (4.74)$$

where

$$\beta_1 = \left(\Delta H_A^0 - \Delta G_A^0\right) \quad (4.75)$$

$$\beta_2 = \left(2Cp_{CO_2} - 3Cp_{H_2O} - Cp_{C_2H_5OH}\right) \quad (4.76)$$

and

$$T^{AC} = \frac{T_4+T_5}{2} \quad (4.77)$$

At the cathode, one must also account for the mixed potential caused by ethanol crossover, and thus the heat generated by the electrochemical oxygen reduction in the CC layer can be determined by [5, 98]:

$$Q^{CC} = \left(i_{cell} + i_{C_2H_5OH}\right)\left(\eta_C - \frac{\Delta H_C - \Delta G_C}{4F}\right) - i_{C_2H_5OH}\left(\frac{\Delta H_A - \Delta G_A}{12F}\right) \quad (4.78)$$

with ΔH_C denoting the cathodic reaction enthalpy and ΔG_C the Gibbs free energy. The third term in the equation denotes the entropy change of the ethanol oxidation reaction on the cathode due to the permeation flux. The previous equation can be rewritten as:

$$Q^{CC} = \left(i_{cell} + i_{C_2H_5OH}\right)\eta_C - \left[\beta_3 + \beta_4\left(T^{CC} - 298\right)\right] - \frac{i_{C_2H_5OH}}{12F}\left[\beta_1 + \beta_2\left(T^{AC} - 298\right)\right] \quad (4.79)$$

considering that:

$$\beta_3 = \frac{i_{cell}+i_{C_2H_5OH}}{4F}\left(\Delta H_C^0 - \Delta G_C^0\right) \quad (4.80)$$

$$\beta_4 = \frac{i_{cell}+i_{C_2H_5OH}}{4F}\left(2Cp_{H_2O} - Cp_{O_2}\right) \quad (4.81)$$

and

$$T^{CC} = \frac{T_6+T_7}{2} \quad (4.82)$$

The heat flux Q_1 occurring within the AAP_2 section in the anode side can be described according to the Newton's law:

$$Q_1 = -h_{heat,\,H_2O} A_a \Delta T \tag{4.83}$$

Additionally, this equation is also used to describe the heat transfer from the AAP_1 and CCP layers to the environment surroundings, and thus:

$$Q_1 = -h_{heat,\,air} A_a \Delta T \tag{4.84}$$

$$Q_2 = -h_{heat,\,air} A_a \Delta T \tag{4.85}$$

Neglecting the Joule heat, the heat flux Q_1 occurring in the APP_1 and AD layers in the anode side can also be related to the temperature gradient across each layer according to equation (4.70):

$$Q_1 = -k^l A_a \frac{dT}{dx} \tag{4.86}$$

where *l* represents AAP_1 or AD. Since the same principle is valid within the membrane and the CD layer on the cathode side, the heat fluxes Q_2 and Q_3 can also be described by this equation. In this case, *l* stands for CD or M, considering Q_2 and Q_3 respectively.
The current collector plates (ACP and CCP) in passive DEFCs are perforated by several holes in order to allow the distribution of the reactants through the catalyst layers, and so the total active area A_a is obtained by:

$$A_a = A_{holes} + A_{surf} \tag{4.87}$$

where A_{holes} denotes the total perforated area, and A_{surf} is the total surface area without the holes. Taking this into consideration, it is assumed that the heat transfer occurs by conduction within the solid material, and by convection within the perforated holes. The thermal resistance regarding the heat conduction is denoted by [38, 134]:

$$R_{cond} = \frac{\delta}{kA_{surf}} \tag{4.88}$$

where δ represents the current collector plate thickness. Additionally, the thermal resistance regarding the perforated area is given by [38, 134]:

$$R_{conv} = \frac{1}{h_{heat} A_{holes}} \tag{4.89}$$

Knowing that the temperature drop across a plane wall is proportional to its thermal resistance $R_{thermal}$, and since conduction and convection resistances are in series, the heat transfer within the ACP and CCP layers can be deduced as [38, 134]:

$$Q = \frac{\Delta T}{R_{thermal}} = \Delta T \left(\frac{1}{R_{cond}} + \frac{1}{R_{conv}} \right) \tag{4.90}$$

Concerning the catalytic layers, the temperature profile in the AC can be determined from [5]:

$$\frac{d^2T}{dx^2} = \frac{Q^{AC}}{k^{AC}\delta^{AC}} \tag{4.91}$$

and the boundary conditions are the temperature of the walls T_4 and T_5 . Accordingly, the temperature profile in the CC layer, with the temperature of the walls T_6 and T_7 as boundary conditions, can be calculated from [5]:

$$\frac{d^2T}{dx^2} = \frac{Q^{CC}}{k^{CC}\delta^{CC}} \tag{4.92}$$

The heat flux occurring within these layers can be described according to the Fourier's law by:

$$Q_1 = -k^{AC}A_a\frac{dT}{dx}, \text{ at } x = x_4 \tag{4.93}$$

$$Q_3 = -k^{CC}A_a\frac{dT}{dx}, \text{ at } x = x_6 \tag{4.94}$$

and $\frac{dT}{dx}$ can be determined from the temperature profiles obtained from equations (4.91) and (4.92).
From a suitable combination of equations 4.73, 4.83, 4.84, 4.86, 4.90 and 4.93, the heat flux Q_1 can be determined from:

$$Q_1 = \frac{T_4 - T_{amb}}{\sum R_A} \tag{4.95}$$

where T_{amb} is the temperature at the environment surrounding, and $\sum R_A$ stands for the total resistance across the distinct layers on the anode side. Analogously,

$$Q_2 = \frac{T_7 - T_{amb}}{\sum R_C} \tag{4.96}$$

which can be deduced from equations 4.78, 4.85, 4.86, 4.90 and 4.94, and $\sum R_C$ stands for the total resistance across the walls on the cathode. From the resolution of the equations presented in this section, it is possible to determine the temperature profile across the cell.

4.3.3. Cell Performance

Taking into account the ethanol and oxygen concentrations determined at the catalyst layers and the temperature distributions, together with the anodic and cathodic overpotentials obtained from the equations previously presented, the cell performance can be determined from [5, 27, 71]:

$$V_{cell} = E_{cell} - \eta_A - \eta_C - i_{cell}\frac{\delta^M}{\kappa} \quad (4.97)$$

where κ is the ionic conductivity of the membrane and E_{cell} is the thermodynamic equilibrium potential of the fuel cell, also known as the electromotive force. Since the atmospheric pressure is considered in this case, E_{cell} is a function of temperature and can be calculated from [5, 71]:

$$E_{cell} = E^0_{cell} + \Delta T\left(\frac{\partial E_{cell}}{\partial T}\right) \quad (4.98)$$

with E^0_{cell} representing the ideal equilibrium electromotive force at standard conditions, and $\partial E_{cell}/\partial T$ the rate of change of the electromotive force.

4.4. Results and Discussion

The developed model, coupling the chemical reactions, as well as the mass and heat transfer processes occurring within the passive feed DEFC is easily implemented using the available numerical tools on Excel.

This model is able to estimate the ethanol, water and oxygen concentrations within the different cell layers, although it cannot predict neither the generation of carbon dioxide occurring on the anode side nor the water drop formation on the cathode. Additionally, the model can be used to estimate the ethanol leakage current due to the fuel crossover through the membrane, as well as the net water transport coefficient, an important parameter concerning the water management in the cell. Concerning the heat transfer, the model is also able to determine the temperature profile across the fuel cell, and to calculate both the anode and the cathode activation overpotentials. Using these results, it is able to adequately estimate the passive feed DEFC performance.

In order to generate the model predictions, the conditions chosen were similar to those used in the experimental studies, described in detail in section 5, and the physical properties of the materials used in the simulations are exhaustively defined in the Appendix B. The values for the parameters used in the simulations were carefully chosen from the literature, and they are listed in Table 4.1. Regarding the parameters that could not be found in the existent literature, the values used in the simulation were prudently chosen having in mind the actual operating conditions. The diffusion coefficients concerning the diffusion and catalytic layers were determined according to the formulation described in Appendix C.

The ethanol concentration profiles predicted by this model through the anode and membrane, are shown in Figure 4.2 assuming current densities of 0.010, 0.015 and 0.200 A cm^{-2}. The membrane considered for the simulation was Nafion™ 117, and the diffusion layers were carbon cloth, on both anode and cathode side. The catalyst loading was Pt–Ru 4 mg cm^{-2} on the anode, and Pt black 2 mg cm^{-2} on the cathode, the initial

concentration of ethanol was considered equal to 1 M, and the operational temperature was 293 K.

Table 4.1 | Values considered for the parameters used in the modeling studies

Parameter	Value	Units	Reference
T_{amb}	293	K	real value
P_{amb}	1	atm	real value
E_{cell}^{0}	1.145	V	[27]
λ	11	n.a.	[58]
κ	$(0.005139\lambda - 0.00326)\exp\left[1268\left(1/303 - 1/T\right)\right]$	S cm^{-1}	[58]
$i_{0,ref}^{C_2H_5OH}$	6.961×10^{-5}	A cm^{-2}	[56]
$i_{0,ref}^{O_2}$	$4.222\times10^{-6}\exp\left[\left(73200/R\right)\left(1/353 - 1/T\right)\right]$	A cm^{-2}	[5]
α_A	0.3	n.a.	assumed
α_C	0.7	n.a.	assumed
A_a	25.0	cm^2	real value
A_{holes}	10.2	cm^2	real value
$\delta^{AAPsectionI,II}$	0.50	cm	real value
δ^{ACP},δ^{CCP}	0.05	cm	real value
δ^{AD},δ^{CD}	0.015	cm	real value
δ^{AC},δ^{CC}	0.0023	cm	real value
δ^{M}	0.0175	cm	[27]
$K_{2\text{-}5}$,$K_{7\text{-}8,H_2O}$	0.8	n.a.	assumed
$K_{7\text{-}8,O_2}$	1.25	n.a.	assumed
K_6	0.001	n.a.	assumed
n_d	$2.9\exp\left[1029\left(1/333 - 1/T\right)\right]$	n.a.	[5]
$n_{C_2H_5OH}$	$0.5\times x_{C_2H_5OH}$	n.a.	[5]

As can be seen in the Figure 4.2, the ethanol concentration within the anode fuel tank is nearly constant. This is due to the fact that the transport of the reactants from the fuel tank to the ACP is mainly dominated by natural convection and fluid flow. Concerning the other layers, the mass transfer diffusion, coupled to the ethanol consumption in the catalyst layer and the ethanol crossover through the membrane, are the responsible phenomena for the decrease of the ethanol concentration. According to these results, the ethanol concentration values are lower for higher current densities, as it should be expected, since the ethanol consumption rises as the current density is increased. Within the membrane, the concentration decreases sharply, due to the occurrence of ethanol crossover to the cathode.

In order to assess the current density effect on the ethanol crossover, the leakage current for different ethanol concentrations is presented in Figure 4.3. The model predictions were simulated considering a Nafion™ 117 membrane, assuming the same diffusion layers and catalyst loadings used for the previous studies.

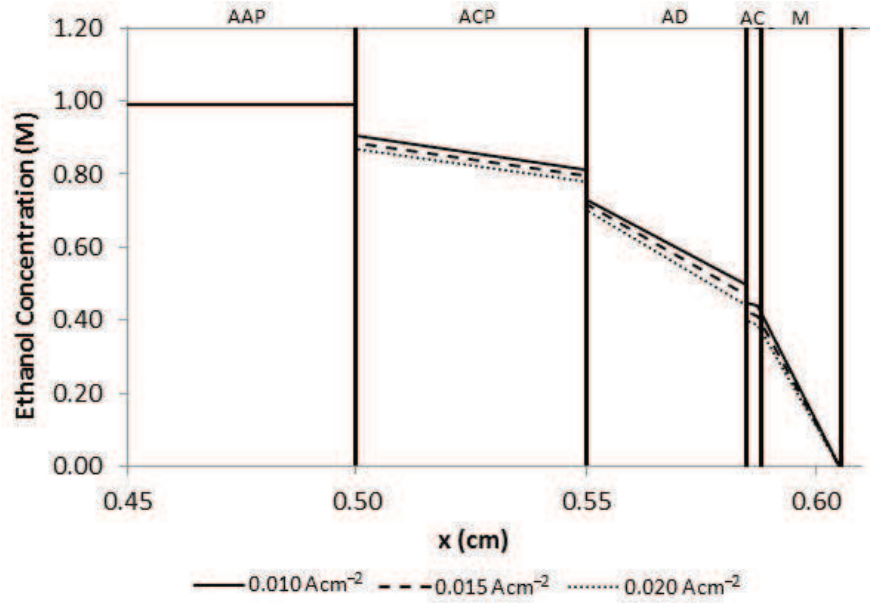

Fig. 4.2 | Predicted ethanol concentration profiles through the DEFC for different current densities. Membrane: Nafion™ 117; Diffusion layers: Carbon Cloth; Anode: ethanol solution 1.0 M, Pt–Ru/C 4.0 mg cm^{-2}; Cathode: Pt/C 2.0 mg cm^{-2}; Temperature: 293 K.

The results shown in Figure 4.3 point toward the leakage current dependency on both ethanol concentration and current density, increasing significantly when the ethanol feed concentration is increased, and decreasing slightly with higher current densities. Higher leakage currents denote higher fuel losses, as the ethanol crossing though the membrane reacts at the cathode, reducing the cell efficiency.

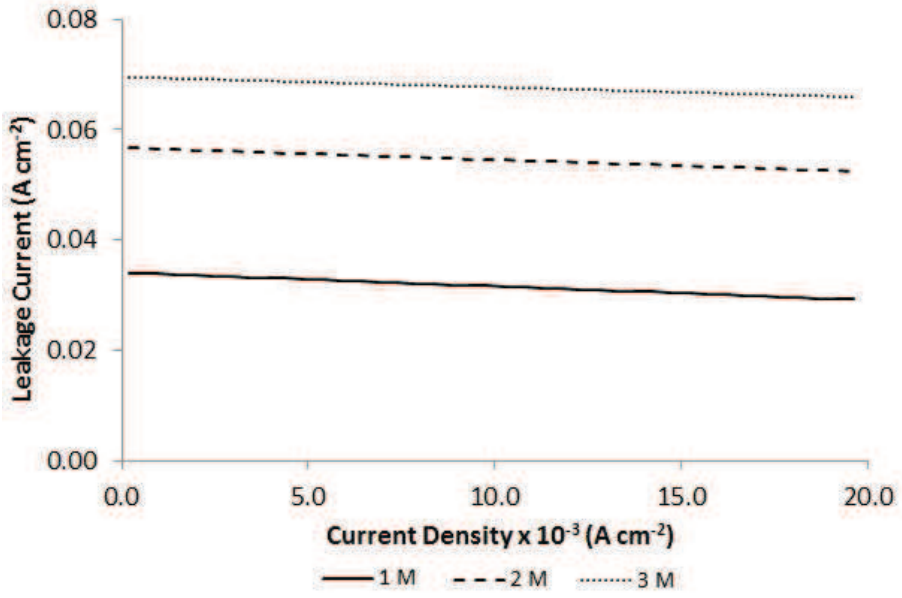

Fig. 4.3 | Predicted leakage current for different ethanol feed concentrations. Membrane: Nafion™ 117; Diffusion layers: Carbon Cloth; Anode: Pt–Ru/C 4.0 mg cm^{-2}; Cathode: Pt/C 2.0 mg cm^{-2}; Temperature: 293 K.

According to these results, the fuel cell efficiency can be optimized by operating with low ethanol concentrations and higher current densities. Besides the leakage current, the water crossover is also a detrimental issue affecting the fuel cell performance and durability. The modeling results for the water concentration profiles across the anode and membrane are depicted in Figure 4.4, considering current densities of 0.010, 0.015 and 0.200 A cm^{-2}. The operating conditions assumed to generate these simulations were the same as those used for the previous studies, considering an initial concentration of ethanol equal to 1M.

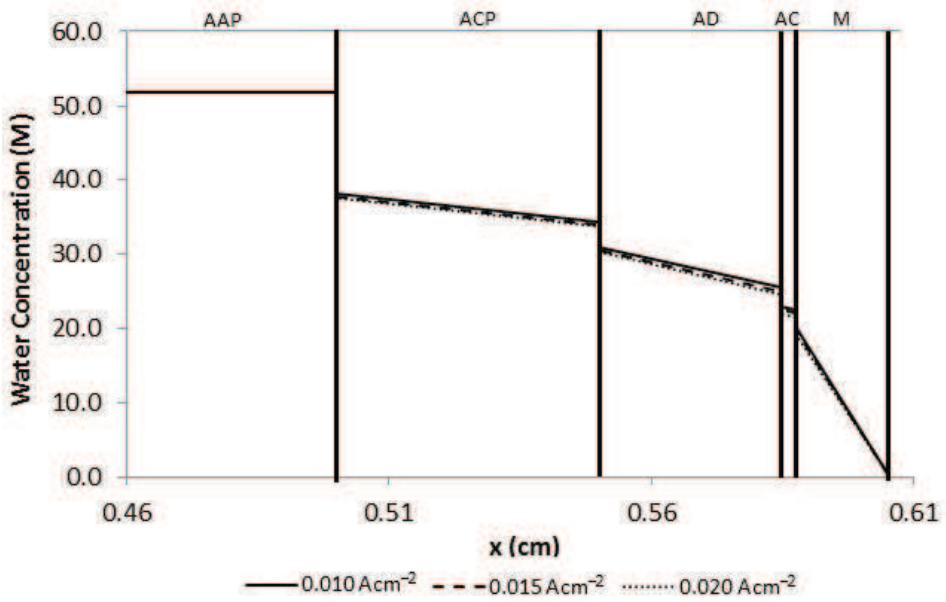

Fig. 4.4 | Predicted water concentration profile across the anode and membrane. Membrane: Nafion™ 117; Diffusion layers: Carbon Cloth; Anode: ethanol solution 1.0 M, Pt–Ru/C 4.0 mg cm^{-2}; Cathode: Pt/C 2.0 mg cm^{-2}; Temperature: 293 K.

From the fuel tank to the current collector, and passing through the diffusion layer to the catalyst layer, the water concentration profile decreases due to the occurrence of water diffusion and electro-osmotic drag.

The water flow from the anode to the cathode can be evaluated through the net water transport coefficient, α. The model predictions for this parameter for different ethanol concentrations using the operating conditions aforementioned are presented in Figure 4.5.

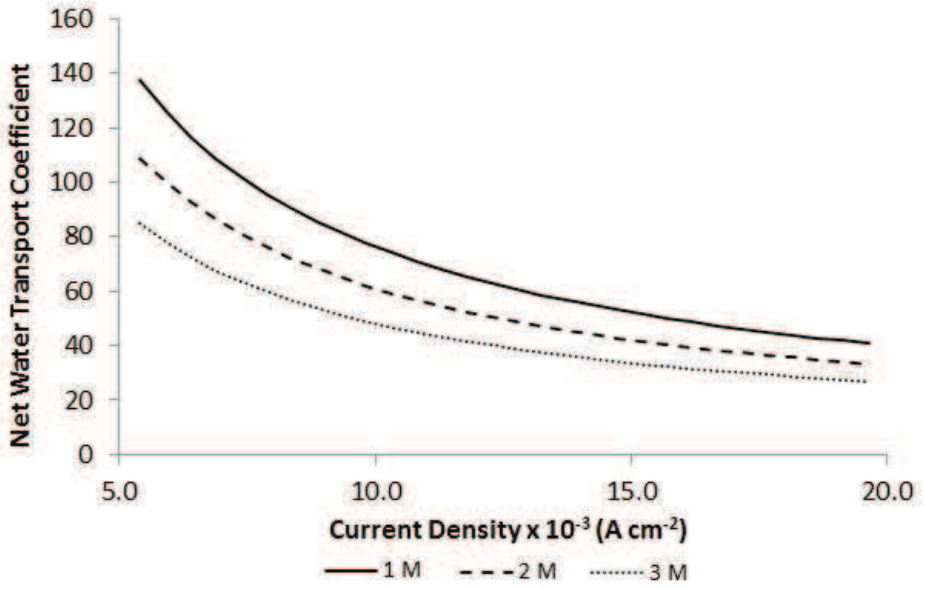

Fig. 4.5 | Predicted net water transport coefficients for different ethanol feed concentrations. Membrane: Nafion™ 117; Diffusion layers: Carbon Cloth; Anode: Pt–Ru/C 4.0 mg cm^{-2}; Cathode: Pt/C 2.0 mg cm^{-2}; Temperature: 293 K.

The positive values of α shown for all the ethanol concentrations investigated indicate that the net water flux in the DEFC occurs from the anode to the cathode and increases with lower ethanol concentrations and lower current densities. This is due to the fact that low ethanol concentrations lead to higher water concentrations at the anode, increasing the water concentration gradient and inducing the water diffusion through the membrane to the cathode side. However, considering higher current densities the impact of the ethanol concentration is slightly decreased, since the chemical reaction generates higher water concentrations at the cathode side. For this reason, the water transport from the anode to the cathode is reduced leading to low values of α, as can be seen in Figure 4.5.

The predicted values for the net water transport coefficient as function of the ethanol feed concentration were inspected for ethanol concentrations ranging from 1 to 3 M. The model simulations are depicted in Figure 4.6, for current densities of 0.010, 0.015 and 0.200 A cm^{-2}. As previously patent in the results shown in Figure 4.5, it is clear from these simulations that the ethanol concentration affects the net water flux. Higher ethanol concentrations lead to lower values of α, especially for high current densities, which correspond to a higher generation of water at the cathode. The simulations also show that the impact of the ethanol concentration is lowered as the current density is increased.

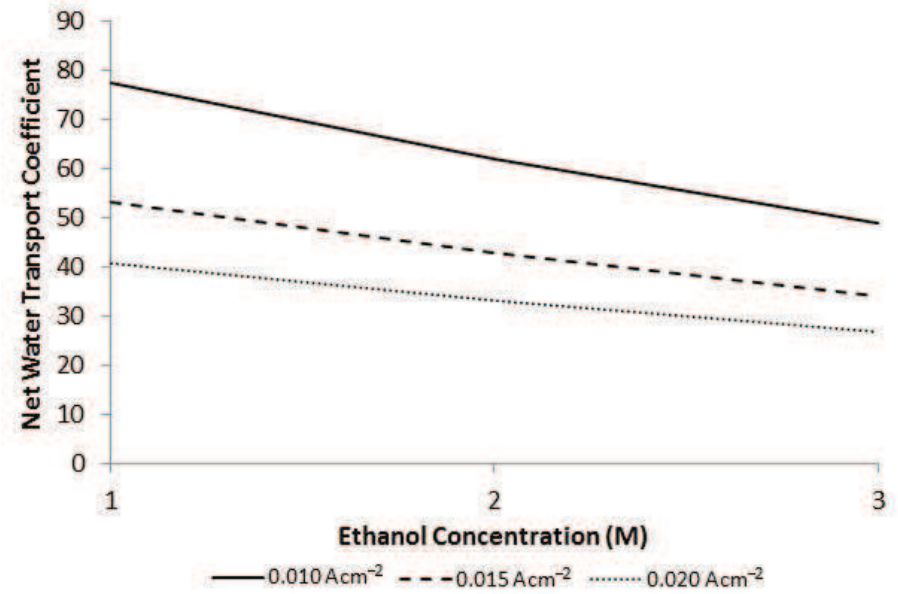

Fig. 4.6 | Influence of ethanol concentration on the net water transport coefficients for different current densities. Membrane: Nafion™ 117; Diffusion layers: Carbon Cloth; Anode: ethanol solution 1.0 M, Pt–Ru/C 4.0 mg cm^{-2}; Cathode: Pt/C 2.0 mg cm^{-2}; Temperature: 293 K.

In addition to the mass transfer processes aforementioned, the reactions taking place in the catalytic layers also generate or consume heat within the fuel cell. The temperature profiles across the DEFC were thus investigated for the operational conditions assumed for the previous studies. The results predicted by the model for these conditions are depicted in Figure 4.7.

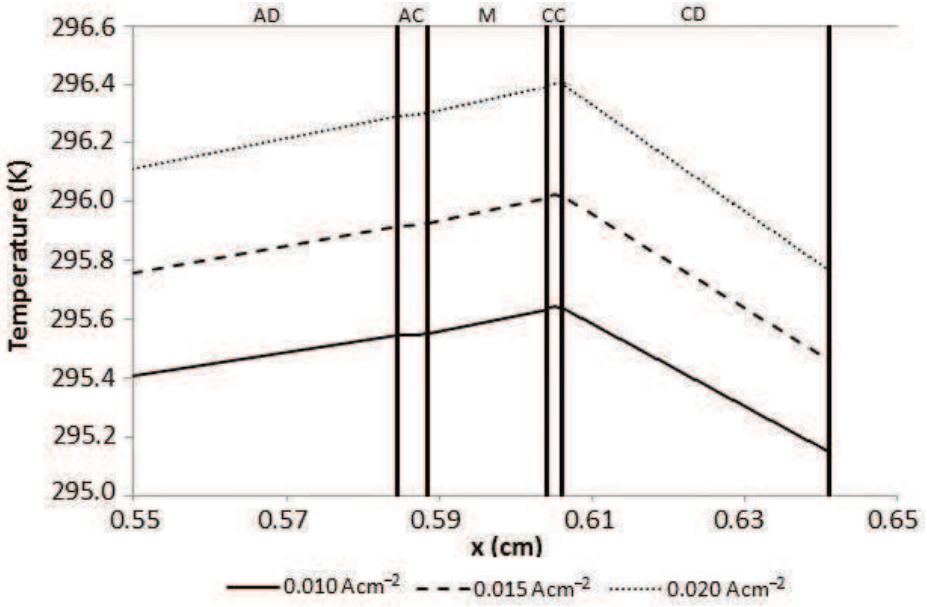

Fig. 4.7 | Predicted temperature profiles across the DEFC for different current densities. Membrane: Nafion™ 117; Diffusion layers: Carbon Cloth; Anode: ethanol solution 1.0 M, Pt–Ru/C 4.0 mg cm^{-2}; Cathode: Pt/C 2.0 mg cm^{-2}; Temperature: 293 K.

Figure 4.7 represents the temperature distribution across the diffusion and catalytic layers, as well as the membrane, for an ethanol concentration of 1 M, and current densities of 0.010, 0.015 and 0.200 A cm^{-2}. The operational temperature is considered to be that of the environment surroundings, and is assumed to be equal to 293 K.
According to the results presented, for the range of values of current densities studied the temperature in the cathode catalytic layer is higher than that on the anode side. A possible explanation for this fact is that the reaction occurring in the cathode is exothermic (ΔH_C = – 484 kJ mol^{-1}), releasing heat. On the other hand, the anodic reaction is endothermic (ΔH_A = 348 kJ mol^{-1}), and thus it absorbs heat from the cathode side. However, on the cathode side the thermal resistances across the fuel cell layers are higher than those on the anode, challenging the heat transfer across the layers. It is clear from the results shown in Figure 4.7 that the temperature on the external walls of the diffusion layers is higher on the anode than on the cathode, where it tends to be more similar to that of the environment surroundings.

4.5. Concluding Remarks

In this section, a steady-state, 1D model accounting for the electrochemical reactions occurring in a passive feed DEFC, as well as the effects of coupled heat and mass transfer, was developed. This model allows the prediction of ethanol, oxygen and water concentration profiles in the anode, cathode and membrane of the fuel cell.
Additionally, the model can also be used to estimate the effect of operating conditions and design parameters on the ethanol and water crossover on the temperature profile across the cell, as well as on fuel cell performance.
Due to its simplicity, the model is easily implemented using numerical tools such as Excel, and allows the investigation of suitable operating conditions to optimize the performance of DEFCs. For this reason, this model can be a useful tool to improve the knowledge on this type of fuel cells.
In order to validate the developed model for the passive DEFC, an “in-house” passive feed DEFC was fabricated and different sets of experiments were performed, so that the model predictions could be compared to the results obtained experimentally. The experimental set-up as well as the experimental results are presented in detail in the following sections.

5. Experimental Setup for a Passive Feed DEFC

All the experimental studies were performed in an "in-house" passive feed direct ethanol fuel cell, where different conditions such as the membrane thickness, diffusion layer material and catalyst loading were deeply investigated. The passive DEFC was developed having into account the use of standard materials easily available on the market, as well as the high flexibility in case of changing the main assembly or cell connections.

5.1. Fuel Cell Design

The cell is composed by the following components, represented in Figures 5.1 to 5.5:

- Membrane electrode assembly (MEA)

The membrane electrode assembly is a membrane coated with catalyst layers, without accounting for the diffusion layers. The MEA used had an active area of 25 cm^2 (5×5 cm^2) and a total area of 110.67 cm^2 (10.52×10.52 cm^2). The membranes tested were made by Nafion™ 117 and 115. The catalyst used on the anode side was Pt–Ru with a loading of 4 mg cm^{-2} or 2 mg cm^{-2}, and on the cathode side was Pt black with a loading of 2 mg cm^{-2} (Figure 5.1).

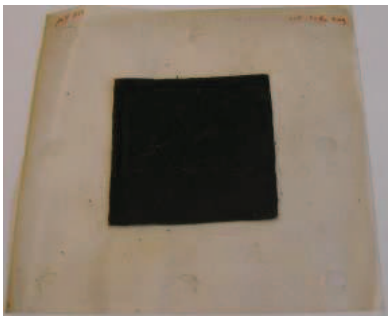

Fig. 5.1 | Nafion-based Membrane Electrode Assembly (MEA)

- Carbon-based diffusion layers

The different materials used in this work as diffusion layers were chosen based on the materials that are commercially available. Therefore, carbon cloth, carbon paper, and an ELAT electrode from E-TEK, fabricated using treated carbon cloth, were selected. For sake of simplification, carbon cloth, carbon paper and ELAT are denoted as CC, CP and ELAT, respectively, in the remaining text.
The carbon paper and the carbon cloth are carbon-fiber-based porous materials. Usually, the CP has a uniform pore size with a peak around 50 µm, while the CC has a broad pore size distribution from 5 to 100 µm. The ELAT material is made of carbon cloth treated on one side with Pt and it is more tortuous, thicker and less porous that carbon cloth.

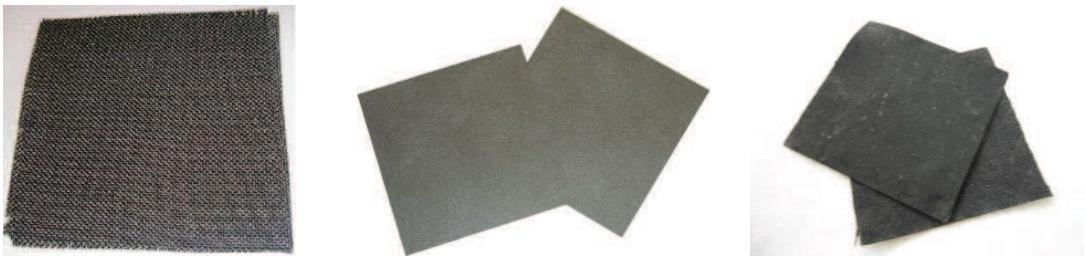

(a) (b) (c)

Fig. 5.2 | Diffusion layers: (a) Carbon cloth; (b) Carbon paper; (c) ELAT

- Perforated current collector plates for electrical contact

For the electrical current collection, two stainless steel plates of 0.5 mm thickness are used. The current collector plates have 36 centered holes with a diameter of 6 mm each, occupying an area of 5×5 cm^2, to allow the reactants supply (Figure 5.3).

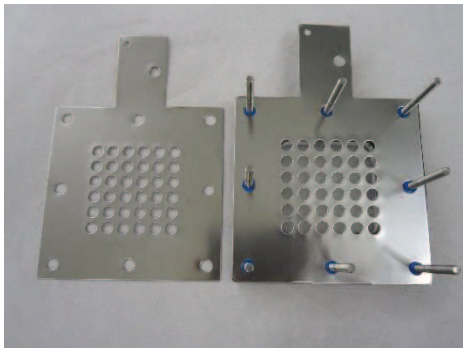

Fig. 5.3 | Current collector plate made of stainless steel

- Isolating Plates

The rubber isolating plates (Figure 5.4) avoid the electrical contact between the current collector plates and the end plates. These rubber plates have a centered hole, 5×5 cm^2, to allow the flow of the reactants, and thus they are not involved in the reaction.

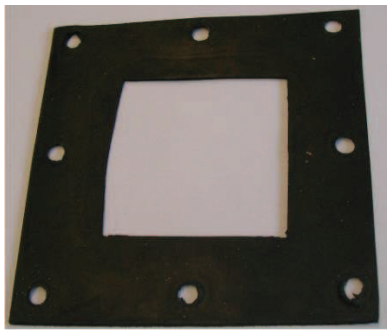

Fig. 5.4 | Isolating rubber plate

- Acrylic end plates

The acrylic plates (Figure 5.5) are used for bracing the cell and they apply a desired tension on the cell elements, in order to prevent flooding. Both plates are 10 mm thick, and they are connected by a total of 8 bolts (diameter 6.2 mm), running through plastic bushes to prevent electrical contact. The anode end plate contains a chamber with 5 mm where the ethanol solution is introduced

(a) (b)

Fig. 5.5 | Acrylic end plates used in the (a) anode side; (b) cathode side

The final "in-house" cell configuration is illustrated in Figure 5.6, and the fabricated DEFC is showed in Figure 5.7.

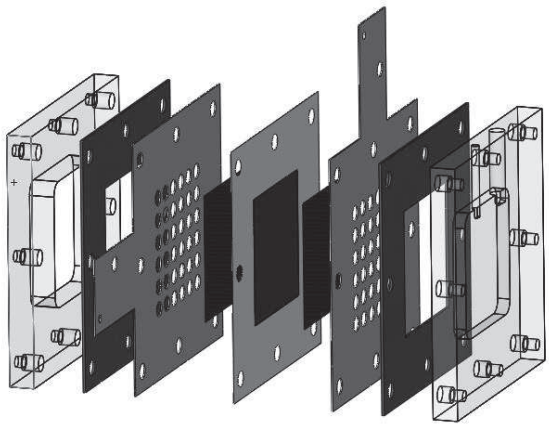

Fig. 5.6 | 3D CAD drawing of the "in-house" passive feed DEFC

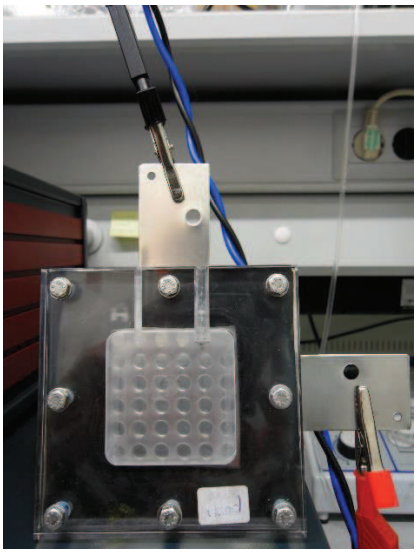

Fig. 5.7 | Fabricated “in-house” passive feed DEFC

The specifications of the components used in the passive feed direct ethanol fuel cell are described in Table 5.1.

Table 5.1 | Specifications of the different components of the passive feed DEFC

Fuel Cell Specifications		
Total Cell Area	100 cm^2	
Cell Active Area	25 cm^2	
Component	Material	Dimensions (cm)
End plates	Acrylic	10×10×1
Isolating plates	Rubber	10×10×0.1
Diffusion layers	Carbon cloth	5×5×0.035
	Carbon paper	5×5×0.019
	ELAT	5×5×0.040
Collector plates	Stainless steel	10×10×0.05
Anode catalyst layer	Platinum–Ruthenium 4 mg cm^{-2}	5×5×0.0023
	Platinum–Ruthenium 2 mg cm^{-2}	5×5×0.0012
Cathode catalyst layer	Platinum black 2 mg cm^{-2}	5×5×0.0012
Membrane	Nafion 115	5×5×0.0127
	Nafion 117	5×5×0.0178

5.2. Test Kit Testing Unit

The tests were performed with a commercial electrochemical impedance test station (Zahner – ElektriK GmbH & Co. kG), and the polarization curves were performed galvanostatically using Thales software. The software constantly monitors both current and voltage, and these parameters are used to calculate and track the cell power during the whole experiment. The experimental set-up is shown in Figure 5.8.

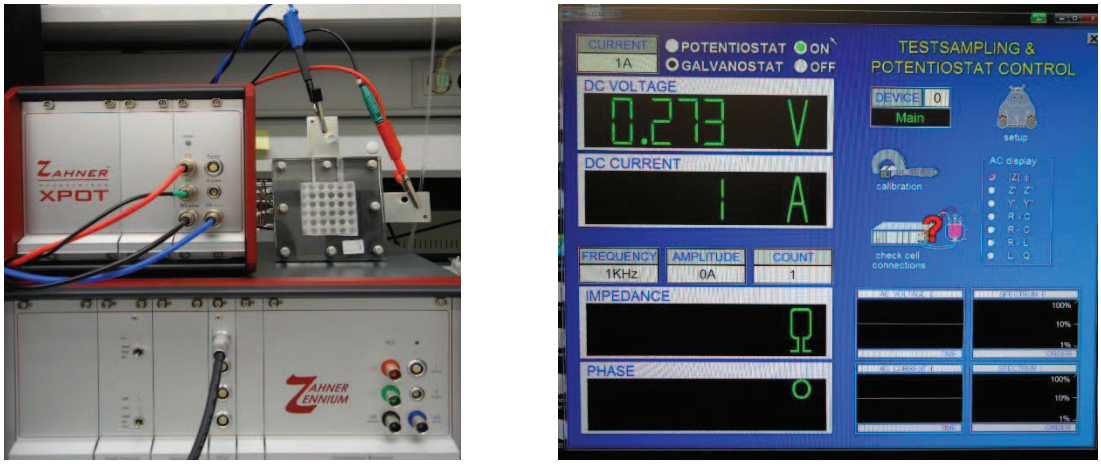

(a) (b)

Fig. 5.8 | Test unit (a) and software (b) used in the experimental studies of the passive feed DEFC

5.3. Experimental Procedure

The procedure for the experimental tests was the following:

a. The fuel tank (recall Figure 5.5(a)) was carefully filled with the ethanol aqueous solution at the desired concentration;

b. The electrical wires were connected to the anode and cathode current collector plates;

c. The computer, as well as the Zahner unit and the Thales software were turned on;

d. The cell was operated in a galvanostatic way, by applying current in the range of 0 till the maximum current allowed by the cell, with an initial step of 5 mA till reaching 40 mA, and then followed by a step of 10 mA. Considering the open circuit the cell was operated for a fifteen minutes interval, while for the other values the cell was operated for three minutes intervals until steady-state conditions;

e. The cell voltage was measured for each value of current applied, and the power density was subsequently calculated. For each set of operating and design conditions, tests were performed until obtaining results with relative errors below 10%.

f. Once the experimental study was finished, the Thales software was turned off, followed by the Zahner unit and the computer.

6. Experimental and Modeling Studies

The performance of the "in-house" developed DEFC was determined by a set of tests, in order to obtain the cell polarization and power density curves. The influence of operating conditions, such as the ethanol concentration, and design parameters, such as the membrane thickness, the diffusion layer material and catalyst loading was carefully investigated. The operating and design conditions studied were selected bearing in mind the present state of the art of passive DEFCs, and the influence of the different parameters on the cell performance was explained under the light of the model predictions. As it was verified in Figure 4.7, in passive feed DEFCs the temperature rises due to the electrochemical reactions, and thus the temperature was controlled along each set of experiments in order to ensure a constant value of approximately 293 K.
The experimental polarization curves were successfully compared with the predictions of the steady-state, 1D model presented in section 4.

6.1. Model Validation

In order to validate the developed model, polarization curves generated in the simulations were compared to the experimental results. The comparison of the experimental results and the predicted polarization curves, as well as the power density curves, are presented in Figure 6.1, considering ethanol feed concentrations of 1 and 2 M. The membrane used for both modeling and experimental studies was Nafion™ 117, with anode catalyst loading of Pt–Ru/C 4.0 mg cm^{-2} and cathode catalyst loading of Pt/C 2.0 mg cm^{-2}. The diffusion layer used on both anode and cathode was carbon cloth.
The results in Figure 6.1 show that the open circuit voltage obtained experimentally is much lower than the thermodynamic equilibrium value of 1.145 V. This fact is mainly due to the phenomena of ethanol crossover, since the fuel that crosses the membrane reacts with oxygen in the cathode side, forming a mixed potential that lowers the cell efficiency. As it can be seen in Figure 6.1, the cell potential and power density is increased by the ethanol feed concentration and, in general, the model is in good agreement with the experimental results especially at low current densities. However, regarding current densities above 5 mA cm^{-2}, it is visible that the values predicted by the model are slightly higher than those obtained experimentally. This is due to the incapability of the model to predict the formation of water drops at the cathode and carbon dioxide on the anode side during the ethanol oxidation reaction, which affects the global efficiency of the process.

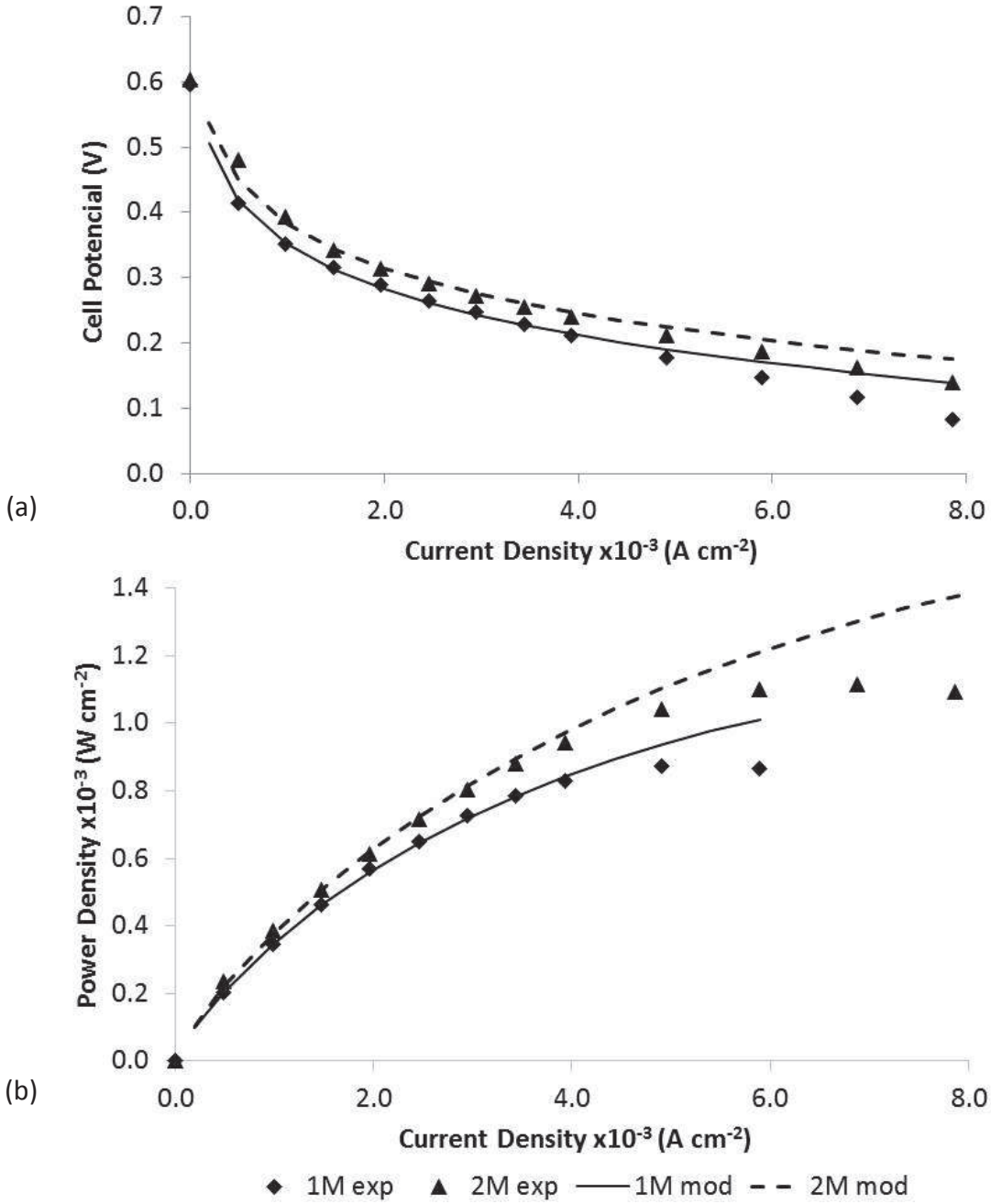

Fig. 6.1 | Comparison of the model predictions for (a) cell potential and (b) power density curves and the experimental results for different ethanol concentrations. Membrane: Nafion™ 117; Diffusion layers: Carbon Cloth; Anode: Pt–Ru/C 4.0 mg cm^{-2}; Cathode: Pt/C 2.0 mg cm^{-2}; Temperature: 293 K. Dots: experimental data; Lines: model predictions.

The carbon dioxide formation was verified during the experimental procedure, and is shown in Figure 6.2. In cases when the gaseous carbon dioxide which is formed in the anode side is not removed from the cell, the bubbles cover the effective active area for ethanol oxidation, decreasing the active sites for reaction and, consequently, decreasing the cell performance.

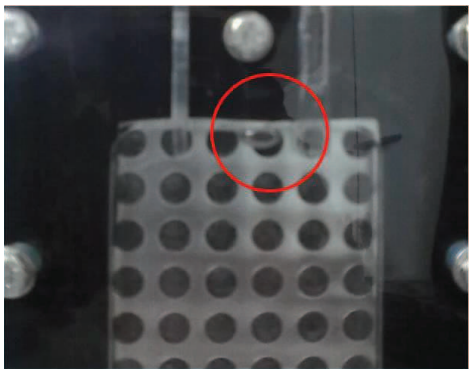

Fig. 6.2 | Carbon dioxide formation on the anode side of the cell during the experimental studies

6.2. Results and Discussion

Several sets of tests were performed to assess the performance of the passive feed DEFC under various operating conditions, by means of cell polarization and power density curves. For each condition investigated the tests were repeated until similar results were achieved, and the results were only accepted when the relative error between corresponding values was lower than 10 %.

6.2.1. Effect of the Ethanol Concentration

The effect of the ethanol feed concentration on the performance of the passive feed DEFC was studied for a range of 1 – 3 M, and the results obtained are presented in Figure 6.3. A Nafion™ 117 membrane, along with an anode catalyst loading of 4 mg cm^{-2} Pt–Ru/C and a cathode catalyst loading of 2 mg cm^{-2} Pt/C were used. Carbon cloth was applied as diffusion layer on both anode and cathode sides.

As was previously mentioned, the open circuit voltage is significantly lower than the thermodynamic equilibrium cell voltage. This occurrence is mainly due to the ethanol crossover, which permeates from the anode to the cathode creating a mixed potential, generating heat but no power.

In Figure 6.3, it is also noticeable that the cell shows better performance with an ethanol concentration of 2 M when compared to the other concentrations of 1 M or 3 M. According to these results, both the fuel cell voltage and power density increase with an increase of the ethanol feed concentration up to a concentration of 2 M, suggesting that higher concentrations have a positive effect on ethanol oxidation. However, considering concentrations beyond this range, the effect of crossover becomes more significant, affecting negatively the fuel cell performance. From this observation, it can be established that the increase of the ethanol concentration enhances the DEFC performance due to the increase on the coverage of the electro-catalytic sites; however, it may also decrease the cell performance due to the enlargement of the concentration

gradient between the anode and the cathode, generating a higher ethanol crossover (see Figure 6.4). At the cathode side, the ethanol reacts with the oxygen and generates a mixed potential leading to lower cell performances.

The increase of ethanol concentration also affects the net water transport coefficient (Figure 6.5). Low ethanol concentrations lead to higher water concentrations at the anode, increasing the water concentration gradient and inducing the water diffusion through the membrane to the cathode side. For this reason, the water transport from the anode to the cathode is lower as the ethanol concentration is increased, as can be seen in Figure 6.5.

When comparing the performances obtained for 1 M and 3 M, it can be seen that although for lower current densities the cell performance is similar concerning these concentrations, for higher current densities, higher concentrations of ethanol lead to higher power densities, and subsequent better cell efficiency. This is due to the intensification of the mass transfer rate of ethanol from the anode fuel tank to the catalyst layer, which reduces the anode voltage loss due to mass transfer polarization.

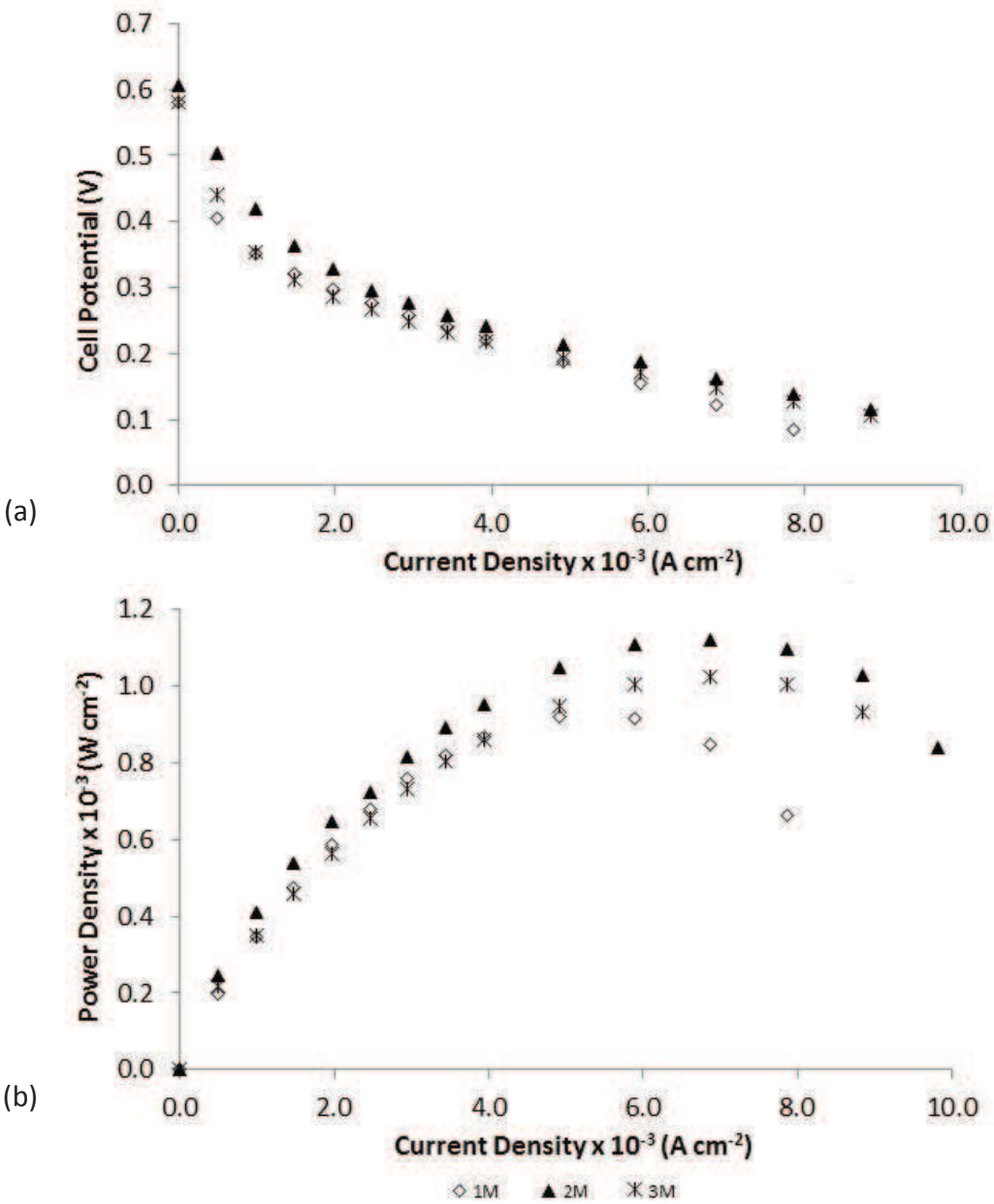

Fig. 6.3 | Influence of ethanol concentration on (a) cell voltage and (b) power density. Membrane: Nafion™ 117; Diffusion layers: Carbon Cloth; Anode: Pt–Ru/C 4.0 mg cm^{-2}; Cathode: Pt/C 2.0 mg cm^{-2}; Temperature: 293 K.

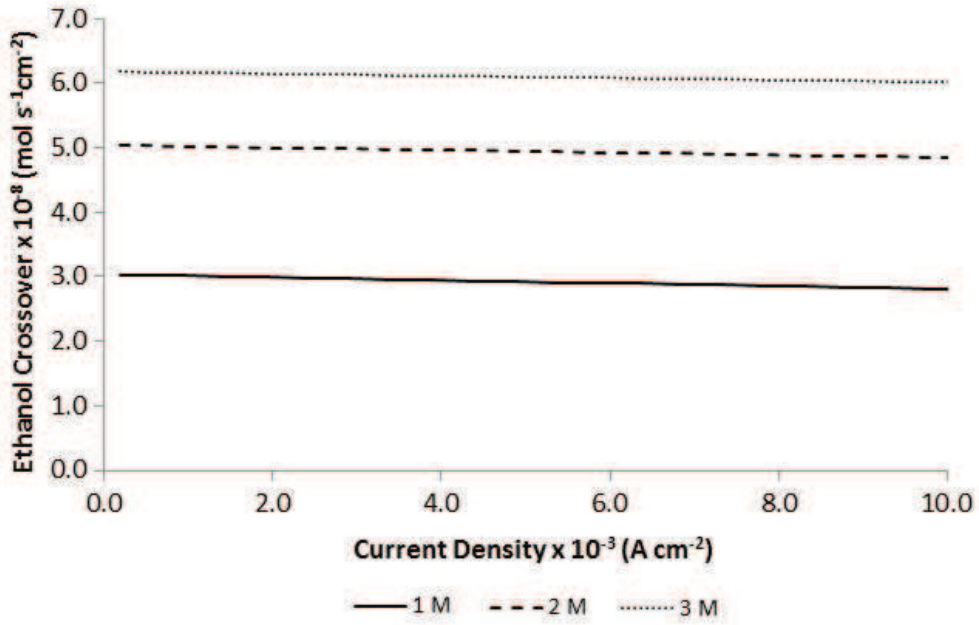

Fig. 6.4 | Predicted ethanol crossover for different ethanol concentrations. Membrane: Nafion™ 117; Diffusion layers: Carbon Cloth; Anode: Pt–Ru/C 4.0 mg cm^{-2}; Cathode: Pt/C 2.0 mg cm^{-2}; Temperature: 293 K.

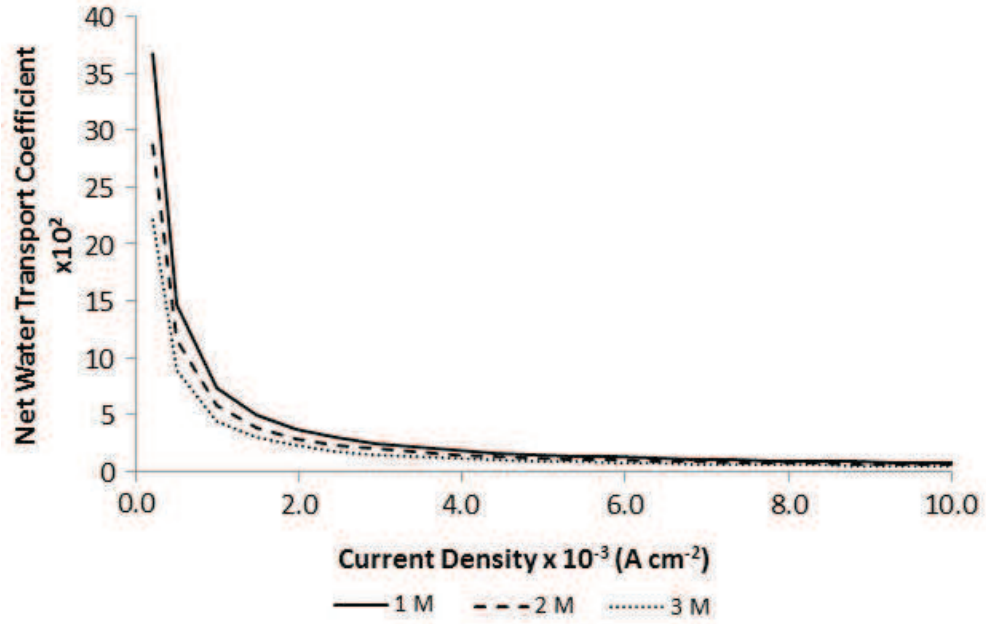

Fig. 6.5 | Predicted net water transport coefficient for different ethanol concentrations. Membrane: Nafion™ 117; Diffusion layers: Carbon Cloth; Anode: Pt–Ru/C 4.0 mg cm^{-2}; Cathode: Pt/C 2.0 mg cm^{-2}; Temperature: 293 K.

6.2.2. Effect of the Membrane Thickness

In order to assess the effect of the Membrane thickness on the performance of the passive DEFC, sets of studies were performed using Nafion™ 115 (thickness 0.127 mm), and Nafion™ 117 (thickness 0.178 mm) membranes.

Figure 6.6 presents the effect of the membrane thickness on the cell voltage (a) and on power density (b) when using ethanol feed concentrations in the range of 1 – 3 M. It is clear from the results that, for the range of ethanol concentrations investigated, the Nafion™ 115 membrane had a lower performance than the Nafion™ 117. This can be explained by the fact that although thinner membranes have lower ohmic resistances, they also present higher crossover rates leading to an increased fuel loss from the anode to the cathode (see Figure 6.7). Due to this, the influence of membrane thickness on the passive DEFC performance is a combined effect of the positive and negative effects. Considering the cell design used in the actual study, it can be concluded that the negative effect of ethanol crossover is more significant than the positive effect on lowering the ohmic resistance.

The model predictions of the ethanol crossover through the membranes Nafion 115™ and Nafion™ 117 are depicted in Figure 6.7, considering an ethanol concentration of 1M. Additionally, in Figure 6.8 it is shown the net water transport coefficient for the different membranes for an ethanol concentrations of 1M. The results presented in Figures 6.7 and 6.8 show that the ethanol crossover, as well as the water net transport coefficient, are increased when using thinner membranes. These occurrences have a negative impact on the fuel cell efficiency, since the ethanol crossover is responsible for the generation of a mixed potential, and the water crossing through the membrane can lead to cathode flooding phenomena. Therefore, the cell performance is considerably lower when thinner membranes are used. These model predictions are in good agreement with what was verified in the experimental results (Figure 6.6).

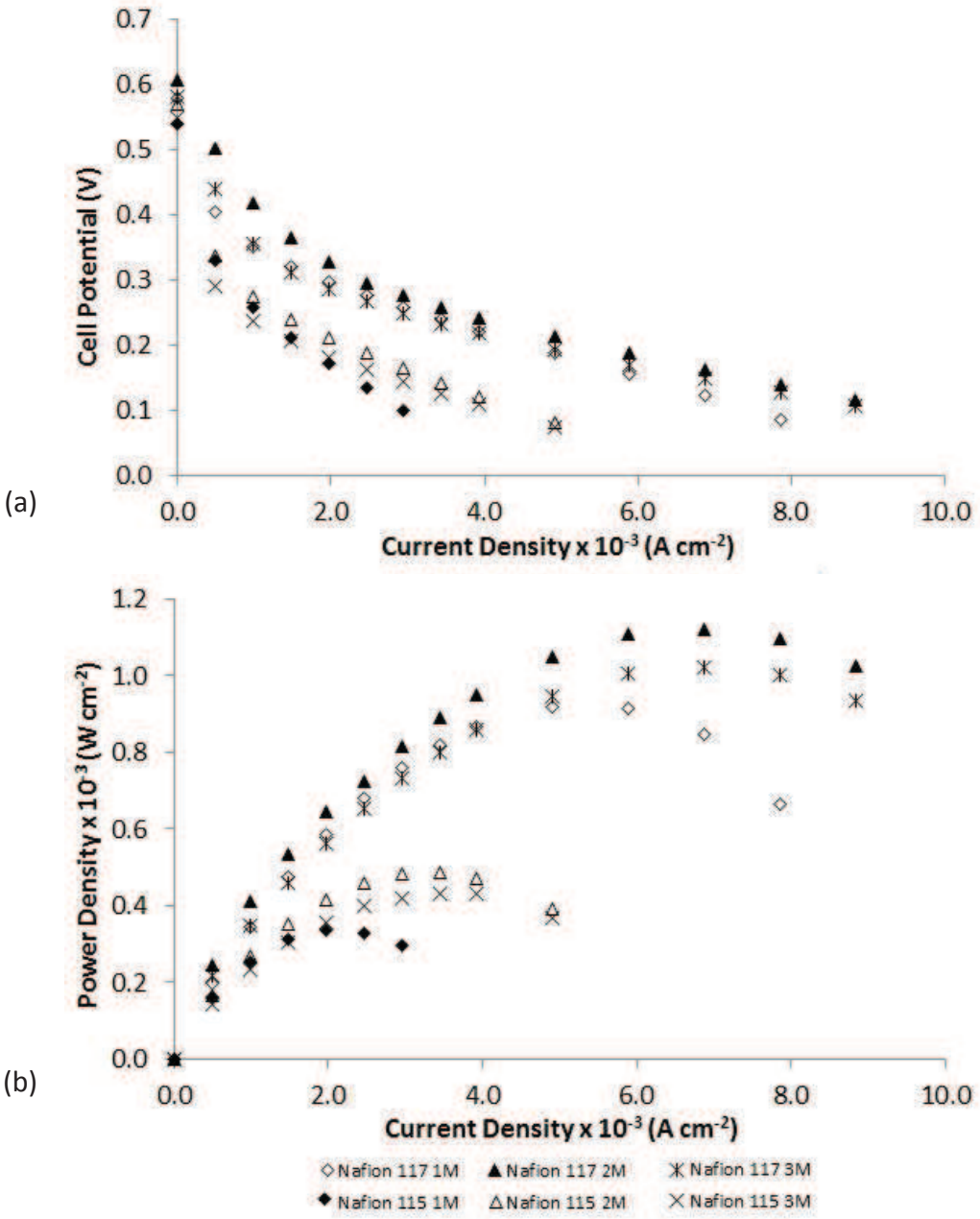

Fig. 6.6 | Influence of membrane thickness on (a) cell voltage and (b) power density for different ethanol concentrations. Diffusion layers: Carbon Cloth; Anode: Pt–Ru/C 4.0 mg cm^{-2}; Cathode: Pt/C 2.0 mg cm^{-2}; Temperature: 293 K.

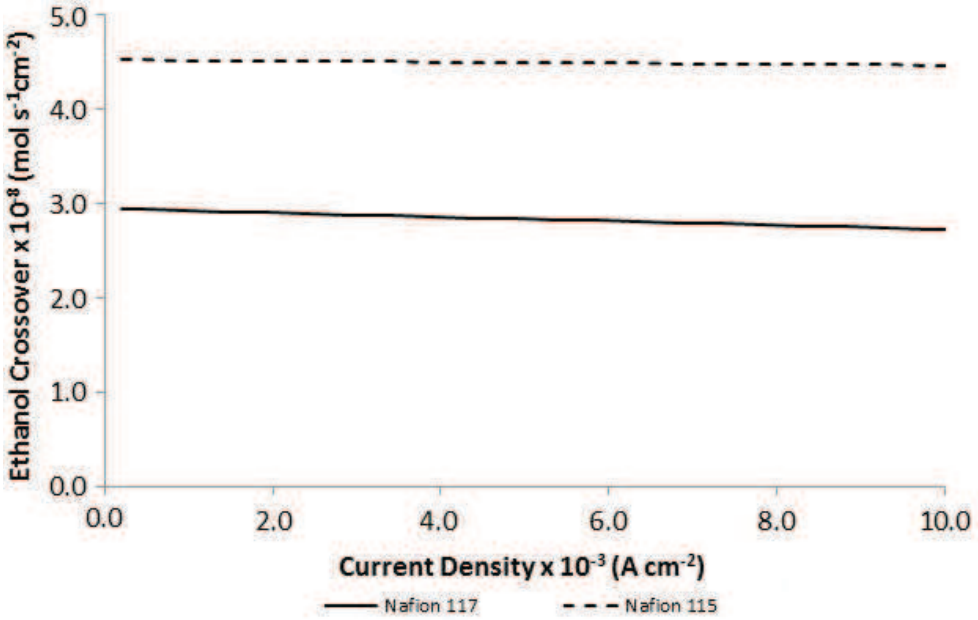

Fig. 6.7 | Predicted ethanol crossover for different membrane thicknesses. Diffusion layers: Carbon Cloth; Anode: ethanol solution 1.0 M, Pt–Ru/C 4.0 mg cm^{-2}; Cathode: Pt/C 2.0 mg cm^{-2}; Temperature: 293 K.

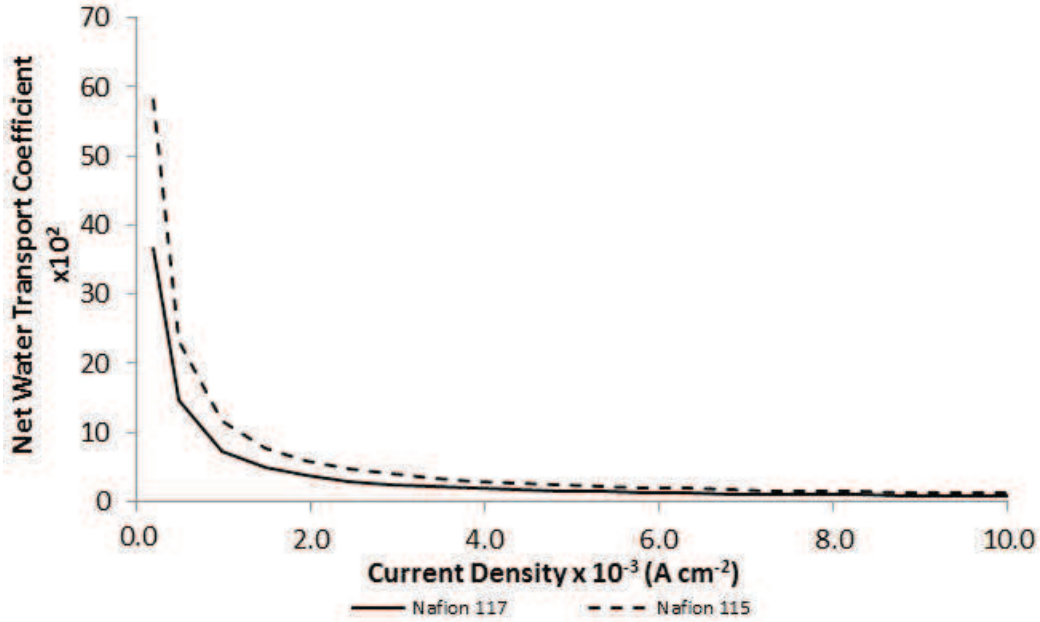

Fig. 6.8 | Predicted net water transport coefficients for different membrane thicknesses. Diffusion layers: Carbon Cloth; Anode: ethanol solution 1.0 M, Pt–Ru/C 4.0 mg cm^{-2}; Cathode: Pt/C 2.0 mg cm^{-2}; Temperature: 293 K.

6.2.3. Effect of the Anode Catalyst Loading

In order to assess the effect of the anode catalyst loading on the performance of the passive DEFC, an investigation was performed where the cathode catalyst layer loading set was Pt black 2 mg cm^{-2}, and the anode catalyst layer loading was Pt–Ru 2 mg cm^{-2} (LL – lower loading) and 4 mg cm^{-2} (HL – higher loading). The results for these conditions are depicted in Figure 6.9 concerning the fuel cell voltage (a) and power density (b).

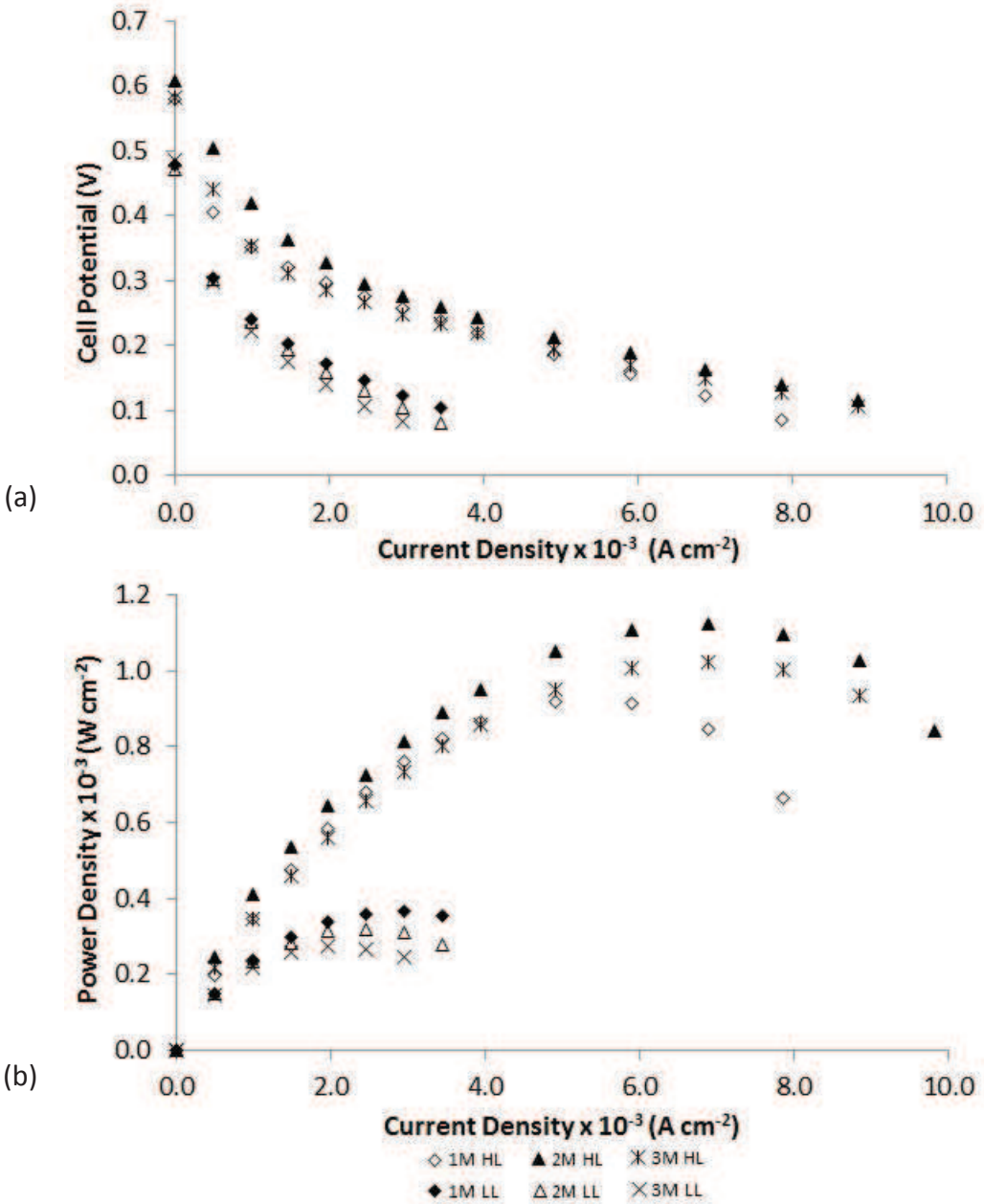

Fig. 6.9 | Influence of the anode catalyst loading on (a) cell voltage and (b) power density for different ethanol concentrations. Membrane: Nafion™ 117; Diffusion layers: Carbon Cloth; Anode: Pt–Ru/C 4.0 mg cm^{-2} (HL) or Pt–Ru/C 2.0 mg cm^{-2} (LL); Cathode: Pt/C 2.0 mg cm^{-2}; Temperature: 293 K.

It is noticeable that the open circuit voltage achieved when using a lower noble metal loading (LL) is lesser than that obtained for the same ethanol concentration when using an anode catalyst loading of 4 mg cm^{-2} Pt–Ru. Moreover, the reduction of the catalyst loading leads to a general decrease in the fuel cell performance, as it is evident in Figure 6.10. In order to understand these results, it is important to take into account the influence of the catalyst loading on the electrodes, since a variation on the catalyst layer loading affects the active surface area, as well as the electronic conductivity and the thickness of the electrode. As a result, a decrease on the catalyst loading leads to a reduction of the active surface area along with a reduction of the layer thickness, and consequently this decreases the ionic conductivity and increases the ionic resistivity.

On the other hand, if the catalyst loading is increased, the active surface area is augmented along with the active sites for the occurrence of the ethanol oxidation. This leads to a reduction of the anode overpotential, and subsequently to an increased cell performance. This is shown in Figure 6.10 where the anode overpotential predicted by the model is represented considering both catalyst loadings. Additionally, the increase of the catalyst loading also leads to an increased layer thickness, which avoids ethanol crossover in some extent, reducing the parasitic current and increasing the cell efficiency (see Figure 6.11).

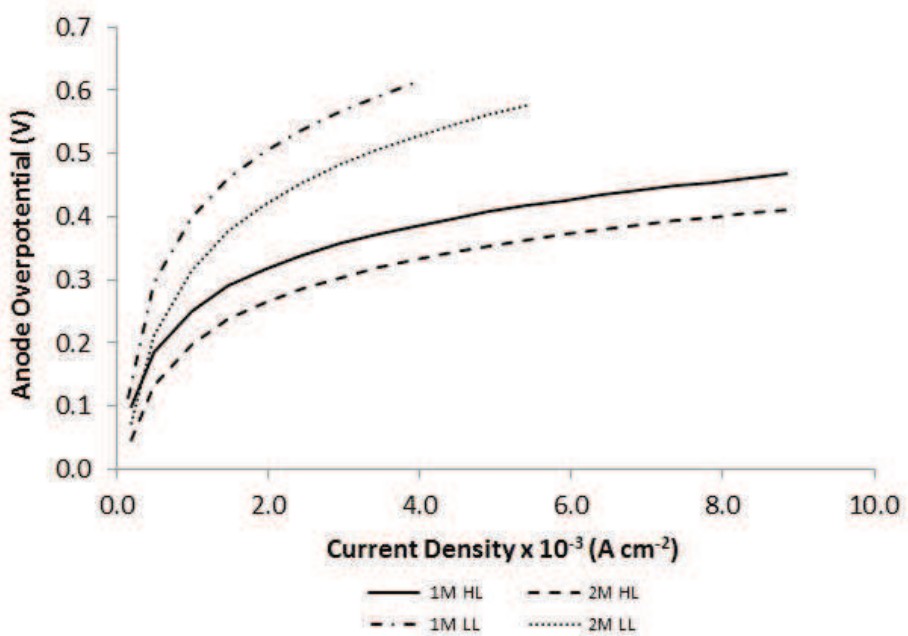

Fig. 6.10 | Model predictions for the effect of the anode catalyst loading on the anode overpotentials for different ethanol concentrations. Membrane: Nafion™ 117; Diffusion layers: Carbon Cloth; Anode: Pt–Ru/C 4.0 mg cm^{-2} (HL) or Pt–Ru/C 2.0 mg cm^{-2} (LL); Cathode: Pt/C 2.0 mg cm^{-2}; Temperature: 293 K.

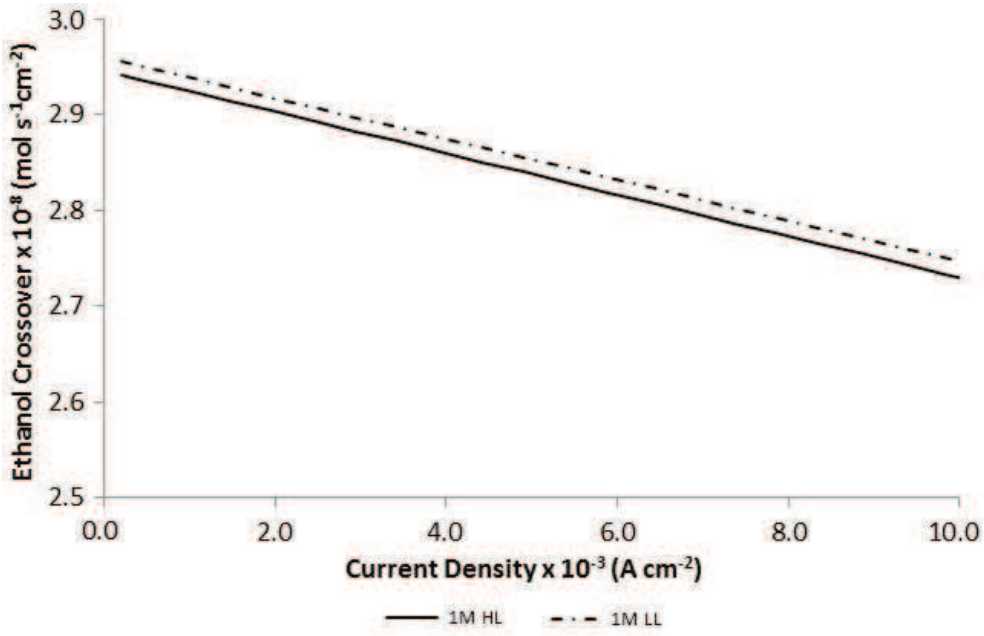

Fig. 6.11 | Model predictions for the effect of the anode catalyst loading on the ethanol crossover. Membrane: Nafion™ 117; Diffusion layers: Carbon Cloth; Anode: ethanol solution 1.0 M, Pt–Ru/C 4.0 mg cm^{-2} (HL) or Pt–Ru/C 2.0 mg cm^{-2} (LL); Cathode: Pt/C 2.0 mg cm^{-2}; Temperature: 293 K.

6.2.4. Effect of the Anode Diffusion Layer Material

The fuel cell performance may also be affected by some characteristics of the diffusion layers used, such as the thickness, wettability, roughness and tortuosity of the materials used. From these different properties may result different transport characteristics, and thus the effect of the anode diffusion layer material on the fuel cell efficiency must be analyzed. In this work, three different materials were used at the anode, namely carbon cloth (CC), carbon paper (CP) and ELAT, while on the cathode side the diffusion layer used was carbon cloth. The carbon cloth is a more porous and thicker material than carbon paper, although it is less tortuous than the latter one. The ELAT material, on the other hand, is made from carbon cloth having one side treated with PT and presents less porosity than CC, even though it is thicker and more tortuous. The characteristics of these materials are specified in Table 6.1.

Table 6.1 | Specifications of the different diffusion layer materials used in the passive feed DEFC as in Ref. [46]

Material	Porosity	Tortuosity	Thickness (cm)
CP	0.78	2.75	0.019
CC	0.83	1.11	0.035
ELAT	0.80	1.50	0.040

In Figure 6.12, the effect of the anode diffusion layer material on the cell voltage and power density is shown, considering ethanol concentrations of 1 and 2 M. As it is clear from the results, the better performances were reached when using ELAT as anode diffusion layer, for both ethanol concentrations. This is mostly due to its higher thickness which prevents ethanol crossover, since the cell efficiency is undoubtedly dependent on the ethanol crossover.

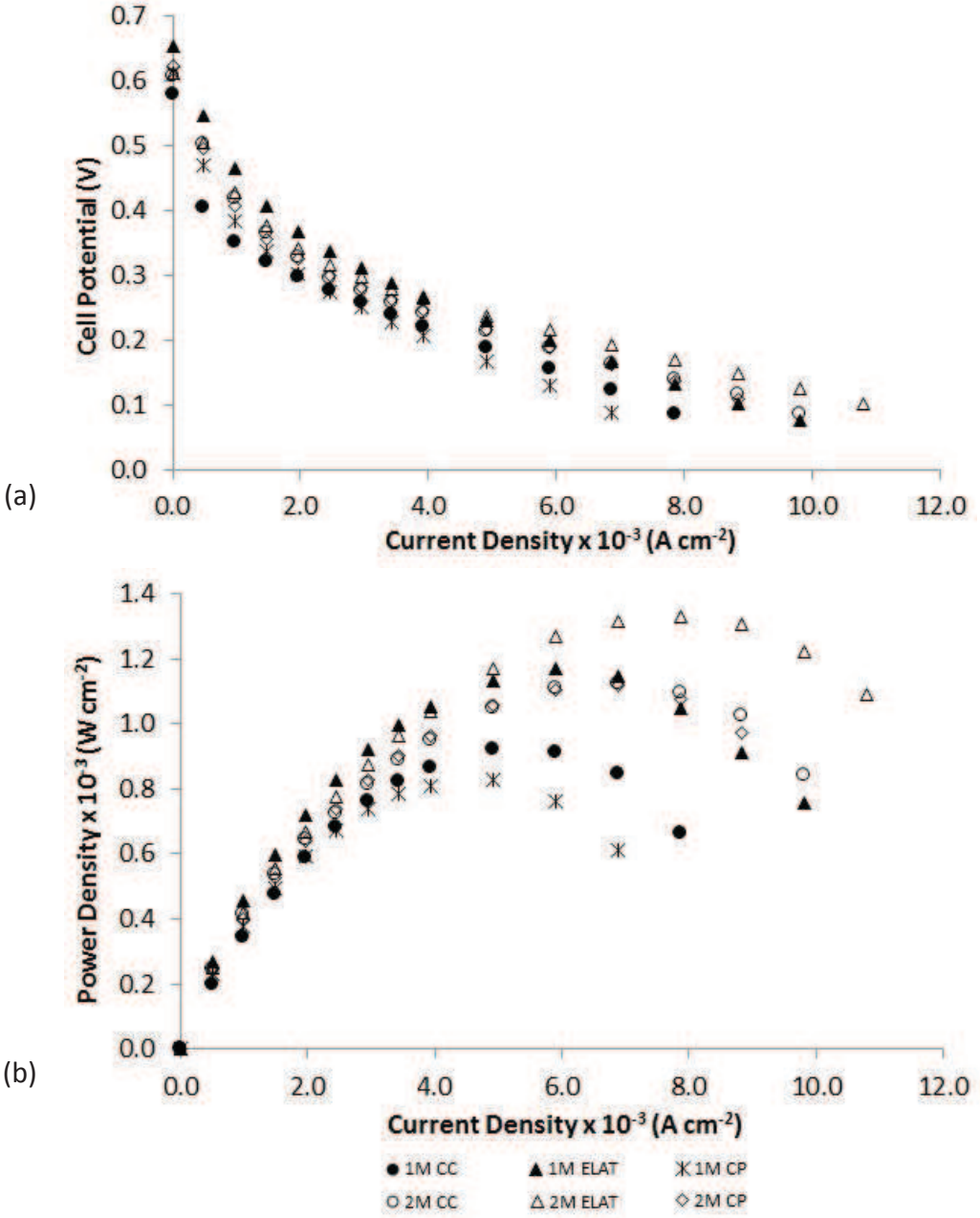

Fig. 6.12 | Influence of the anode diffusion layer material on (a) cell voltage and (b) power density for different ethanol concentrations. Membrane: Nafion™ 117; Anode: Pt–Ru/C 4.0 mg cm^{-2}; Cathode: Pt/C 2.0 mg cm^{-2}; Temperature: 293 K.

Compared to the other diffusion layer materials, it is clear from the model predictions that ELAT prevents crossover much more efficiently (see Figure 6.13). However, materials such as ELAT and carbon cloth have similar thickness layers, as it is specified in Table 6.1, and the cell performance is much higher when ELAT is used as diffusion layer. This suggests that the thickness is not the only important factor affecting the cell performance. As already referred, the ELAT suffers a previous treatment where Pt is applied on the side that is in contact with the catalyst layer, enhancing the catalyst loading in terms of noble metal. For this reason, the number of active sites for ethanol oxidation is increased, substantially reducing the anode overpotential when compared to the other materials. This is clearly shown in Figure 6.14.

In addition, the material capacity to prevent the water and the carbon dioxide accumulation at the surface of the layers greatly influences the cell performance. In Figure 6.15, the net water transport coefficient predicted by the model for the three materials used as diffusion layers is presented, for an ethanol concentration of 1M. ELAT presents the lower net water transfer coefficient, as expected, due to its higher thickness. The results show that the CP material presents a greater water flow through the membrane to the cathode, and for this reason, the use of carbon paper diffusion layers leads to a lower cell performance. Moreover, this material presents a high tortuosity, and the water molecules, as well as the carbon dioxide gas, tends to remain attached to the diffusion layer surface, blocking the active sites and preventing the ethanol oxidation reaction from occurring.

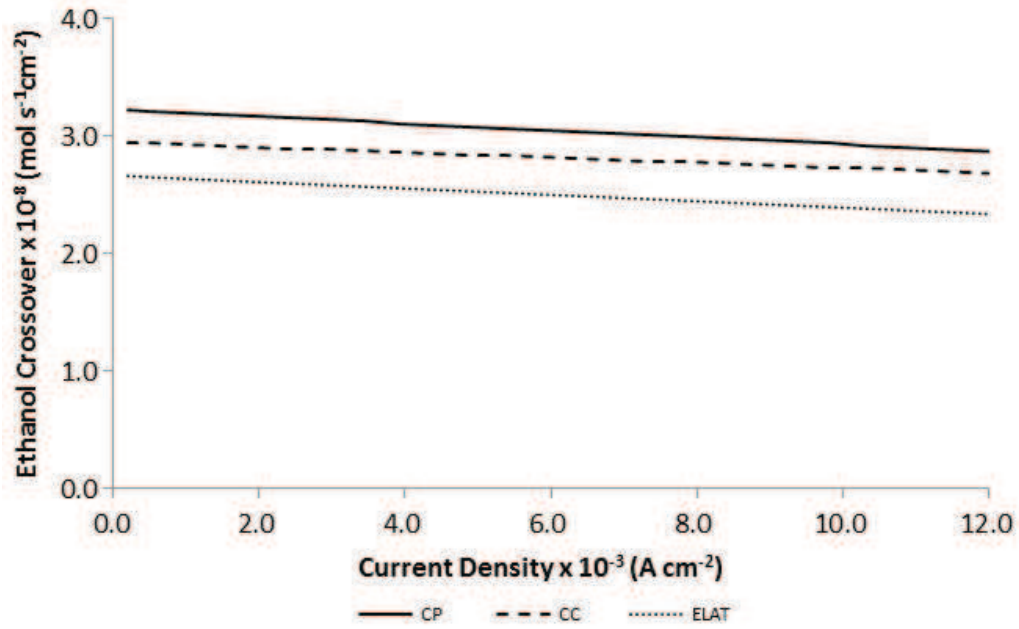

Fig. 6.13 | Predicted ethanol crossover for different anode diffusion layer materials. Membrane: Nafion™ 117; Anode: Ethanol concentration: 1M; Pt–Ru/C 4.0 mg cm^{-2}; Cathode: Pt/C 2.0 mg cm^{-2}; Temperature: 293 K.

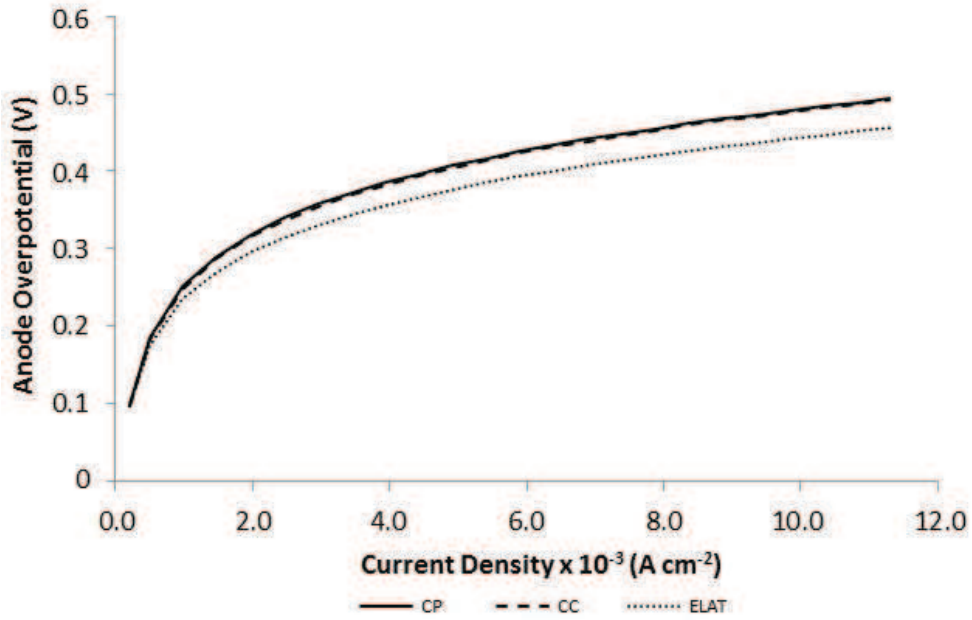

Fig. 6.14 | Predicted anode overpotentials for different anode diffusion layer materials. Membrane: Nafion™ 117; Anode: Ethanol concentration: 1M; Pt–Ru/C 4.0 mg cm^{-2}; Cathode: Pt/C 2.0 mg cm^{-2}; Temperature: 293 K.

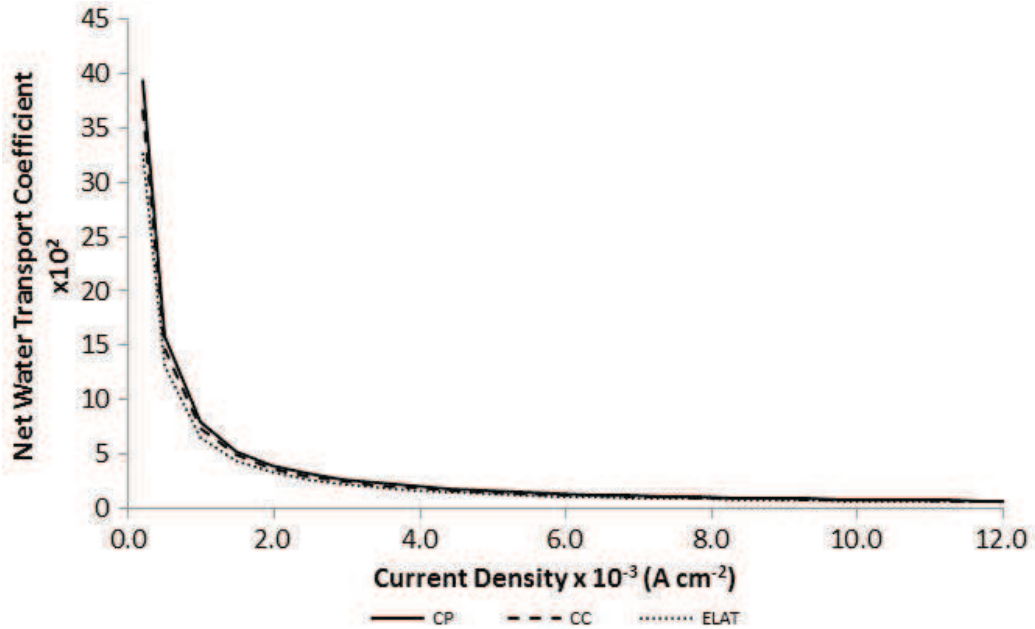

Fig. 6.15 | Predicted net water transport coefficient for different anode diffusion layer materials. Membrane: Nafion™ 117; Anode: Ethanol concentration: 1M; Pt–Ru/C 4.0 mg cm^{-2}; Cathode: Pt/C 2.0 mg cm^{-2}; Temperature: 293 K.

6.3. Concluding Remarks

The performance of a passive direct ethanol fuel cell operating at ambient conditions has been studied to systematically evaluate the effect of ethanol concentration, membrane thickness and anode diffusion layer material and loading on cell voltage and power density.

The model developed in section 4 was successfully compared to the experimental data and predicted the correct trends of the effect of ethanol concentration on fuel cell performance. Most of the experimental results were explained under the light of the predictions of the ethanol crossover rate, net water transport coefficient and anode overpotential from the developed and validated model.

In this work, it was found that simple changes concerning the design parameters of DEFCs could significantly reduce ethanol and water crossover. Increasing the membrane thickness, the anode catalyst loading or the anode diffusion layers proves to be an effective way to prevent both ethanol and water crossover. Moreover, it was found that the use of thinner membranes leads to an increase on both ethanol crossover and net water transport coefficient. On the other hand, the use of thicker diffusion layer materials such as ELAT significantly decreases the water transport from the anode to the cathode and reduces the ethanol crossover, resulting in enhanced cell performances.

The best performance was reached with an ethanol concentration of 2 M for higher current densities. It was verified that higher ethanol concentrations lead to a reduction on the net water transport coefficient, however an increase of ethanol concentration above 2 M lead to lower cell performances due to higher rates of ethanol crossover.

The results achieved in this work provide very interesting and useful information for the development of passive DEFCs. For this specific cell design, a thick anode diffusion layer coupled with a thick catalyst layer and thick membrane are suggested to reduce both water and ethanol crossover.

7. Conclusions and Suggestions for Future Work

The main goal of the present work was to allow a better comprehension of the mass and heat transport phenomena occurring in a passive feed direct ethanol fuel cell, and to evaluate the effect of the different parameters on fuel cell performance and power density. One of the main motivations of this work was to develop modeling and experimental studies that were able to counterbalance the lack of experimental characterization of DEFCs operating under ambient conditions, bearing in mind the portable applications of this type of fuel cells, as well as the introduction of passive DEFCs in the actual market. The accomplishment of the goals proposed in this work involved the following steps:

- The development of a mathematical model for passive feed DEFCs;
- Design and construction of a passive feed direct ethanol fuel cell;
- The execution of several experimental sets in order to evaluate the efficiency of the designed passive feed direct ethanol fuel cell;
- The validation of the developed mathematical model with data obtained from experimental results;
- The intensive use of the developed model to explain the results obtained experimentally.

The conclusions achieved from the investigation performed, as well as recommendations for future work are discussed below.

7.1. Conclusions

In this work, a steady-state, one-dimensional (1D) model was developed, coupling the effects of heat and mass transfer as well as the electrochemical reactions occurring in a passive feed DEFC. This model was based on the previous work developed for passive DMFCs by Oliveira et al. [5], and one of the main objectives was to accomplish a reduced model, with a comprehensive modeling of heat and mass transfer phenomena, and easily extendable structure. The model developed in this work uses simple numerical tools, like Excel, which allows the rapid prediction of the passive DEFC performance, and can be a useful tool to optimize the fuel cell design. This model allows the prediction of the effect of key operating conditions, such as ethanol feed concentration and current density, and design parameters, such as different materials used in the cell design, on both temperature and concentration profiles across the cell, and subsequently, on the general

fuel cell performance. Using this feature, the influence of these parameters on important issues such as ethanol and water crossover was deeply investigated.
The model proved to describe satisfactorily the experimental results, concerning a range of low current densities. However, it was verified that some divergences arise between the model and the experimental results for high current densities, especially due to the fact that the model neglects two-phase flow effects. Under the conditions assumed in this model, the carbon dioxide bubbles which are generated on the anode side, and the water droplets accumulating on the cathode side are neglected. Experimentally, it is known that these occurrences considerably reduce the limiting current density of the cell.
Nevertheless, the experimental studies of the passive feed DEFC were in accordance with the main results presented in the existent literature concerning active feed DEFCs. The results obtained showed that high ethanol concentrations generate lower fuel cell performances due to the higher ethanol crossover rates. However, using low ethanol concentrations considerably decreases the energy density, since a larger water volume occupies the fuel reservoir on the anode side, without generating power. For this specific cell design, the optimum ethanol concentration seems to be 2M.
Moreover, the experimental studies show that changes in the structure of the diffusion layers, in the catalyst loadings and membrane thickness, constitute effective ways of control water and methanol crossover. In particular, increasing the thicknesses of the membrane and anode diffusion layer could significantly enhance the cell performance due to the reduction of ethanol crossover. Additionally, the enlargement of the anode catalyst layer by increasing the catalyst loading could also help to improve the cell performance due to the augmentation of active sites for ethanol oxidation.
In this work the maximum power density, 1.33 mW cm^{-2}, was obtained using a Nafion™ 117 membrane, 4 mg cm^{-2} of Pt–Ru and 2 mg cm^{-2} of Pt, as respectively, anode and cathode catalyst layers, ELAT as anode diffusion layer, carbon cloth as cathode diffusion layer and an ethanol concentration of 2M.

7.2. Suggestions for Future Work

The present work is assumed as a starting point for the development of detailed experimental studies aiming to find adequate tailored membrane electrode assemblies that can provide low ethanol and water crossover rates, critical conditions needed for DEFC portable applications. In the future, additional experimental work concerning passive feed DEFCs is necessary in order to investigate the influence of parameters, such as temperature and different materials available for the MEAs, on the cell performance. The use of different and more active catalysts for the anode would also be essential.
It is known that mathematical models are a useful tool to understand the main processes occurring within a fuel cell which cannot be observed directly in the experimental work,

namely the electrochemical reactions, as well as mass and heat transport phenomena. For this reason, it is crucial to refine the present mathematical model, especially concerning the exploration of the two-phase flow effects occurring at both the anode and the cathode.

Also, an interesting suggestion for future work would be the development of a mechanistic model for the anode, which could supply details as the concentration profiles of the intermediate components within the anode and the coverage of adsorbed species on the electrode surface. This is of great significance, since the electro-oxidation of ethanol in the catalyst layer generates numerous intermediate products that block the active catalyst sites, reducing the efficiency of the fuel cell.

Additionally, the possible permeation of oxygen to the anode catalyst layer and resulting mixed potential was not discussed in this work, but this occurrence could influence the anode potential as well as the cell voltage. It would be also interesting for future work to perform an investigation of this issue.

8. References

1. Höök M. and Tang X., Depletion of fossil fuels and anthropogenic climate change—A review. Energy Policy, 2013. 52(0): p. 797-809.
2. Achmad F. et al., Passive direct methanol fuel cells for portable electronic devices. Applied Energy, 2011. 88(5): p. 1681-1689.
3. Kamarudin S.K., Achmad F., and Daud W.R.W., Overview on the application of direct methanol fuel cell (DMFC) for portable electronic devices. International Journal of Hydrogen Energy, 2009. 34(16): p. 6902-6916.
4. Faghri A., Li X., and Bahrami H., Recent advances in passive and semi-passive direct methanol fuel cells. International Journal of Thermal Sciences, 2012. 62(0): p. 12-18.
5. Oliveira V.B., Rangel C.M., and Pinto A.M.F.R., One-dimensional and non-isothermal model for a passive DMFC. Journal of Power Sources, 2011. 196(21): p. 8973-8982.
6. IEA, Key World Energy Statistics. http://www.iea.org/, 2012.
7. Thomas S. and Zalbowitz M., Fuel Cells: Green Power. 1999.
8. Bagotsky V.S., Fuel Cells: Problems and Solutions. 2012: Wiley.
9. Larminie J. and Dicks A., Fuel Cell Systems Explained. 2nd ed. ed. 2003, West Sussex, England: John Wiley & Sons Ltd. 433.
10. O'Hayre R.P., Fuel cell fundamentals. 2006: John Wiley & Sons.
11. Oliveira V.B. et al., A comparative study of approaches to direct methanol fuel cells modelling. International Journal of Hydrogen Energy, 2007. 32(3): p. 415-424.
12. Kamarudin M.Z.F. et al., Review: Direct ethanol fuel cells. International Journal of Hydrogen Energy, (0).
13. Song, S. and Tsiakaras P., Recent progress in direct ethanol proton exchange membrane fuel cells (DE-PEMFCs). Applied Catalysis B: Environmental, 2006. 63(3–4): p. 187-193.
14. Bentley J. and Derby R., Ethanol & Fuel Cells: Converging Paths of Opportunity. Renewable Fuels Association, 2002: p. 14.
15. Lamy C., et al., Recent advances in the development of direct alcohol fuel cells (DAFC). Journal of Power Sources, 2002. 105(2): p. 283-296.
16. Alzate V., Fatih K., and Wang H., Effect of operating parameters and anode diffusion layer on the direct ethanol fuel cell performance. Journal of Power Sources, 2011. 196(24): p. 10625-10631.
17. Andreadis G.M., Podias A.K.M., and Tsiakaras P.E., A model-based parametric analysis of a direct ethanol polymer electrolyte membrane fuel cell performance. Journal of Power Sources, 2009. 194(1): p. 397-407.

18. Antolini E., Catalysts for direct ethanol fuel cells. Journal of Power Sources, 2007. 170(1): p. 1-12.

19. Heysiattalab S., et al., Investigation of key parameters influence on performance of direct ethanol fuel cell (DEFC). Journal of Industrial and Engineering Chemistry, 2011. 17(4): p. 727-729.

20. Li G. and Pickup P.G., Analysis of performance losses of direct ethanol fuel cells with the aid of a reference electrode. Journal of Power Sources, 2006. 161(1): p. 256-263.

21. Jiao K. and Li X., Water transport in polymer electrolyte membrane fuel cells. Progress in Energy and Combustion Science, 2011. 37(3): p. 221-291.

22. Jablonski A., Kulesza P.J., and Lewera A., Oxygen permeation through Nafion 117 membrane and its impact on efficiency of polymer membrane ethanol fuel cell. Journal of Power Sources, 2011. 196(10): p. 4714-4718.

23. Jablonski A. and Lewera A., Electrocatalytic oxidation of ethanol on Pt, Pt-Ru and Pt-Sn nanoparticles in polymer electrolyte membrane fuel cell—Role of oxygen permeation. Applied Catalysis B: Environmental, 2012. 115–116(0): p. 25-30.

24. Andreadis G. and Tsiakaras P., Ethanol crossover and direct ethanol PEM fuel cell performance modeling and experimental validation. Chemical Engineering Science, 2006. 61(22): p. 7497-7508.

25. James D.D. and Pickup P.G., Effects of crossover on product yields measured for direct ethanol fuel cells. Electrochimica Acta, 2010. 55(11): p. 3824-3829.

26. Song S. et al., The effect of the MEA preparation procedure on both ethanol crossover and DEFC performance. Journal of Power Sources, 2005. 140(1): p. 103-110.

27. Suresh N.S. and Jayanti S., Cross-over and performance modeling of liquid-feed Polymer Electrolyte Membrane Direct Ethanol Fuel Cells. International Journal of Hydrogen Energy, 2011. 36(22): p. 14648-14658.

28. Song S. et al., The effect of methanol and ethanol cross-over on the performance of PtRu/C-based anode DAFCs. Applied Catalysis B: Environmental, 2005. 55(1): p. 65-72.

29. Song S. et al., Ethanol crossover phenomena and its influence on the performance of DEFC. Journal of Power Sources, 2005. 145(2): p. 266-271.

30. Wan C.H. and Chen C.L., Mitigating ethanol crossover in DEFC: A composite anode with a thin layer of Pt50–Sn50 nanoparticles directly deposited into Nafion® membrane surface. International Journal of Hydrogen Energy, 2009. 34(23): p. 9515-9522.

31. Ghumman A. et al., Online analysis of carbon dioxide from a direct ethanol fuel cell. Journal of Power Sources, 2009. 194(1): p. 286-290.

32. Gupta S.S. and Datta J., An investigation into the electro-oxidation of ethanol and 2-propanol for application in direct alcohol fuel cells (DAFCs). J. Chemical Science, 2005. 117(4): p. 337-344.

33. Iwasita T., The Electrocatalysis of Ethanol Oxidation, in 3rd LAMNET Workshop2002: Brazil. p. 8.

34. Kutz R.B. et al., Reaction pathways of ethanol electrooxidation on polycrystalline platinum catalysts in acidic electrolytes. Journal of Catalysis, 2011. 278(2): p. 181-188.

35. Pierozynski B., Kinetic Aspects of Ethanol Electrooxidation on Catalytic Surfaces of Pt in 0.5 MH2so4. Int. J. Electrochem. Sci, 2012. 7: p. 3327-3338.

36. Song S., Wang Y., and Shen P., Thermodynamic and Kinetic Considerations for Ethanol Electrooxidation in Direct Ethanol Fuel Cells. Chinese Journal of Catalysis, 2007. 28(9): p. 752-754.

37. Taneda K. and Yamazaki Y., Study of direct type ethanol fuel cells: Analysis of anode products and effect of acetaldehyde. Electrochimica Acta, 2006. 52(4): p. 1627-1631.

38. Spiegel C., PEM Fuel Cell Modeling and Simulation Using Matlab. 2008: Elsevier Science.

39. www.fuelcelltoday.com

40. Zhang J., PEM Fuel Cell Electrocatalysts and Catalyst Layers: Fundamentals and Applications. 2008: Springer-Verlag.

41. Oliveira V.B., Rangel C.M., and Pinto A.M.F.R., Effect of anode and cathode flow field design on the performance of a direct methanol fuel cell. Chemical Engineering Journal, 2010. 157(1): p. 174-180.

42. Oliveira V.B., Rangel C.M., and Pinto A.M.F.R., Performance of a Direct Methanol Fuel Cell Operating Close to Room Temperature. Journal of Fuel Cell Science and Technology, 2011. 8.

43. García B.L. et al., Mathematical Model of a Direct Methanol Fuel Cell. Journal of Fuel Cell Science and Technology, 2004. 1: p. 43-48.

44. Meyers J.P. and Newman J., Simulation of the Direct Methanol Fuel Cell-II. Modeling and data analysis of transport and kinetic phenomena. Journal of the Electrochemical Society, 2002. 149: p. A718-A728.

45. Oliveira V.B. et al., Heat and mass transfer effects in a direct methanol fuel cell: A 1D model. International Journal of Hydrogen Energy, 2008. 33(14): p. 3818-3828.

46. Oliveira V.B., Rangel C.M., and Pinto A.M.F.R., Modelling and experimental studies on a direct methanol fuel cell working under low methanol crossover and high methanol concentrations. International Journal of Hydrogen Energy, 2009. 34(15): p. 6443-6451.

47. Oliveira V.B., Rangel C.M., and Pinto A.M.F.R., Water management in direct methanol fuel cells. International Journal of Hydrogen Energy, 2009. 34(19): p. 8245-8256.

48. Davis S.C., Anderson-Teixeira K.J., and DeLucia E.H., Life-cycle analysis and the ecology of biofuels. Trends in Plant Science, 2009. 14(3): p. 140-146.

49. Barbora L. et al., A novel composite Nafion membrane for direct alcohol fuel cells. Journal of Membrane Science, 2009. 326(2): p. 721-726.

50. Basu S., Agarwal A., and Pramanik H., Improvement in performance of a direct ethanol fuel cell: Effect of sulfuric acid and Ni-mesh. Electrochemistry Communications, 2008. 10(9): p. 1254-1257.

51. Chikh L., Delhorbe V., and Fichet O., (Semi-)Interpenetrating polymer networks as fuel cell membranes. Journal of Membrane Science, 2011. 368(1–2): p. 1-17.

52. Elliott J.A. et al., The swelling behaviour of perfluorinated ionomer membranes in ethanol/water mixtures. Polymer, 2001. 42(5): p. 2251-2253.

53. Gomes A.d.S. and Dutra Filho J.C., Hybrid membranes of PVA for direct ethanol fuel cells (DEFCs) applications. International Journal of Hydrogen Energy, 2012. 37(7): p. 6246-6252.

54. Maab H. and Nunes S.P., Modified SPEEK membranes for direct ethanol fuel cell. Journal of Power Sources, 2010. 195(13): p. 4036-4042.

55. Roelofs K.S. and Schiestel T., sPEEK based composite membranes for direct ethanol fuel cell applications. Desalination, 2010. 250(3): p. 1051-1052.

56. Andreadis G., Song S., and Tsiakaras P., Direct ethanol fuel cell anode simulation model. Journal of Power Sources, 2006. 157(2): p. 657-665.

57. Meyer M., Melke J., and Gerteisen D., Modelling and simulation of a direct ethanol fuel cell considering multistep electrochemical reactions, transport processes and mixed potentials. Electrochimica Acta, 2011. 56(11): p. 4299-4307.

58. Pramanik H. and Basu S., Modeling and experimental validation of overpotentials of a direct ethanol fuel cell. Chemical Engineering and Processing: Process Intensification, 2010. 49(7): p. 635-642.

59. Siegel C., Review of computational heat and mass transfer modeling in polymer-electrolyte-membrane (PEM) fuel cells. Energy, 2008. 33(9): p. 1331-1352.

60. Sousa Jr R. et al., Modeling and simulation of the anode in direct ethanol fuels cells. Journal of Power Sources, 2008. 180(1): p. 283-293.

61. Zhu Y. et al., Development of a passive direct methanol fuel cell (DMFC) twin-stack for long-term operation. Journal of Power Sources, 2009. 193(2): p. 649-655.

62. Cao J. et al., Double microporous layer cathode for membrane electrode assembly of passive direct methanol fuel cells. International Journal of Hydrogen Energy, 2010. 35(10): p. 4622-4629.

63. Eccarius S. et al., Passively operated vapor-fed direct methanol fuel cells for portable applications. Journal of Power Sources, 2008. 182(2): p. 565-579.

64. Ward T., Li X., and Faghri A., Performance characteristics of a novel tubular-shaped passive direct methanol fuel cell. Journal of Power Sources, 2011. 196(15): p. 6264-6273.

65. Cai W. et al., Transient behavior analysis of a new designed passive direct methanol fuel cell fed with highly concentrated methanol. Journal of Power Sources, 2011. 196(8): p. 3781-3789.

66. Yuan W. et al., Structural diversity and orientation dependence of a liquid-fed passive air-breathing direct methanol fuel cell. International Journal of Hydrogen Energy, 2012. 37(11): p. 9298-9313.

67. Chen R. and Zhao T.S., Porous current collectors for passive direct methanol fuel cells. Electrochimica Acta, 2007. 52(13): p. 4317-4324.

68. Zhang J. et al., The function of hydrophobic cathodic backing layers for high energy passive direct methanol fuel cell. Journal of Power Sources, 2011. 196(22): p. 9510-9515.

69. Faghri A. and Guo Z., An innovative passive DMFC technology. Applied Thermal Engineering, 2008. 28(13): p. 1614-1622.

70. Feng L. et al., Fabrication and performance evaluation for a novel small planar passive direct methanol fuel cell stack. Fuel, 2012. 94(0): p. 401-408.

71. Chen R. and Zhao T.S., Mathematical modeling of a passive-feed DMFC with heat transfer effect. Journal of Power Sources, 2005. 152(0): p. 122-130.

72. Chan Y.H. et al., A self-regulated passive fuel-feed system for passive direct methanol fuel cells. Journal of Power Sources, 2008. 176(1): p. 183-190.

73. Liu J.G. et al., Effect of membrane thickness on the performance and efficiency of passive direct methanol fuel cells. Journal of Power Sources, 2006. 153(1): p. 61-67.

74. Higa M. et al., Performance of passive direct methanol fuel cell with poly(vinyl alcohol)-based polymer electrolyte membranes. International Journal of Hydrogen Energy, 2012. 37(7): p. 6292-6301.

75. Guo Z. and Cao Y., A passive fuel delivery system for portable direct methanol fuel cells. Journal of Power Sources, 2004. 132(1–2): p. 86-91.

76. Yousefi S. and Ganji D.D., Experimental investigation of a passive direct methanol fuel cell with 100cm2 active areas. Electrochimica Acta, 2012. 85(0): p. 693-699.

77. He Y.L., Miao Z., and Yang W.W., Characteristics of heat and mass transport in a passive direct methanol fuel cell operated with concentrated methanol. Journal of Power Sources, 2012. 208(0): p. 180-186.

78. Pan Y.H., Advanced air-breathing direct methanol fuel cells for portable applications. Journal of Power Sources, 2006. 161(1): p. 282-289.

79. Cai W., et al. Design and simulation of a liquid electrolyte passive direct methanol fuel cell with low methanol crossover. Journal of Power Sources, 2011. 196(18): p. 7616-7626.

80. Oliveira V.B. et al., Water management in a passive direct methanol fuel cell. International Journal of Energy Research, 2012.

81. Xu C. et al., Methanol and water crossover in a passive liquid-feed direct methanol fuel cell. International Journal of Hydrogen Energy, 2010. 35(4): p. 1769-1777.

82. Xu C., Faghri A., and Li X., Improving the water management and cell performance for the passive vapor-feed DMFC fed with neat methanol. International Journal of Hydrogen Energy, 2011. 36(14): p. 8468-8477.

83. Li X., Faghri A., and Xu C., Water management of the DMFC passively fed with a high-concentration methanol solution. International Journal of Hydrogen Energy, 2010. 35(16): p. 8690-8698.

84. Bae B. et al., Performance evaluation of passive DMFC single cells. Journal of Power Sources, 2006. 158(2): p. 1256-1261.

85. Zheng W. et al., A new structure of a passive direct methanol fuel cell. Chemical Engineering Science, 2012. 76(0): p. 188-191.

86. Torres N. et al., Performance optimization of a passive silicon-based micro-direct methanol fuel cell. Sensors and Actuators B: Chemical, 2008. 132(2): p. 540-544.

87. Feng L. et al., Single passive direct methanol fuel cell supplied with pure methanol. Journal of Power Sources, 2011. 196(5): p. 2750-2753.

88. Li X., Faghri A., and Xu C., Structural optimization of the direct methanol fuel cell passively fed with a high-concentration methanol solution. Journal of Power Sources, 2010. 195(24): p. 8202-8208.

89. Lufrano F. et al., Investigation of sulfonated polysulfone membranes as electrolyte in a passive-mode direct methanol fuel cell mini-stack. Journal of Power Sources, 2010. 195(23): p. 7727-7733.

90. Yuan T. et al., Enhanced performance of a passive direct methanol fuel cell with decreased Nafion aggregate size within the anode catalytic layer. International Journal of Hydrogen Energy, 2011. 36(16): p. 10000-10005.

91. Bahrami H. and Faghri A., Exergy analysis of a passive direct methanol fuel cell. Journal of Power Sources, 2011. 196(3): p. 1191-1204.

92. Jewett G., Guo Z., and Faghri A., Performance characteristics of a vapor feed passive miniature direct methanol fuel cell. International Journal of Heat and Mass Transfer, 2009. 52(19–20): p. 4573-4583.

93. Kim D. et al., Recent progress in passive direct methanol fuel cells at KIST. Journal of Power Sources, 2004. 130(1–2): p. 172-177.

94. Shaffer C.E. and Wang C.Y., High concentration methanol fuel cells: Design and theory. Journal of Power Sources, 2010. 195(13): p. 4185-4195.

95. Sundarrajan S., Allakhverdiev S.I., and Ramakrishna S., Progress and perspectives in micro direct methanol fuel cell. International Journal of Hydrogen Energy, 2012. 37(10): p. 8765-8786.

96. Yang W.W., Zhao T.S., and Wu Q.X., Modeling of a passive DMFC operating with neat methanol. International Journal of Hydrogen Energy, 2011. 36(11): p. 6899-6913.

97. Yeh T.K. and Chen C.H., Modeling and optimizing the performance of a passive direct methanol fuel cell. Journal of Power Sources, 2008. 175(1): p. 353-362.

98. Zhao T.S. et al., Small direct methanol fuel cells with passive supply of reactants. Journal of Power Sources, 2009. 191(2): p. 185-202.

99. Shimizu T. et al., Design and fabrication of pumpless small direct methanol fuel cells for portable applications. Journal of Power Sources, 2004. 137(2): p. 277-283.

100. Yuan W. et al., Operational characteristics of a passive air-breathing direct methanol fuel cell under various structural conditions. International Journal of Hydrogen Energy, 2011. 36(3): p. 2237-2249.

101. Ye Q. and Zhao T.S., A natural-circulation fuel delivery system for direct methanol fuel cells. Journal of Power Sources, 2005. 147(1-2): p. 196-202.

102. Tang Y. et al., Effects of structural aspects on the performance of a passive air-breathing direct methanol fuel cell. Journal of Power Sources, 2010. 195(17): p. 5628-5636.

103. Quadros F.M. et al., Estudo de eletrocatalisadores PtNiRu para célula a combustível de etanol direto passiva. Sociedade Brasileira de Química, 2010: p. 1.

104. Yuan W. et al., Porous metal materials for polymer electrolyte membrane fuel cells – A review. Applied Energy, 2012. 94(0): p. 309-329.

105. Song S.Q. et al., Direct ethanol PEM fuel cells: The case of platinum based anodes. International Journal of Hydrogen Energy, 2005. 30(9): p. 995-1001.

106. Zhou W.J. et al., Performance comparison of low-temperature direct alcohol fuel cells with different anode catalysts. Journal of Power Sources, 2004. 126(1–2): p. 16-22.

107. Zhou W. et al., Pt based anode catalysts for direct ethanol fuel cells. Applied Catalysis B: Environmental, 2003. 46(2): p. 273-285.

108. Zhou W.J. et al., Pt-based anode catalysts for direct ethanol fuel cells. Solid State Ionics, 2004. 175(1–4): p. 797-803.

109. Zhou W.J. et al., Direct ethanol fuel cells based on PtSn anodes: the effect of Sn content on the fuel cell performance. Journal of Power Sources, 2005. 140(1): p. 50-58.

110. Antolini E., Colmati F., and Gonzalez E.R., Effect of Ru addition on the structural characteristics and the electrochemical activity for ethanol oxidation of carbon

supported Pt–Sn alloy catalysts. Electrochemistry Communications, 2007. 9(3): p. 398-404.

111. Cunha E.M. et al., Preparation, characterization and application of Pt–Ru–Sn/C trimetallic electrocatalysts for ethanol oxidation in direct fuel cell. International Journal of Hydrogen Energy, 2011. 36(17): p. 11034-11042.

112. Camara G.A., de Lima R.B., and Iwasita T., The influence of PtRu atomic composition on the yields of ethanol oxidation: A study by in situ FTIR spectroscopy. Journal of Electroanalytical Chemistry, 2005. 585(1): p. 128-131.

113. Lee C.G., Umeda M., and Uchida I., Cyclic voltammetric analysis of C1–C4 alcohol electrooxidations with Pt/C and Pt–Ru/C microporous electrodes. Journal of Power Sources, 2006. 160(1): p. 78-89.

114. Liu Z. et al., Preparation and characterization of Pt/C and PtRu/C electrocatalysts for direct ethanol fuel cells. Journal of Power Sources, 2005. 149(0): p. 1-7.

115. Purgato F.L.S. et al., Direct ethanol fuel cell: Electrochemical performance at 90ºC on Pt and PtSn/C electrocatalysts. Journal of Power Sources, 2012. 198(0): p. 95-99.

116. Simões F.C. et al., Electroactivity of tin modified platinum electrodes for ethanol electrooxidation. Journal of Power Sources, 2007. 167(1): p. 1-10.

117. Spinacé E.V. et al., PtSn/C electrocatalysts prepared by different methods for direct ethanol fuel cell, in Studies in Surface Science and Catalysis, M.D.D.E.D.V.S.H.P.A.J.J.A.M. E.M. Gaigneaux and P. Ruiz, Editors. 2006, Elsevier. p. 617-624.

118. Antolini E., An empirical model to evaluate the contribution of alloyed and non-alloyed tin to the ethanol oxidation reaction on Pt-Sn/C catalysts based on the presence of SnO2 and a Pt(1−x)Snx solid solution: Application to DEFC performance. International Journal of Hydrogen Energy, 2011. 36(17): p. 11043-11047.

119. Ribadeneira E. and Hoyos B.A., Evaluation of Pt–Ru–Ni and Pt–Sn–Ni catalysts as anodes in direct ethanol fuel cells. Journal of Power Sources, 2008. 180(1): p. 238-242.

120. Nakagawa N. et al., Product distribution and the reaction kinetics at the anode of direct ethanol fuel cell with Pt/C, PtRu/C and PtRuRh/C. Journal of Power Sources, 2012. 199(0): p. 103-109.

121. Neto O.A. et al., Eletro-oxidação de etanol sobre eletrocatalisadores PtRh/C, PtSn/C e PtSnRh/C preparados pelo método da redução por álcool. ECLÉTICA Química, 2006. 31(1): p. 81-88.

122. Tayal J., Rawat B., and Basu S., Bi-metallic and tri-metallic Pt–Sn/C, Pt–Ir/C, Pt–Ir–Sn/C catalysts for electro-oxidation of ethanol in direct ethanol fuel cell. International Journal of Hydrogen Energy, 2011. 36(22): p. 14884-14897.

123. Goel J. and Basu S., Pt-Re-Sn as Metal Catalysts for Electro-Oxidation of Ethanol in Direct Ethanol Fuel Cell. Energy Procedia, 2012. 28(0): p. 66-77.

124. Tayal J., Rawat B., and Basu S., Effect of addition of rhenium to Pt-based anode catalysts in electro-oxidation of ethanol in direct ethanol PEM fuel cell. International Journal of Hydrogen Energy, 2012. 37(5): p. 4597-4605.

125. Iwasita T., Electrocatalysis of methanol oxidation. Electrochimica Acta, 2002. 47(22–23): p. 3663-3674.

126. Li G. and Pickup P.G., The promoting effect of Pb on carbon supported Pt and Pt/Ru catalysts for electro-oxidation of ethanol. Electrochimica Acta, 2006. 52(3): p. 1033-1037.

127. Oliveira Neto A. et al., Electro-oxidation of methanol and ethanol on Pt–Ru/C and Pt–Ru–Mo/C electrocatalysts prepared by Bönnemann's method. Journal of the European Ceramic Society, 2003. 23(15): p. 2987-2992.

128. Lee E., Murthy A., and Manthiram A., Effect of Mo addition on the electrocatalytic activity of Pt–Sn–Mo/C for direct ethanol fuel cells. Electrochimica Acta, 2011. 56(3): p. 1611-1618.

129. Lopes T., Antolini E., and Gonzalez E.R., Carbon supported Pt–Pd alloy as an ethanol tolerant oxygen reduction electrocatalyst for direct ethanol fuel cells. International Journal of Hydrogen Energy, 2008. 33(20): p. 5563-5570.

130. Belchor P.M., Forte M.M.C., and Carpenter D.E.O.S., Parallel serpentine-baffle flow field design for water management in a proton exchange membrane fuel cell. International Journal of Hydrogen Energy, 2012. 37(16): p. 11904-11911.

131. Nowak A.P. et al., A conductive and hydrophilic bipolar plate coating for enhanced proton exchange membrane fuel cell performance and water management. Journal of Power Sources, 2012. 210(0): p. 138-145.

132. http://www.h2carblog.com/

133 http://worldlesstech.com/

134. Çengel Y.A., Heat Transfer - A Practical Approach. 2nd edition ed. 2003: McGraw-Hill. 932.

135. Barbir F., PEM Fuel Cells: Theory and Practice, Elsevier Academic Press, Oxford, 2005.

136. Perry, R.H. and Chilton, C.H., Chemical Engineers' Handbook, Fifth edition, McGraw-Hill, 1973.

137. Reid R.C., Prausnitz J.M., Sherwood T.K., The Properties of Gases and Liquids, McGraw-Hill, 1977.

138. Sherwood T.K., Pigford R.L., Wilke C.R., Mass Transfer, McGraw-Hill, 1975.

139. Wang Y., Wang C.Y. and Chen K.S., Elucidating differences between carbon paper and carbon cloth in polymer electrolyte fuel cells, Electrochimica Acta 2007 (52): p. 3695–9375.

Appendices

Appendix A: Uncertainty Analysis

For a given parameter $X = f(x_1, x_2, \ldots, x_n)$, where the uncertainty of each measured variable is denoted by $\delta x_1, \delta x_2, \ldots, \delta x_n$, it is known that the uncertainty of the parameter X is given by the uncertainty analysis approach according to [136]:

$$(\delta X)^2 = \left(\frac{\partial X}{\partial x_1}\delta x_1\right)^2 + \left(\frac{\partial X}{\partial x_2}\delta x_2\right)^2 + \cdots + \left(\frac{\partial X}{\partial x_n}\delta x_n\right)^2 \quad \text{(A.1)}$$

Thus, this approach was used to evaluate the uncertainty of the parameters affecting the experimental results as described in the following sections.

A.1. Ethanol concentration

The ethanol solutions used in the tests performed with the passive feed DEFC were prepared in agreement with the following equation:

$$C_{final} = \frac{V_{initial}}{V_{final}} C_{initial} \quad \text{(A.2)}$$

where $C_{initial}$ and C_{final} stand for the initial and final ethanol concentrations, respectively, and $V_{initial}$ and V_{final} are the initial and final solution volumes. According to the general uncertainty approach, the uncertainty of C_{final} can be determined from:

$$\left(\delta C_{final}\right)^2 = \left(\frac{\partial C_{final}}{\partial V_{initial}}\delta V_{initial}\right)^2 + \left(\frac{\partial C_{final}}{\partial V_{final}}\delta V_{final}\right)^2 \quad \text{(A.3)}$$

where $\delta V_{initial}$ and δV_{final} represent the uncertainties related to the measured volumes.

Equation A.3 can be written in the following form:

$$\left(\frac{\delta C_{final}}{C_{final}}\right)^2 = \left(\frac{\delta V_{initial}}{V_{initial}}\right)^2 + \left(\frac{\delta V_{final}}{V_{final}}\right)^2 \quad \text{(A.4)}$$

And the relative uncertainty of the ethanol concentration can thus be determined from:

$$\frac{\delta C_{final}}{C_{final}} = \sqrt{\left(\frac{\delta V_{initial}}{V_{initial}}\right)^2 + \left(\frac{\delta V_{final}}{V_{final}}\right)^2} \quad \text{(A.5)}$$

The ethanol solutions were prepared in a volumetric flask with a final volume of 50 $\pm$ 0.06 mL. The values of the uncertainties regarding the ethanol concentrations used in the passive DEFC are in table A.1.

Table A.1 | Values of parameters and uncertainties regarding the ethanol concentration

Ethanol concentration (M)	$V_{initial}$ (mL)	$\delta V_{initial}$ (mL)	$\delta C_{final} / C_{final}$ (%)
1	2	0.01	0.51
2	4	0.03	0.76
3	6	0.03	0.51

A.2. Current

The overall uncertainty of the current given by the system is ± 5 % of the current applied to the fuel cell. The values of the cell currents I_{cell} and the uncertainties concerning this parameter are depicted in Table A.2.

Table A.2 | Values of parameters and uncertainties regarding the cell current

I_{cell} (mA cm^{-2})	δI_{cell} (A cm^{-2})	$\delta I_{cell} / I_{cell}$ (%)
1.0		
3.0		
5.0	± 5 % $\times$ I_{cell}	5
7.0		
9.0		

A.3. Potential

The uncertainty associated with the cell potential V_{cell} is mainly related to the uncertainty of the measurement. The overall uncertainties for this parameter are showed in Table A.3.

Table A.3 | Values of parameters and uncertainties regarding the cell potential

V_{cell} (V)	δV_{cell} (V)	$\delta V_{cell} / V_{cell}$ (%)
0.1		0.50
0.2		0.25
0.3	0.0005	0.17
0.4		0.13
0.5		0.10

A.4. Power

The power density presented in the results is determined by using the following formula:

$$P = I_{cell} V_{cell} \quad \text{(A.6)}$$

The uncertainty of the resulting variable P is given by the general uncertainty approach by:

$$(\delta P)^2 = \left(\frac{\partial P}{\partial I_{cell}}\delta I_{cell}\right)^2 + \left(\frac{\partial P}{\partial V_{cell}}\delta V_{cell}\right)^2 \quad \text{(A.7)}$$

Equation A.7 can be rewritten in the following form:

$$\frac{\delta P}{P} = \sqrt{\left(\frac{\delta I_{cell}}{I_{cell}}\right)^2 + \left(\frac{\delta V_{cell}}{V_{cell}}\right)^2} \quad \text{(A.8)}$$

and the uncertainties regarding the cell potential can be determined. The calculated uncertainties for the cell power are shown in Table A.4.

Table A.4 | Values of parameters and uncertainties regarding the cell power

P (mW cm^{-2})	$\delta I_{cell}/I_{cell}$ (%)	$\delta V_{cell}/V_{cell}$ (%)	$\delta P/P$ (%)
0.1	0.05	0.0050	5.02
0.2	0.05	0.0025	5.00
0.3	0.05	0.0017	5.00
0.4	0.05	0.0013	5.00
0.5	0.05	0.0010	5.00

Appendix B: Physical properties of the materials used

B.1. Densities

Table B.1 | Densities

Species	ρ (g cm^{-3})	Reference
Water (l)	1.000	[134]
Air (g)	1.186×10^{-3}	[134]
Platinum, Pt	21.450	[134]
Ruthenium, Ru	12.400	[135]
Nafion	1.970	[135]
Teflon, PTFE	2.200	[134]
Carbon	1.950	[134]
Carbon paper TGP-H-060	0.440	[135]
Carbon cloth E-TEK	0.310	[135]

B.2. Specific heat

Table B.2 | Specific heat

Species	Cp (J mol^{-1} K^{-1})	Reference
Water (l)	75.29	[134]
Water (g)	33.58	[134]
Air (g)	29.11	[134]
Ethanol (l)	113.33	[134]
Oxygen (g)	$4.187\times (6.713 - 8.79\times10^{-5}\,T + 4.17\times10^{-6}\,T^2 - 2.544\times10^{-9}\,T^3)$	[136]
Carbon Dioxide (g)	$4.187\times(4.728 + 0.01754\,T - 1.338\times10^{-5}\,T^2 + 4.097\times10^{-9}\,T^3)$	[136]

B.3. Specific enthalpies

Table B.3 | Standard enthalpies of formation

Species	H_0 (J mol^{-1})	Reference
Water (l)	-285826	[38]
Water (g)	-241826	[38]
Ethanol (l)	-277690	[38]
Oxygen (g)	0	[38]
Carbon Dioxide (g)	-393522	[38]

B.4. Gibbs free energy

Table B.4 | Standard Gibbs free energy

Species	G^0 (J mol^{-1})	Reference
Water (l)	-237180	[38]
Water (g)	-228590	[38]
Ethanol (l)	-174891	[38]
Oxygen (g)	0	[38]
Carbon Dioxide (g)	-394360	[38]

B.5. Viscosities

Table B.5 | Viscosities

Species	μ (Pa s)	Reference
Water (l)	$\exp(-52.843 + 3703.6\,T^{-1} + 5.866\ln T - 5.879\times10^{-29}\,T^{10})$	[136]
Ethanol (l)	$\exp(7.875 + 781.98\,T^{-1} - 3.0418\ln T)$	[136]
Air (g)	$(1.425\times10^{-6}\,T^{0.5039})/(1 + 108.3\,T^{-1})$	[136]

B.6. Liquid molar volumes

Table B.6 | Liquid molar volumes

Species	V (cm^3 mol^{-1})	Reference
Water (l)	18.015	[137]
Ethanol (l)	58.83	[137]

B.7. Parachors

Table B.7 | Parachor values

Species	P ($cm^3\ g^{1/4}\ s^{-1/2}\ mol^{-1}$)	Reference
Water (l)	51.0	[137]
Ethanol (l)	125.3	[137]

B.8. Diffusion volumes

Table B.8 | Diffusion volumes

Species	$\sum \upsilon$ ($cm^3\ mol^{-1}$)	Reference
Water	12.7	[138]
Oxygen	16.6	[138]
Air	20.1	[138]

B.9. Tortuosity

Table B.9 | Tortuosity

Species	τ	Reference
Carbon cloth	1.11	[139]
Carbon paper	2.75	[139]

B.10. Porosity

Table B.10 | Porosity

Species	ε^{untr}	Reference
Carbon cloth	0.83	[135]
Carbon paper	0.78	[135]

B.10.1. Porosity of the diffusion layers

The carbon paper and carbon cloth are PTFE treated, and thus the real porosity must be determined accounting for the PTFE content, according to:

$$\varepsilon^{tr} = \varepsilon^{untr} - \frac{W_{PTFE}}{1\text{-}W_{PTFE}} \times \frac{\rho_{carbon}}{\rho_{PTFE}} (1 - \varepsilon^{untr}) \qquad \text{(B.1)}$$

where W_{PTFE} is the PTFE mass content (usually 0.3), ε^{untr} is the porosity of the diffusion layer material before the PTFE treatment, and ε^{tr} is the porosity of the diffusion layer after the treatment.

B.10.2. Porosity of the catalytic layers

Concerning the catalytic layer, the porosity is given by:

$$\varepsilon = \delta^{-1} \times \left(\delta - \frac{W_{cat}}{\rho_{cat}}\right) \quad \text{(B.2)}$$

with W_{cat} as the catalyst loading and δ the thickness of the catalytic layer.

B.11. Thermal conductivities

Table B.11 | Thermal conductivities

Species	k (W cm^{-1} K^{-1})	Reference
Water (l)	$0.00341 + 9.26\times10^{-6}\,T$	[136]
Air (g)	$0.000034 + 7.6\times10^{-7}\,T$	[136]
Stainless Steel	0.15	[135]
Platinum, Pt	0.71	[135]
Ruthenium, Ru	1.17	[135]
Nafion	0.0043	[135]
Teflon, PTFE	0.0035	[135]
Carbon paper untreated	0.017	[135]
Carbon cloth untreated	0.0015	[135]

B.12. Effective thermal conductivities

B.12.1. Effective thermal conductivity of the diffusion layers

The effective thermal conductivities of the anode and cathode diffusion layers are determined correspondingly according to:

$$k^{AD} = (1 - \varepsilon^{untr})k_A + (1 - \varepsilon^{tr})k_{PTFE} + \varepsilon^{untr}k_{H_2O} \quad \text{(B.3)}$$

$$k^{CD} = (1 - \varepsilon^{untr})k_A + (1 - \varepsilon^{tr})k_{PTFE} + \varepsilon^{untr}k_{air} \quad \text{(B.4)}$$

and k_A represents the thermal conductivity of carbon paper or carbon cloth.

B.12.2. Effective thermal conductivity of the catalytic layers

The effective thermal conductivities of the anode and cathode catalytic layers are determined respectively according to:

$$k^{AC} = (1 - \varepsilon)k_{Pt\text{-}Ru} + \varepsilon k_{H_2O} \quad \text{(B.5)}$$

$$k^{CC} = (1 - \varepsilon)k_{Pt} + \varepsilon k_{air} \quad \text{(B.6)}$$

Appendix C: Diffusion coefficients

C.1. Diffusion in the anode diffusion and catalytic layers

Considering a binary mixture of a given solute *A* in a solvent *B*, the binary diffusion coefficient D_{AB} of the mobile species *A* within the anode diffusion and catalytic layers can be estimated by the Tyn and Calus Method using the following relation [137]:

$$D_{AB} = 8.93 \times 10^{-8} \left(\frac{V_A}{V_B^2}\right)^{1/6} \left(\frac{P_B}{P_A}\right)^{3/5} \frac{T}{\mu_B} \quad \text{(C.1)}$$

where *V* is the molar volume, μ is the viscosity, and *P* is the parachor parameter. The parachor is related to the liquid surface tension, and may be estimated from additive group contributions, as tabulated by Quayle [137].

C.2. Diffusion in the cathode diffusion and catalytic layers

At the cathode it is assumed that the mobile species behave as ideal gases, and thus the molecular diffusion of a binary gas system of a given solute *A* in a solvent *B* can be determined by the empirical correlation of Fuller, Schettler and Giddings [138]:

$$D_{AB} = \frac{0.001 T^{7/4} \left(1/M_A + 1/M_B\right)^{1/2}}{P\left[(\sum \upsilon)_A^{1/3} + (\sum \upsilon)_B^{1/3}\right]^2} \quad \text{(C.2)}$$

where *P* is the pressure, and *M* is the molecular weight of the species *A* and *B*.

The effective diffusion coefficients can be obtained from D_{AB} by:

$$D_{AB}^{eff} = \frac{\varepsilon}{\tau} D_{AB} \quad \text{(C.3)}$$

where τ is the tortuosity factor, and ε is the porosity.